Pattern formation in complex systems

By

Neeraj Kumar Kamal

PHYS10200704002

The Institute of Mathematical Sciences, Chennai

A thesis submitted to the

Board of Studies in Physical Sciences

In partial fulfillment of requirements

For the Degree of

DOCTOR OF PHILOSOPHY

of

HOMI BHABHA NATIONAL INSTITUTE

October, 2013

Homi Bhabha National Institute

Recommendations of the Viva Voce Board

As members of the Viva Voce Board, we recommend that the dissertation prepared by Neeraj Kumar Kamal titled "Pattern formation in complex systems" may be accepted as fulfilling the dissertation requirement for the Degree of Doctor of Philosophy.

____ **Date :**
Chair/Guide:

____ **Date :**
Member 1 :

____ **Date :**
Member 2 :

____ **Date :**
Member 3 :

____ **Date :**
External Examiner :

Final approval and acceptance of this dissertation is contingent upon the candidate's submission of the final copies of the dissertation to HBNI.

I hereby certify that I have read this dissertation prepared under my direction and recommend that it may be accepted as fulfilling the dissertation requirement.

Date :
Place : Guide

STATEMENT BY AUTHOR

This dissertation has been submitted in partial fullfillment of requirements for an advanced degree at Homi Bhabha National Institute (HBNI) and is deposited in the Library to be made available to borrowers under rules of HBNI.

Brief quotations from this dissertation are allowable without special permission, provided that accurate acknowledgement of source is made. Request for permission for extended quotation from or reproduction of this manuscript in whole or in part may be granted by the Competent Authority of HBNI when in his or her judgment the proposed use of the material is in the interests of scholarship. In all other instances, however, permission must be obtained from the author.

Neeraj Kumar Kamal

DECLARATION

I, hereby declare that the investigation presented in the thesis has been carried out by me. The work is original and has not been submitted earlier as a whole or in part for a degree/diploma at this or any other Institute/University.

Neeraj Kumar Kamal

AKNOWLEDGMENTS

It is a great pleasure to thank all those people who, via discussions, suggestions or otherwise, have directly or indirectly contributed towards this thesis.

First and foremost, I would like to express my sincere gratitude to my thesis advisor, Prof. Sudeshna Sinha, for her guidance and valuable advice on my thesis work. I would like to thank her for being a person open to ideas, and for encouraging and helping me to shape my interest. I would also like to thank her for her patience, motivation and enthusiasm.

Besides my advisor, I would like to thank the rest of my doctoral committee: Prof. Sitabhra Sinha, Prof. G. I. Menon and Prof. R. Rajesh, for their encouragement and insightful comments during my work.

My sincere thanks also goes to Prof. A. K. Mishra and Prof. S. R. Hassan for their motivation and encouragement.

I am also grateful to IMSc for all its support during my work here. I would also like to thank IISER, Mohali for the support whenever I visited there.

I would also like to thank all my friends who were always a constant source of joy, laughter and support in these difficult years. Without them I would not have made it this far.

Finally I would like to thank my family, especially my mother and father for always believing in me, for their continuous love and their support in my decisions.

List of Publications arising from the thesis

Journal

1. *Imbalance of positive and negative links induces regularity.* **Neeraj K. Kamal**, and Sudeshna Sinha

   Chaos, Solitons & Fractals **44**, 71 (2011)

2. *Pattern formation in arrays of chemical oscillators.* **Neeraj K. Kamal**

   Pramana **78**, 705 (2012)

3. *Cluster formation in populations of coupled chaotic neurons.* **Neeraj K. Kamal**, and Sudeshna Sinha

   EPJ-ST **222**, 905 (2013)

Others(communicated)

1. *Emergent patterns in coupled neuronal population with different sizes and types.* **Neeraj K. Kamal**, and Sudeshna Sinha

2. *Interplay of diversity and random connection on coupled neuronal populations.* **Neeraj K. Kamal**, and Sudeshna Sinha

List of corrections and changes as suggested by the Thesis and Viva Voce Examiners

1. Corrected typos as suggested by the referees in all the Chapters.

The corrections and changes suggested by the Thesis and Viva Voce Examiners have been incorporated in the thesis.

Guide

Contents

Synopsis

An interacting network of nonlinear dynamical elements is a simple prototype of a complex system and has been used to describe various self-organizing phenomena, ranging from biological systems and ecosystems, to physical and chemical systems. Understanding the structure and dynamics of such networks lies at the core of complex systems research. These systems are comprised of two basic components: (i) local nodal dynamics, modeled by nonlinear maps or differential equations capable of yielding a rich variety of temporal patterns, and (ii) transmission of information among these local dynamical units by coupling connections of varying strengths and underlying topologies, described by a connectivity matrix. The study of emergent spatiotemporal patterns in an extended system of interactive dynamical elements, under varying nodal dynamics and coupling architectures, is the main theme of this thesis.

There are various types of complexity inherent in the dynamical networks. For example, there may be *dynamical complexity* where the nodal dynamics, namely the evolution of the state of the individual nodes, is complex. One may also have *spatial diversity* in the system, where the nodes have different intrinsic dynamical behaviors. Further, there may be complexity in coupling as well, such as *diversity in connections* where the links of the network have different (positive/negative) weights. One can even consider *dynamic network architectures* where the links between nodes change over time, introducing another time-scale in the problem. In this thesis, we will incorporate a range of complexity, in both nodal dynamics and connections, and study their effects on the spatiotemporal

behavior of the extended system.

The thesis is organized as follows: In the introductory *Chapter* 1 we briefly review the literature dealing with the study of collective behavior of the networks of interacting dynamical systems, in particular, work related to our studies. *Chapter* 2 provides a brief overview of the models used to describe the dynamics of a single node in the networks that are studied in this thesis. Here we will describe discrete-time neuron models which can yield the basic modes of activity of a single neuron, as well as the Brusselator model, which is a minimal mathematical model predicting oscillations in chemical reactions. The results obtained from our extensive numerical and analytical studies will be presented in subsequent chapters described briefly below.

In *Chapter* 3, the effect of the interplay of positive and negative links, on the dynamical regularity of a random weighted network, with neuronal dynamics at the nodes is investigated. We study how the mean $\overline{J}$ and the variance of the weights of links, influence the spatiotemporal regularity of this dynamical network. We find that when the connections are predominantly positive (i.e., the links are mostly excitatory, with $\overline{J} > 0$) the spatiotemporal fixed point is stable. A similar trend is observed when the connections are predominantly negative (i.e., the links are mostly inhibitory, with $\overline{J} < 0$). However, when the positive and negative feedback is quite balanced (namely, when the mean of the connection weights is close to zero) one observes spatiotemporal chaos. So, counter-intuitively, it appears that in this random weighted network of neuronal maps, *balanced excitatory and inhibitory connections leads to the destabilization of the fixed (rest) state, resulting in large irregular spiking.* To be stabilized to a inactive state one needs one type of connection (either excitatory or inhibitory) to dominate. Further we observe that larger network size leads to greater spatiotemporal regularity.

In *Chapter* 4, we investigate cluster formation in populations of coupled chaotic model neurons under homogeneous global coupling, and distance dependent coupling, where the coupling weights between neurons depend on their relative distance in the lattice. We observed three types of clusters emerge for global coupling: synchronized cluster, two state cluster and anti-phase cluster. In addition to these, we find a novel three state-cluster for distance dependent coupling, where the population splits into two synchronized groups and one incoherent group. Lastly, we study a system with random inhomogeneous coupling strengths, in order to discern if the special pattern found in distance-dependent coupling arises from the underlying lattice structure or from the inhomogeneity in coupling. We found that emergent patterns depend not only on coupling heterogeneity but also on the coupling architecture in the lattice.

In *Chapter* 5, we investigate the spatiotemporal dynamics of an ensemble of coupled model neurons, consisting of sub-populations with varying sizes that possess different dynamical behavior, ranging from periodic to chaotic. This system is motivated by the phenomena of *Event Related Synchronization/Desynchronization* (ERD/ERS) which are event related response of the brain. Here, an event is a dynamic signal which induces synchrony (ERS) or desynchronization (ERD) in the brain. In our model, we observe that this coupled system yields a wide variety of patterns, ranging from different distinct sets of synchronized clusters to anti-phase clusters. The nature of clustering is determined by the sizes and dynamics of the interacting sub-populations. For instance, for two interacting chaotic groups, we observe that the anti-phase clusters within a group occurs only in the minority population. Further, for interacting chaotic and periodic groups, when large chaotic groups are strongly coupled to small periodic groups there is complete synchronization in the chaotic population. However, when a majority periodic group couples strongly to a minority chaotic group, it desynchronizes. It is then evident that the emergent clusters are strongly governed by the interplay of the sizes and the intrinsic dynamics of the sub-populations.

In *Chapter* 6, we investigate the influence of diversity and random connections on the temporal regularity of spiking in coupled model neurons. Both static and dynamic random connections are considered in this study. We find *diversity induced coherence* in the spike events for connections ranging from regular to random, with the coherence being most pronounced for the regular coupling case. We also observe that for higher coupling strengths and random rewiring probabilities, larger coherence in the spike events emerges when the random links are dynamic, while the temporal regularity of spike events is not enhanced for quenched random connections. Lastly, we report the effect of coupling strength and rewiring probability on the diversity required to induce *optimal coherence*.

In *Chapter* 7, we describe a simple model mimicking diffusively coupled chemical micro-oscillators. Our study here draws its motivation from experiments of diffusively coupled chemical oscillators in micro-fluidic assemblies. These experiments have nanoliter volume aqueous drops containing reactants of the oscillating reaction, separated by gaps containing typically octane. A variety of dynamics was observed in such systems, most notably in-phase and anti-phase synchronization. So, we seek a simple model capable of showing the observed spatiotemporal patterns. The physical gap between the "droplets" of chemical oscillators is modeled by delay in the coupling interaction in our model. So, we mimic the micro-fluidic array by a delay-coupled array of oscillatory chemical systems. In here we have characterize the patterns in time and space that arise in this arrays under varying forms of coupling. We observed rich variety of dynamical states emerging from the model under variation of time delay in coupling, coupling strength and boundary conditions. The spatiotemporal patterns obtained include clustering, mixed dynamics, inhomogeneous steady states and amplitude death. Further, under delay in coupling the model yields transitions from phase to anti-phase oscillations, reminiscent of that observed in experiments.

Finally, in *Chapter* 8, we present the principal conclusions that emerge from the work in this thesis, as well as some potential extensions and applications of our results.

List of Figures

List of Tables

Chapter 1

Introduction

The primary focus of this thesis is to study the patterns or spatiotemporal dynamics arising from *the interplay of local dynamics and coupling interactions* in *complex systems*. In this chapter, we will start with a minimal broad definition of a *Complex System*, commonly used in the context of spatially extended systems. Then we will briefly discuss the modeling of such complex systems based on a hierarchy of discretization schemes. We will then outline the nodal complexity and connection diversity in the systems we focus on in our work. Finally we present the organization of the chapters in this thesis.

1.1 Complex Systems

A complex system is defined as a system consisting of a large number of interacting components and has following two salient properties, (a) *emergence* and (b) *self-organization* [1]. Emergence refers to the appearance of a behavior which could not be expected or anticipated from the knowledge of the constituents of the system alone, namely the "whole" is more than merely the sum of the "parts". Self-organization refers to spontaneous appearance of the emergent features and collective patterns in the system, even in the absence of external influences.

These systems are ubiquitous in nature and often described by spatially extended systems and complex dynamical networks [2, 3]. Examples of these include food webs [4] and ecosystem [5], biological neural networks [6], electrical power grids [7], social [8, 9]and economic relations [10], co-authorship and citation networks of scientists [11, 12], cellular and metabolic networks [13], etc. The spatiotemporal behavior or formation of patterns in these system has been studied both theoretically and experimentally, such as in fluid dynamical systems [14], biological systems [15] and chemical systems [16, 17]. The diverse collective behavior of these systems, which have many degrees of freedom, include captivating phenomena such as: synchronization [18, 19], seen in a group of fireflies [20], chemical oscillators [21], ecological systems [22], plasma discharges [23], chaotic lasers [24] etc.; frequency locking in chemical systems [25], Josephson junction arrays [26] etc.; pattern formation in reaction diffusion systems [27]; and spatiotemporal chaos, eg. in plasma discharge [28]. As a reasonable understanding of the behavior of low dynamical systems has been achieved [29, 30], a lot of recent research effort has gone into modeling spatially extended systems, namely large interactive systems with many distributed degrees of freedom [31]. Such novel formalisms and models have paved a new way of understanding a wide range of complex physical, biological, chemical and social systems.

1.2 Models of complex systems

Modeling the collective behavior of a spatially extended system is very difficult and remains theoretically challenging. The evolution of these spatially extended systems mentioned above are often modeled by partial differential equations of various kinds. A comprehensive review of these nonlinear partial differential equations is to be found in Ref. [27]. It was found that these partial differential equations are analytically tractable only in the simplest of the cases. From numerical point of view, the solutions of these are not only cumbersome, but very time-consuming too. So, a lot of effort has been made over the years to *construct simple but effective models which are capable of capturing the essence of complicated dynamic processes as they occur in nature and whose dynamics can be easily analyzed and simulated*. Also, these simple models should also provide a suggestive conceptual frameworks for understanding complex phenomena which are generic in complex systems.

Discretization is one of the simplest and most straightforward routes to obtain model equations which describe the dynamics of spatially extended systems. There are three quantities in these systems that are to be accounted for, in any spatiotemporal behavior or pattern: (a) *time* (b) *space* and (c) *state variables*, corresponding to physical entities of interest e.g. - temperature, pressure, velocity in fluids, concentrations in chemical systems, populations in ecosystems etc. That is, in order to capture the behavior of these complex systems, one needs to follow a set of relevant state variables over space and time.

Thus, any combination of these three quantities can be discretized to obtain model equations which describe complex systems. A broad classification of models, obtained from the discretization of these three quantities, are summarized in Table 1.1.

One such class of the models is: *Coupled Oscillators Chain*. These models are based on a discrete space, while the evolution of the state variables are given by coupled ordinary differential equations, namely continuous time and state variables. This class of models has been used extensively in studying a variety of phenomena, such as mode locking in Josephson junction arrays [26] and neural dynamics [32].

Another popular class of models is the *Coupled Map Lattice*. These are obtained, when is addition to discrete space, time is also discretized. So these models can be thought of as stroboscopic snapshots of the system. Here the evolution of the state variable(s) on the lattice, which are continuous, is given by a map. Typically such models consist of a local dynamical map describing the dynamics at a site on the lattice, with the different sites interacting with sub-sets of other sites on the lattice via a prescribed coupling scheme. This class of models is widely used in various contexts, as they are computationally very

Model	Time	Space	State Variables
Partial Differential Equations	Continuous	Continuous	Continuous
Coupled Oscillators	Continuous	Discrete	Continuous
Coupled Map Lattices	Discrete	Discrete	Continuous
Cellular Automata	Discrete	Discrete	Discrete

Table 1.1: Table showing the classification of models resulting from different possible discretization schemes.

efficient and are analytically more tractable [31].

The furthest simplification in modeling is obtained by discretization of state variables also, along with space and time. This class of models is known as *Cellular Automata* [33], and it has provided many useful insights by yielding very simple models of complicated phenomena. For example, the well known sand-pile model [34] has been found to capture the essential qualitative features of the self-organized criticality.

As mentioned above, complex systems can be considered as a lattice of large number of nonlinear dynamical elements and a general strategy to model a complex system is to split the model equations describing the dynamics of the system into two parts: one part will give the local dynamics of the site of lattice and the other part will give the interaction between the sites of the lattice. This set of maps or differential equations obtained from the discretization scheme are an important prototype of the complex systems. But, there are strong reasons to re-visit the fundamental issue of interactions defined on a regular lattice-like structure in coupled map/oscillators lattices. It was found in various studies that many systems of biological, technological and physical significance are better described by randomizing some fraction of the regular links. Hence, apart from the models of complex systems shown in Table 1.1, other models that fall under the broad class of *complex networks* were proposed [1, 2, 3]. In the network picture we consider a collection of elemental dynamical units, the *nodes*, which are connected to other units through connections which may be described by (directed or undirected) edges of a graph. In this thesis we will consider, dynamics on networks with a wide range of topologies.

1.2.1 Principal Components of the Models

In this thesis, we have utilized the coupled map lattices/networks and coupled oscillators chain framework to describe the spatiotemporal behavior and formation of patterns in spatially extended systems. We will now briefly discuss the basic ingredients of the model equations which describe the system, obtained in this framework.

Local dynamics: The local dynamics gives the rule, in the form of a map or a set of differential equations, which prescribe how the state variables at a local site (or node) changes with time. It is the source of local temporal patterns. One can choose an appropriate low dimensional system to model the local dynamics, depending on the phenomena of interest. For example, in order to describe the behavior of a network of neurons, a map [35] or a set of differential equations [36] mimicking the dynamics of a single neuron is an appropriate choice for the local dynamics.

Interactions: The interaction term in these systems attempts to model the transmission of information from one site (node) to another in a lattice (network). This transmission of information drives the global organization in the system. The interaction term can be of various types depending on the phenomena of interest. For example, in chemical dynamical systems, the relevant interaction term captures the diffusion of concentration from one site to another. Similarly, in neural networks a basic form of interaction can represent electrical synapses which conduct electrical potential directly from one neural cell to another via diffusion, or chemical synapses which are described by pulse coupling [36].

In general, there are many different coupling classes. For example, the coupling can be *local* where the nodes interact only with nearest nodes, that is the interaction term only involves spatially close neighboring sites. Coupling also may be *non-local*, where the nodes can interact with far away nodes. Further, the coupling form may be *homogeneous*, with the coupling weight between any two node being constant. On the other hand, in certain situations the coupling may be *heterogeneous*, where the coupling weight between the two nodes depends on a kernel.

In many models the topology of the connection network and the coupling weights of the interaction is represented by a connectivity matrix, $\mathbf{J}$. In this matrix, the element, J_{ij}, represents the connection strength between the two sites (nodes) i and j of a lattice (network). Specifically we will consider many different forms of such connection matrices in this thesis, ranging from sparsely connected to globally connected ones, and varying from regular lattices to completely random networks.

Boundary conditions: For coupled map lattices and coupled oscillator chains the specification of the boundary is also very important. The most commonly used boundary condition is periodic boundary condition. Also, free and fixed boundary conditions are used for coupled map/oscillator chains depending on the the phenomena of interest.

Interaction with the environment: The model system may also incorporate noise terms, as well as external periodic signals, in order to provide more realistic descriptions of certain naturally occurring and human engineered phenomena. These terms describe the interaction of the system with its environment and are responsible for many self-organizing phenomena. For example, in the case of circadian rhythm, the system of coupled biological oscillators is acted upon by the daily variations of sunlight experienced by the organism [37]. Similarly, noise in a system of coupled maps/oscillators has been found to assist amplification and optimization of feeble input information such as a weak external signal [38].

Using these basic ingredients, the model equations describing the system of interest are obtained. These are solved numerically for initial conditions drawn from a random distribution, in order to obtain the behavior of a generic system. The patterns are then characterized by space-time plots and bifurcation diagrams, which captures the qualitative change of dynamical behavior under variation of the system parameters. Further, the stability of the patterns are quantitatively determined by calculating the Lyapunov exponents of the system.

In these systems, the conflict between the dynamics at the node and interaction among the nodes accounts for the formation of a rich variety of spatiotemporal patterns. For example, consider a globally coupled nonlinear system. Here, the coupling is via a mean field, which involves an average over the states of all elements in the system. The mean field is conducive to synchronization among the elements, while the local(nodal) nonlinear behavior induces destruction of this coherence. The balance between these two trends is responsible for rich pattern formation in this system [39, 40]. Typically, for globally coupled maps, when the interaction is diffusive in nature, it is expected that strong enough coupling will drive the elements to a state of *complete synchronization*, but at intermediate coupling strengths stable clusters or condensates of elements may form. Within a cluster all the elements are completely synchronized, but the dynamics of the different clusters are not synchronized and may even be qualitatively different. A number of coherent clusters have been reported in numerical investigations of relatively simple systems such as coupled logistic and circle map systems [41, 42, 43], randomly coupled maps [44], coupled chaotic Rössler oscillators [45, 46], coupled genetic oscillators [47, 48], globally coupled inhibitory neurons [49], as well as in experiments on salt water oscillators [50] and in arrays of electrochemical oscillators [51, 52].

1.3 Complexity in the Models

In order to gain an understanding of complex systems and their emergent patterns or spatiotemporal dynamics, various levels of complexity should be explored in the model equations which describe these system [2]. In this thesis, we have tried to investigate the following complexities in our models:

(i) **Dynamical Complexity:** This complexity refers to the local dynamics at a site/node in the lattice/network. Namely, the local dynamical elements comprising the lattice or network can be nonlinear systems capable of yielding a wide variety of qualitatively distinct dynamics, ranging from fixed points to chaos.

(ii) **Connection Diversity:** This complexity refers to the properties of the directed or undirected links between the sites/node in the lattice/network, including the connection weight between each pair of nodes/sites and the sign of the connection weight indicating positive or negative feedback.

Most existing research work on complex network models have concentrated on network structures with binary connection weights, i.e. the links between any two nodes is either 1 or 0, for example in various models describing the ecosystem [53, 54, 55]. But the properties and dynamics of many social, technological, biological and financial systems are found to depend on the connection weights among their nodes [56, 57] and so they are best described by weighted networks. Also, the sign of the connection weight is very important for neuronal networks, where the positive sign in the connection weight represents excitatory and the negative sign represents a inhibitory connection. The profound effect on the dynamical behavior of the network arising from these two aspects of diversity in connection weights is discussed in the Chapter 3.

Now, the inhomogeneity in the coupling connections, can also arise from asymmetric coupling, time delays [58], etc. For example, in electrochemical systems, we have nonlocal coupling among reactive sites due to the electric field. Here, the long range coupling is not global as its effect dies out with increasing distance, thus making the coupling distance dependent. The transition to desynchronization is studied in a system of coupled phase oscillators [59] and sine-circle maps [60] for non-local coupling. In these works, the strength of the interaction decays with the lattice distance as a power-law, in such a way that one can pass continuously from a local (nearest-neighbor) to a global (mean-field) type of coupling. Map clusters, or spatially coherent structures with similar temporal evolutions, are found in Hamiltonian systems [61] for this non-local coupling. Apart from decaying power law interactions, for networks with time-delayed coupling, where the delay depends on spatial distance between the nodes, various clustered states are found [62, 63, 64, 65]. Taking motivation from the above mentioned work we also tried to employ this kind inhomogeneity in coupling connection where the coupling weight between two nodes depends on the relative distance between the nodes. The effect on the formation of cluster due to this type of coupling weight is described in the Chapter 4.

(iii) **Local Diversity at the Nodes:** This kind of complexity refers to diversity in the dynamical properties of the nodal dynamics, i.e. the dynamical domain of the nodes in the network are different. Several studies have been reported which incorporate this kind of complexity in the network. For example, Daido and Nakanishi [66, 67], have considered a globally coupled network consisting of two types of populations, (a) active or self-oscillatory and (b) inactive or non-self oscillatory, and studied the robustness of macroscopic synchronized oscillations. In a similar vein, a mixed population composed of self-oscillatory elements and excitable elements have been considered in [68]. Also, mixed populations consisting of two types of self- oscillatory elements with different periods, has been investigated in [69].

Related to this kind of complexity, studies have been devoted to the emergence of mutual synchronization among groups which are in different dynamical domains in a system. For example, the onset of coherent collective behavior in networks of interacting populations of phase oscillators, with both node and coupling heterogeneity, is described in [70]. In [71], all possible routes to synchronization for two interacting populations of different phase oscillators with asymmetric coupling functions is presented. Also, richer dynamical behavior is found for this case vis-a-vis symmetrically coupled populations. The effects of coupling, noise, and phase asymmetries on inter-ensemble synchronization in two coupled ensembles of phase oscillators, is considered in [72].

In this thesis, we have investigated this class of complexity in a neural network consisting of periodic and chaotic groups. The effect of the interplay of the sizes and the intrinsic dynamics of these two populations, on the formation of clusters, is presented in Chapter 5

.

(iv) **Network Evolution:** This addresses the dynamic properties of the connectivity matrix. In commonly used models, the connection between any two nodes in a network is considered static throughout the evolution i.e. if the two nodes in the network are connected, they will remain connected and vice-versa. But in the real systems, the connection between two nodes is likely to change in time. Dynamically varying links add one more time scale to the problem and may have counter-intuitive consequences [73, 74, 75]. Motivated by this, in Chapter 6, we study the effect of dynamic switching of random links on the temporal regularity of spiking in a neural network.

(v) **Parametric Heterogeneity:** The elements of an extended system may certainly differ from each other. So it is natural to incorporate heterogeneity in the parameters governing the nodal dynamics. This can also be considered as *parametric noise*, which is *quenched* in time.

In spatially extended systems, the constructive role of disparity in a characteristic parameter of the local dynamical element, has been a focus of recent research interest. For example, it is found that the spatiotemporal chaos in an array of coupled pendulums can be tamed by an optimal magnitude of disorder, induced by disparity in pendulum lengths [76, 77]. Similarly, it was found by Tessone *et. al.* that different sources of diversity, such as those represented by quenched disorder or noise, can induce a resonant collective behavior in an ensemble of coupled bistable or excitable systems [78]. This phenomena is termed as diversity induced resonance and it is quite similar to noise induced resonance phenomena in spatially extended systems [38, 79]. Thus, diversity can play a constructive role analogous to that of the noise. Taking this further, in Chapter 7 we have explored the effect of such diversity on the temporal regularity of spiking in a neuronal network.

In this thesis we explored all the above levels of complexity in our models, and determined the consequences of each type of complexity on spatiotemporal pattern formation.

1.4 Organization of the chapters

The organization of the chapters in this thesis are as follows. In *Chapter* 2, we start with a brief overview of models which describe the dynamics of spiking neurons and oscillating chemical reactions. Then we discuss in some detail the particular models which describe the local dynamics at the nodes of the networks studied in this thesis. In *Chapter* 3, we present results on the dynamical regularity of a random weighted network, with neuronal dynamics at its nodes, where the connection weights are skewed towards positive (excitatory connections) or negative (inhibitory connections) links. In *Chapter* 4, we present our results on the cluster formation in populations of coupled chaotic model neurons under homogeneous global coupling, and distance dependent coupling where the coupling weights between neurons depend on their relative distance in the lattice. *Chapter* 5 investigates the spatiotemporal dynamics of an ensemble of coupled model neurons, consisting of sub-populations with varying sizes that possess different dynamical behavior, ranging from periodic to chaotic. In *Chapter* 6, we explore the influence of disparity of elements, along with random connections, on the temporal regularity of spiking in coupled model neurons. Here, we consider the effect of both static and dynamic random connections. In *Chapter* 7, we describe a simple model mimicking diffusively coupled chemical micro-oscillators and characterize the rich variety of dynamical states emerging from the model under variation of time delay in coupling, coupling strength and boundary conditions. Finally, in *Chapter 8*, we present the principal conclusions that emerge from the work in this thesis, as well as some potential extensions and applications of our results.

Chapter 2

Models : Neurons and Chemical Oscillators

In this Chapter, we will briefly discuss the models that will be used to describe the nodal dynamics of the networks explored in the thesis.

2.1 Modeling Neuronal Activity

Neurons are very complex biophysical and biochemical entities. To understand the dynamics of neurons and neural networks, phenomenological models have to be developed (see the review in Ref. [32]). The Hodgkin-Huxley (H-H) system is a prototype among such phenomenological descriptions of all ion channel-based models describing a single neuron [80]. It was introduced to model the firing dynamics observed in the giant squid axon. This model has two fast and two slow variables. It also considers the large number of voltage-gated ion channels of a neuron. There is a large list of models derived from this one, and it serves as a principal test-bed in computational neuroscience. Viewing this seminal work from the perspective of dynamical systems, much effort has been made to use the tools of classical nonlinear dynamics, for example bifurcation theory, to understand the dynamics of the neuron [81]. The study of bifurcations in neural models and in *in vitro* experiments is a keystone for understanding the dynamical origin of many single-neuron firing patterns. A comprehensive review of the bifurcations in neuronal models is to be found in [36]).

The H-H model is not very suitable for modeling a neural network consisting of large number of elements due to its high dimensionality. Thus, a new series of models, called conductance based models, appeared as a simplification of H-H models. They capture the basic ingredients of the phenomenology of a neuron. The FitzHugh-Nagumo [82, 83] model is one such model which is widely and successfully used to describe, not only the neuronal dynamics, but also chemical reactions. Similarly, a simplified model of a neuron was proposed by Morris *et. al.* [84] which reduces the number of dynamical variables of the H-H model and also displays action potential generation when changing the external current, arising from a saddle-node bifurcation to a limit cycle. Also, a neuron model has been proposed by Hindmarsh *et. al.* [85], which uses a polynomial approximation to the right-hand side of a H-H model.

Apart from these coupled differential equation systems, many discrete time phenomenological model of a single neurons have also been introduced, which are known in literature as map-based models (see review of these models in Ref. [86, 35]). These map-based models are one of a class of simple phenomenological models for spiking, bursting neurons. These models can be computationally very fast, but have little biophysical foundation. Also, these map-based models should be considered as compact abstractions of dynamical properties of neurons which can shed light over the mechanisms that give rise to neuronal phenomena ranging from chaotic spike trains to synchronized oscillations [35].

In next two subsections we will briefly review two such map based models which will be used extensively in this thesis to describe the dynamics of a single neuron.

2.1.1 Chialvo Map

The dynamical equation(s) describing a neuron must have following properties: It must have a globally attracting equilibrium point called the resting state. The phase space must contain sub-threshold and supra-threshold domains which are partitioned by a threshold. These two domains are defined by the response of the state variables after a small instantaneous perturbation acts on the system. If the system is in the sub-threshold domain, after perturbation the state variables will eventually return to the rest state. But, if the system is in the supra-threshold domain, there is a large excursion in the state variables before returning to the resting state. This response in nerve cells is known as an action potential. Further, the system must be capable of exhibiting periodic oscillations under constant bias input, and some parameter values in the dynamical equations must lead to chaotic solutions.

Based on the above, a simple two-dimensional map was proposed by Dante R. Chialvo [87] to model the dynamics of an isolated neuron. The map has following form:

$$x_{n+1} = f_1(x_n, y_n) = x_n^2 exp(y_n - x_n) + k, \tag{2.1a}$$

$$y_{n+1} = f_2(x_n, y_n) = ay_n - bx_n + c, \tag{2.1b}$$

where, the variable x mimics the evolution of the activation variable or the membrane potential and y acts as a recovery-like variable. Subscript n represents iteration steps corresponding to the discretized time evolution of the system.

The equations describing the neuron have four parameters, a, b, c and k. The first three parameters control the dynamics of the recovery variable as follows: a is a time constant of recovery ($a < 1$); b is the activation-dependence of the recovery process ($b < 1$); and c is the offset. In the activation variable, the parameter k can act either as a constant bias or as a time-dependent additive perturbation. The typical values of the three parameters were set to values $a = 0.89$, $b = 0.6$, and $c = 0.28$, and the parameter k acts as the control parameter of the map.

In order to get a qualitative understanding of this model, we first consider the case where the value of k is 0. In this case, the fixed points (x^*, y^*) of the map in Eq. (2.1) is given by following relations,

$$x^* = x^{*2}\exp(y^* - x^*), \tag{2.2a}$$

$$y^* = ay^* - bx^* + c. \tag{2.2b}$$

One of fixed point is $(0, \frac{c}{1-a})$, which is stable as the eigenvalues of the Jacobian are $(0, a)$ and $a < 1$. Now consider the case where the value of the state variable y is fixed at r. With the parameter $b = 0$, the above system now can be described as,

$$x_{n+1} = f(x_n, r) = x_n^2 \exp(r - x_n), \tag{2.3a}$$

$$r = \frac{c}{1-a} \tag{2.3b}$$

For the above map, the fixed point solution will depend on the value of r. When $r < 1$, we have only one fixed point at $x = 0$. When $r > 1$, we have three fixed points. There will be one fixed point, x_{mid}, between $x = 0$ & $x = 1$ which is always unstable and one fixed point, x_{up} at $x > 1$ which is either stable or unstable depending on the value of r. A plot of the function $f(x, r)$ vs x is shown in Fig. 2.1 for three representative values of r.

For $r > 1$, all initial conditions of $x < x_{mid}$ converge to the fixed point $x = 0$. But, the values of $x > x_{mid}$ either converge to fixed point x_{up} or are trapped in the interval $[x_{mid}, f(x, r)]$, depending on the value of r. The bifurcation diagram shown in the Fig. 2.2(i) captures the above features. It also shows the cascade of period-doubling leading to chaos as the value of r is increased, for all the initial conditions $x > x_{th}$. The lyapunov exponents as a function of r, shown in the Fig. 2.2(ii) also corroborate the above mentioned features of the map.

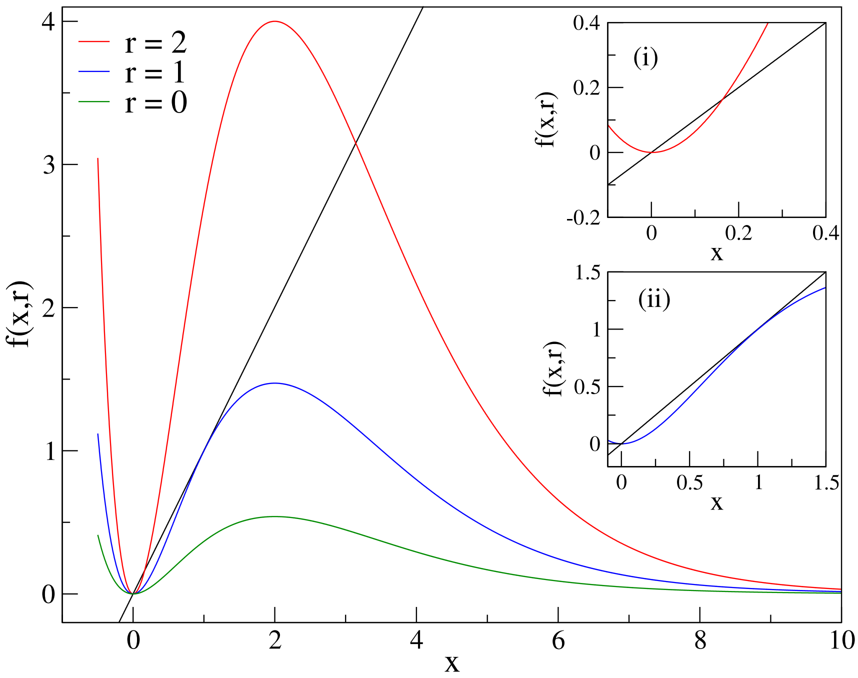

Figure 2.1: Plot of function $f(x,r)$, given by Eq. (2.3), vs x for various values of r. Here the black line is the diagonal line $y = x$. Inset (i) shows the two intersections of the function $y = f(x,r)$ with the line $y = x$ for $r = 2$. Also notice that for $r = 1$, the line $y = x$ is tangent to the function $y = f(x,r)$ in inset (ii).

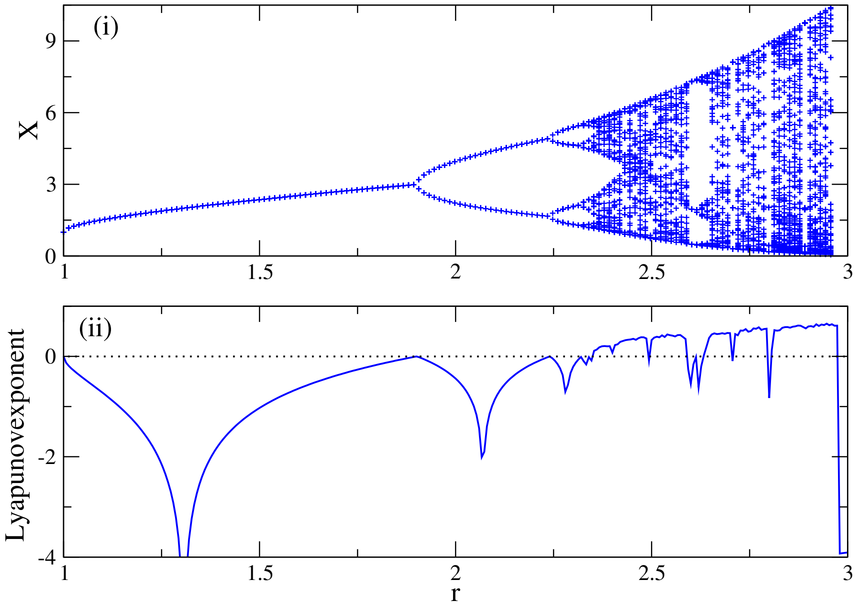

Figure 2.2: Here in (i) the bifurcation diagram of the map given by Eq. (2.3) is plotted against r, for the initial conditions $x > 1$. All initial conditions $x < 1$ leads to fixed point $x = 0$ (ii) the Lyapunov exponents of the map is plotted against r.

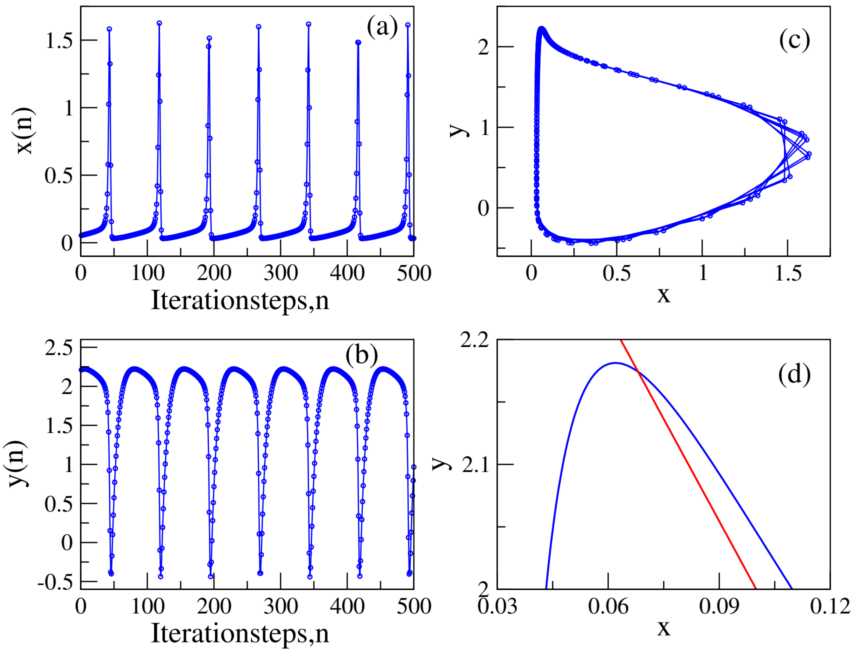

Figure 2.3: Periodic solutions of the map given by Eq. (2.1) for the parameter values $a = 0.89$, $b = 0.18$, $c = 0.28$ and $k = 0.03$. (a) Time series of the state variable, x, (b) Time series of state variable, y, (c) Phase space plot (d) Nullcline of both state variables (x-nullcline shown by color blue) showing the stable fixed point at the intersect of both the nullclines.

An understanding of the full system given by Eq. (2.1) can be obtained by considering the properties of the map in the phase plane. The x and y- nullclines are given by the equations,

$$y = x + \ln \frac{x-k}{x}, \tag{2.4a}$$

$$x = \frac{c-(1-a)y}{b} \tag{2.4b}$$

It is found that the intersections of the these two nullclines depends on the parameters (a, b, c, k) of the map. The oscillatory and the chaotic solutions of the map can be obtained, by treating k as a bifurcation parameter and keeping the other parameters constant. Increase in the value of k in this model is equivalent to an increasing bias current applied to a neuron.

Periodic solutions: The oscillatory solutions appear for parameter values $a = 0.89$, $b =$

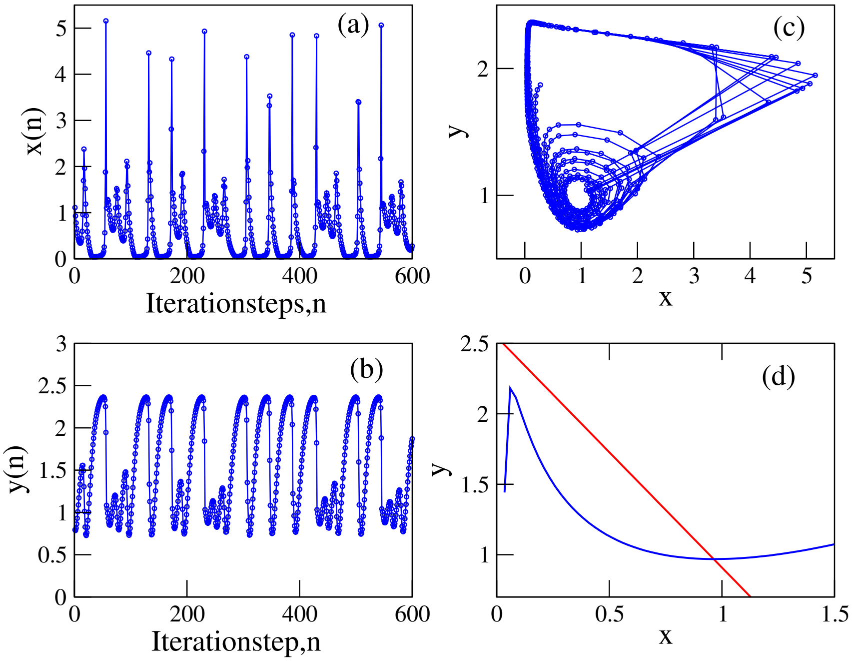

Figure 2.4: Chaotic solutions of the map given by Eq. (2.1) for the parameter values $a = 0.89$, $b = 0.18$, $c = 0.28$ and $k = 0.03$. (a) Time series of the state variable, x, (b) Time series of state variable, y, (c) Phase space plot (d) Nullcline of both state variable (X-nullcline shown by color blue) showing the unstable fixed point near $(x, y) \sim (1, 1)$.

0.6, $c = 0.28$ and $k = 0.03$. Here the nullclines intersect near the negative slope region of x-nullcline, as shown in the Fig. 2.3(d). This results in the co-existence of a stable focus and a stable oscillatory solution. The dynamics of the map converges to either of the attractors depending on the initial conditions. The time series of the state variables along with phase space of state variables is shown in the Fig. 2.3.

Chaotic solutions: For the aperiodic bursting solution the parameter values are, $a = 0.89$, $b = 0.18$, $c = 0.28$ and $k = 0.03$. Existence of chaotic solutions at these parameter values is due to the following two reasons: (i) for these parameter values there is a single unstable fixed point which is near $(x, y) \sim (1, 1)$ as shown in the Fig. 2.4(d), (ii) the value of parameter, b, which is the activation-dependence of recovery variable, y, is relatively small.

Due to the smallness of the value of the parameter b, the value of y remains more or less frozen. This allows several iterates of the map to remain around the unstable fixed point near $(x, y) \sim (1, 1)$, before spiraling out to produce a large oscillation. Thus, the basic rhythm of the map will consist of some large amplitude oscillations followed by small amplitude oscillations around the unstable fixed point. The interval between the large spikes, as well as the number of small oscillations, vary randomly. All these above mentioned features of the map can be seen in the time series of state variables, and in the phase potrait of the state variables, displayed in the Fig. 2.4.

2.1.2 Rulkov Map

This is a map describing a model neuron proposed by Rulkov [88]. It is a two dimensional map, consisting of two dynamical variables which capture the slow and fast dynamics of a neuron, given as,

$$x_{n+1} = f(x_n, y_n + \beta_n), \tag{2.5a}$$

$$y_{n+1} = y_n - \mu(1 + x_n) + \mu\sigma_n \tag{2.5b}$$

where, x_n is the fast and y_n is the slow dynamical variable. Slow time evolution of the variable y is due to small values of the parameter, μ ($\mu = 0.001$). Here β_n and σ_n describe external influences applied to the map. These terms model the dynamics of the neuron under the action of the external dc bias current I_{dc} and synaptic inputs I_{syn}. The term β_n can also be used as the control parameter to select the regime of dynamical behavior. The function $f(x, y)$ is a piecewise nonlinear function which is designed to shape spiking oscillations in fast subsystems. It contains three intervals which can be described as follows,

$$f(x, y) = \begin{cases} \alpha/(1 - x) + y, & \text{for} \quad x \leq 0, \\ \alpha + y, & \text{for} \quad 0 < x < \alpha + y, \\ -1, & \text{for} \quad x \geq \alpha + y, \end{cases} \tag{2.6}$$

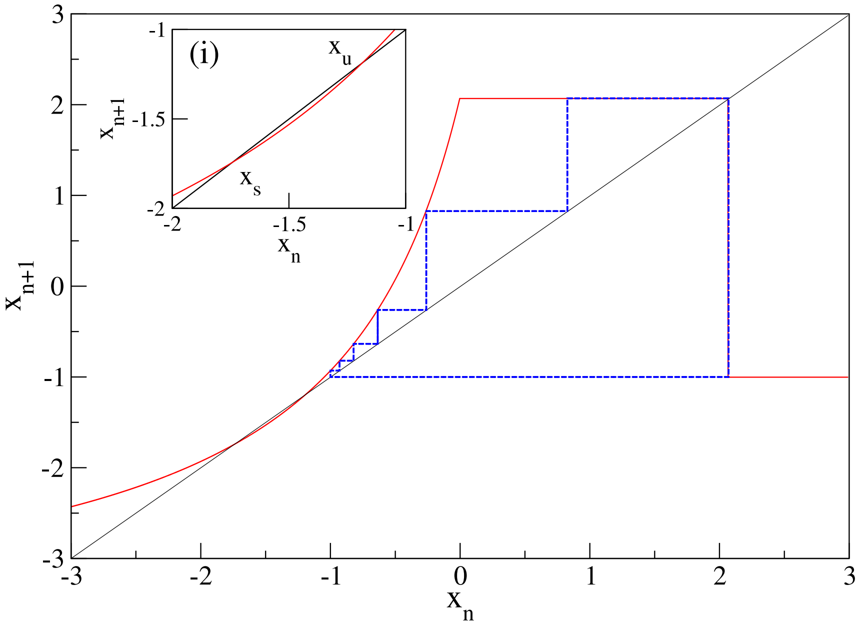

Figure 2.5: Plot of the discontinuous function $f(x, y)$, vs x given by Eq. (2.6), vs x for a constant value of $y = -3.93$ and $\alpha = 6.0$. Here the black line is the diagonal line $y = x$. Inset (i) shows the two intersections of the function $y = f(x, y)$ with the line $y = x$ resulting two fixed points: x_s which is stable and x_u which is unstable. Here the blue line shows the co- existence of a limit cycle along with the two fixed points corresponding to spiking oscillations in Eq. (2.5a).

where, α is the control parameter of the map. A representative of the function $f(x, y)$ is shown in the Fig. 2.5, where the co-existence of two fixed points along with a limit cycle which corresponds to spiking oscillation can be seen. It is clear from the Eq. (2.6) that the function $f(x, y)$ can move up or down when there is an increase or decrease in the value of the variable y, except in the interval $x \geq \alpha + y$.

Now consider a single model neuron whose dynamics is given as,

$$x_{n+1} = f(x_n, y_n), \tag{2.7a}$$

$$y_{n+1} = y_n - \mu(1 + x_n) + \mu\sigma. \tag{2.7b}$$

with the inputs $\beta_n = \beta$ and $\sigma_n = \sigma$ taken to be constants, and a change of variable $y_n + \beta \to y_n$ in Eq. (2.5). Clearly, the individual dynamics of the map now depends on two parameter α and σ. Typical time series of the map are shown in the Fig. 2.6 for various values of α and σ showing silence, tonic spiking and spiking-bursting behavior.

The dynamical behavior of a single unit, given by Eq. (2.7), can be analyzed by treating the fast and slow variable separately. The slow variable y does not change for $x = x^*$ where,

$$x^* = -1 + \sigma \tag{2.8}$$

Since, $y_{n+1} = y_n - \mu(x_n - x^*)$, the value of variable y increase when $x_n < x^*$ and decreases when $x_n > x^*$. For this fixed point x^* where $x^* \leq 0$, the Eq. (2.7a) can be written as,

$$y = x^* - \frac{\alpha}{1 - x^*} \tag{2.9}$$

This equation defines the branches of slow dynamics in the phase space (x_n, y_n). Solving for x^* and treating α and y as a bifurcation parameter we have,

$$x^* = \frac{(1 + y) \pm \sqrt{(1 + y)^2 - 4(\alpha + y)}}{2} \tag{2.10}$$

Thus, for a single value of y we have two values of x^*, meaning two fixed points. These two values of x^* merge when,

$$(1 + y)^2 = 4(\alpha + y) \Rightarrow (1 - y)^2 = 4\alpha \Rightarrow y = 1 - 2\sqrt{\alpha}$$

The stability of x^* can be gauged from the Jacobian of the map,

$$x_{n+1} = y + \frac{\alpha}{1 - x_n}$$

For stable fixed point x_s^* the Jacobian must be less than one, i.e.,

$$J = \left|\frac{\partial x_{n+1}}{\partial x_n}\right|_{x^*} < 1$$

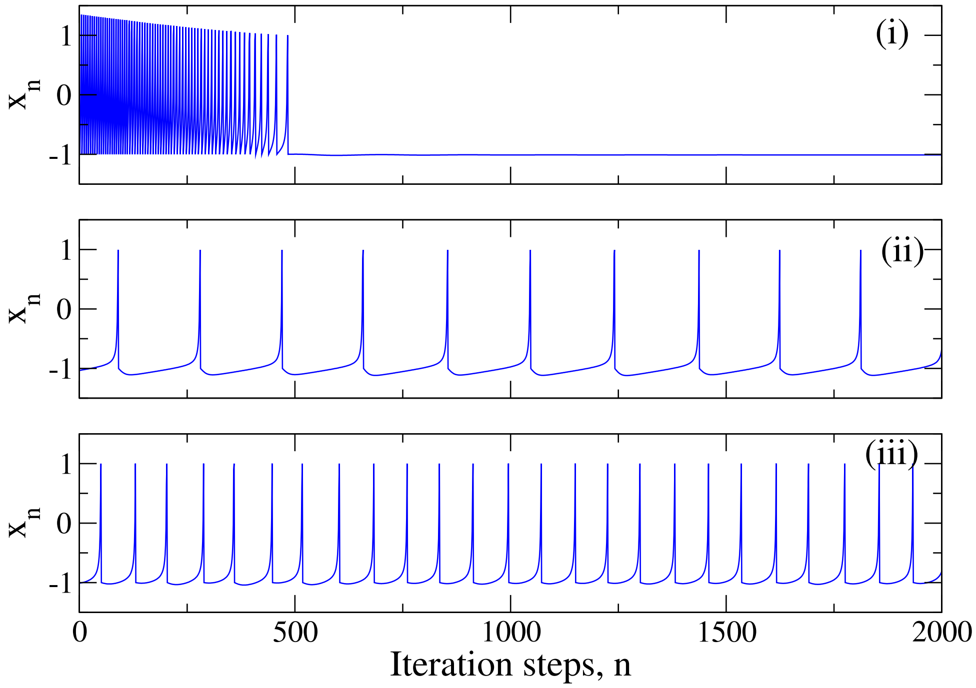

(a) Spiking behaviour

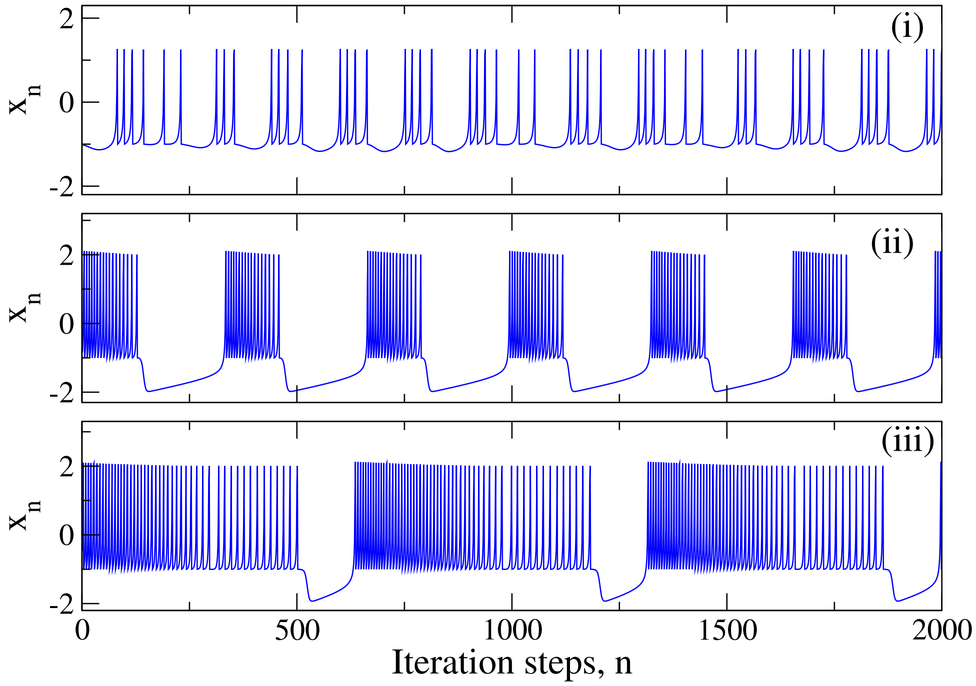

(b) Spiking-bursting behavior

Figure 2.6: Time series of Rulkov map given by Eq. (2.7). In panel (a) the parameter value σ is (i) -0.01, (ii) 0.01, (iii) 0.1 and $\alpha = 4$. In panel (b), the parameter values are: (i) $\alpha = 4.5\,\sigma = 0.14$, (ii) $\alpha = 6\,\sigma = -0.1$, (iii) $\alpha = 6\,\sigma = 0.38$. The value of the parameter $\mu = 0.001$ in both.

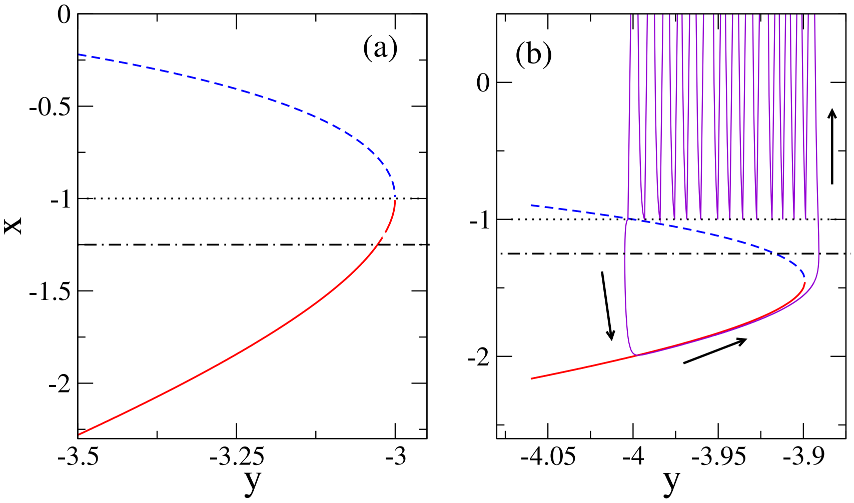

Figure 2.7: The stable (shown in red) and unstable (shown in blue) branches of the slow dynamics of Eq. (2.7) are shown in the plane of phase variables (y, x). Here the value of parameter α is 4 and 6 for (a) and (b) respectively and the value of parameter σ is 0.25. The dashed horizontal black line is for slow nullcline $x^* = -1 + \sigma$ and the dotted horizontal black line shows the reset voltage level $x = -1$. Notice the intersection of the line $x = -1$ and unstable branch in (b). The black arrows shown in (b) gives the direction of slow evolution. The homoclinic orbit which corresponds spiking-bursting behavior is also superimposed in (b).

which gives,

$$1 > \frac{\alpha}{(1 - x^*)^2} \Rightarrow x^* < 1 - \sqrt{\alpha}$$

Thus, when $x^* < 1 - \sqrt{\alpha}$ the stable branch exists but when $1 - \sqrt{\alpha} \geq x^* \geq 0$ the unstable branch exists. These branches which are given by Eq. (2.10) are shown in the Fig. 2.7. The oscillation in the map will appear when σ crosses the threshold value σ_{th}, which is given by (using Eq. (2.8)),

$$\sigma_{th} = 2 - \sqrt{\alpha} \tag{2.11}$$

The curve of σ_{th} can also be obtained by considering the dynamics of the map given by Eq. (2.7) in the regime where $x \leq 0$. In this case the map is given by following two equations,

$$\begin{aligned} x_{n+1} &= \alpha/(1 - x_n) + y_n, \\ y_{n+1} &= y_n - \mu(x_n + 1 - \sigma) \end{aligned}$$

The Jacobian matrix J for this case is,

$$J = \begin{pmatrix} \frac{\alpha}{(1-x^*)^2} & 1 \\ -\mu & 1 \end{pmatrix}$$

For the fixed point $x^* = -1 + \sigma$, the determinant of the Jacobian becomes,

$$\det(J) = \frac{\alpha}{(2-\sigma)^2} + \mu$$

The critical value for the occurrence of Subcritical Andronov Hopf Neimark Sacker bifurcation is given by $\det(J) = 1$ which leads to the following equation,

$$\alpha = (2-\sigma)^2(1-\mu). \tag{2.12}$$

which reduces to (2.11) for $\mu = 0$.

Clearly, a *homoclinic orbit*, which is defined as a trajectory of a flow of a dynamical system which joins a saddle equilibrium point to itself, originating from the unstable fixed point, can only occur when $\alpha > 4$. This fast map bifurcation, associated with the occurrence of a homoclinic orbit, happens when the co-ordinate of the unstable fixed point is -1 (for a representative see Fig. 2.7(b)). Here, the unstable branch crosses the line $x = -1$. When the map is spiking and the value of y gets to the bifurcation point, the limit cycle merges into the homoclinic orbit, disappears, and then trajectory of the map jumps to the stable branch and the whole process repeats itself. This process leads to spiking-bursting behavior in the map.

Thus, we see that this simple phenomenological model captures the complex dynamics of spiking-bursting behavior of neurons. The shape of the function $f(x, y)$ defined by Eq. (2.6) is chosen due to following reasons. The fast map is able to generate limit cycles whose wave forms mimic those of the spikes. There is only one iteration in the rightmost interval $x \geq \alpha + y$, whose appearance in the trajectory can be used to define the time of a spike. This feature is important for modeling the dynamics of chemical synapses in a group of coupled neurons. The analytic expression of the nonlinear function in the interval $x < 0$ is simple and allows a rigorous analysis of bifurcations of fixed points of the fast map. Use of the fixed level, -1, in the rightmost interval of the function simplifies the analysis of dynamics at the end of the bursts. The end of a burst is associated with the formation of a homoclinic orbit that corresponds to the case when the trajectory from this interval maps into the unstable fixed point.

However, some modification in the fast map is required to enhance the region of parameters where the model can still be used to mimic neural dynamics properties. The trajectory of the fast system is found to stay in the middle interval of the function $f(x, y)$ for several iterations thus leading to increase in duration of a spike. Introduction of one additional condition to the fast map removes this problem. The modified function $f(x_n, y)$ is written as,

$$f(x_n, y) = \begin{cases} \alpha/(1 - x_n) + y, & \text{for} \quad x_n \leq 0, \\ \alpha + y, & \text{for} \quad 0 < x_n < \alpha + y \text{ and } x_{n-1} \leq 0 \\ -1, & \text{for} \quad x_n \geq \alpha + y, \text{ or } x_{n-1} > 0 \end{cases} \tag{2.13}$$

Clearly, the low dimensionality of this model helps one understand the dynamical mechanisms behind the spiking and spiking-bursting behavior using simple phase plane analysis.

2.2 Modeling Oscillations in Chemical Reactions

Oscillations in a chemical reaction is a non-equilibrium phenomena. It manifests itself as a periodic change in a characteristic color corresponding to a chemical reactant in the system. The observation and characterization of this phenomena leads to the systematic study of oscillating chemical reactions and of the broader field of nonlinear chemical dynamics. Here we will start with a brief history of this fascinating subject and then go on to describe the prototypical *Brusselator* model.

In 1828, Fechner described an electrochemical cell that produced an oscillating current, which is the first published report of oscillations in a chemical system [89]. Similarly, Ostwald observed in 1899 that the rate of chromium dissolution in acid periodically increased and decreased [90]. As both the systems were inhomogeneous, it was believed that homogeneous oscillating reactions were impossible. However, the first homogeneous chemical oscillation was observed by William C. Bray in 1921 [91, 92] in a reaction among iodate, iodine and hydrogen peroxide. Here the concentrations of oxygen and iodine showed approximate periodicity during the reaction.

The study of the dynamics and chemistry of oscillating reactions can be traced to *Boris Pavlovich Belousov* (1893-1970), who was looking for an inorganic analog of the Krebs cycle, a key metabolic process in which citric acid is an intermediate. He found that a certain mixture of chemicals containing citric acid and bromate shows periodic changes in the concentrations of species [93]. Another Soviet physical chemist, *Anatoly Zhabotinsky*, noticed the work and modified the reaction by changing some reactants and made the appearance of the phenomena more dramatic by achieving bright, easy to observe colors. This reaction known as *Belousov-Zhabotinsky* (B-Z) reaction occupies a central place in the area of nonlinear chemical phenomena and pattern formation. (For more on the history see Ref. [94] and for complete bibliography along with article reviews on B-Z reaction see Ref. [95]).

These oscillating chemical reactions were dismissed by most chemist earlier as they thought that these are non reproducible phenomena or are the artifacts due to impurities. Also, according to Second Law of Thermodynamics, at constant temperature and pressure in a closed system, the Gibbs free energy, G, of a reacting mixture must continually decrease as the reaction approaches equilibrium [96] (p. 98). Thus, an oscillating reaction would seem to violate the Second Law. The skeptics objected to the notion of oscillating reactions and mistakenly, considered an oscillating reaction to be analogous to a pendulum, which passes through its equilibrium point during each cycle of oscillation.

They concluded that an oscillating reaction would require the free energy of the system to oscillate as the reactants were converted to products and then back to reactants, thus contradicting the Second Law of Thermodynamics.

The thermodynamical explanation of these oscillating reactions comes from the Belgian chemist *Ilya Prigogine* (1917-2004). Since reaction in a closed system cannot oscillate about their equilibrium state because such behavior is prohibited by the most fundamental principle of microscopic reversibility. However, according to Prigogine, periodic oscillations in the concentration of intermediate species in a chemical reaction can occur, if a system is far from equilibrium. Also, for an open systems, i.e., systems open to exchange of matter and/or energy with their surroundings, kept far from equilibrium, could exhibit spontaneous self-organization by dissipating energy to the surroundings to compensate for the entropy decrease in the system [97].

A closed system must reach equilibrium and so can exhibit only transitory oscillations as it approaches equilibrium. Sustained oscillations require an open system with a constant influx of new reagents and the removal of waste products. It was found that in the BZ reaction in a beaker the concentrations of reactants (bromate and malonic acid) and products (carbon dioxide and bromomalonic acid) do not oscillate but he concentrations of intermediates such as bromide and bromous acid oscillate. For a complete review on this topic see Ref. [98].

The B-Z reaction has been thoroughly studied from both chemical and mathematical perspectives. It has also inspired new areas of study in which similar chemical systems are studied, which are later used in the prediction of the behavior of their complex reaction mechanisms. There are now a large number of both ‘real’ and ‘toy’ systems that provide insight into the complex behavior of oscillating chemical systems, for example, Lotka-Volterra model [99, 100, 101], Oregonator model [102] etc. We will now describe the Brusselator model, which is a toy model system and describe the system’s dynamics in the phase plane.

2.2.1 Brusselator

It is a mathematical model which captures the dynamics of a chemical reaction. This model proposed by Prigogine and Lefever in 1968 [103] and dubbed the “Brusselator" by Tyson in 1973 [104]. It is an example of an *autocatalytic*, oscillating chemical reaction. An autocatalytic reaction is a chemical reaction in which at least one of the reactants is also a product. Here the rate equations for the reaction are nonlinear which can lead to the spontaneous generation of order. This spontaneous order creation seems to contradict the Second Law of Thermodynamics but the contradiction is resolved when the disorder of both the system and its surroundings are taken into account. In many autocatlytic systems complex dynamics are seen, including multiple steady-states and periodic orbits.

The Brusselator describes the simplest chemical reaction of the transformation of the initial substances called substrates A and B into products C and D,

$$A + B \longrightarrow C + D$$

as a reaction consisting of the following stages:

$$\begin{aligned} A &\xrightarrow{k_1} X \\ 2X + Y &\xrightarrow{k_2} 3X \\ B + X &\xrightarrow{k_3} Y + C \\ X &\xrightarrow{k_4} D \end{aligned}$$

The two species of interest to us are X and Y, the autocatalytic species. The differential equations given in dimensionless form for these species are:

$$\dot{x} = f_1(x, y) = a - (b + 1)x + x^2 y, \tag{2.14a}$$

$$\dot{y} = f_2(x, y) = bx - x^2 y. \tag{2.14b}$$

These equation depends only on the two parameters a and b, where, a is the rate by which x is produced from outside and b is the rate at which y is produced from x. The only nonlinear term is x^2y which gives the rate of x production from both x and y.

Steady states: The steady state of the system (x_f, y_f) can be calculated by the following two equations for which, $\dot{x} = \dot{y} = 0$,

$$a - (b+1)x_f + x_f^2 y_f = 0$$

$$bx_f - x_f^2 y_f = 0$$

The above two equations are simultaneously satisfied by the points $(x_f, y_f) = (a, \frac{b}{a})$, which are the only equilibrium of the system. The Jacobian of the system is given as,

$$J(x,y) = \begin{pmatrix} 2xy - (b+1) & x^2 \\ b - 2xy & -x^2 \end{pmatrix}$$

which for the fixed point $(x_f, y_f) = (a, \frac{b}{a})$ reduces to,

$$J(x_f, y_f) = \begin{pmatrix} b-1 & a^2 \\ -b & -a^2 \end{pmatrix}$$

To analyze the stability of the above system we compute the trace (τ) and determinant (Δ) of the Jacobian matrix, J, which are,

$$\begin{aligned} \tau &= b - a^2 - 1 \\ \Delta &= a^2 \end{aligned}$$

Since, $a > 0$ the determinant, $\Delta > 0$ which implies the fixed point, $(a, \frac{b}{a})$ is not a saddle point. If $b < a^2 + 1$ then $\tau < 0$, and the fixed point is an attractor. But if $b > a^2 + 1$, then

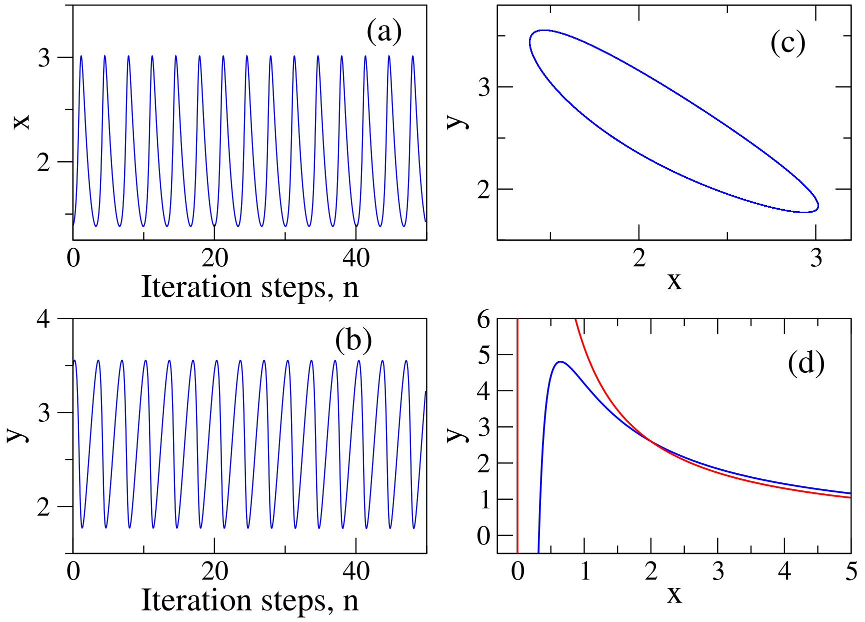

Figure 2.8: Plot showing the time-series of x-variable in (a), y-variable in (b), phase-space of both variables in (c) and the nullclines in (d) of the Brusselator system. In (d), the blue curve is for Eq. (2.17) and the red curve is for Eq. (2.16). The parameter values are $a = 2$ and $b = 5.2$.

$\tau > 0$ and the fixed point is a repellor. The eigenvalues of the Jacobian matrix, J will be,

$$\lambda_{1,2} = \frac{-\tau \pm \sqrt{\tau^2 - 4\Delta}}{2} = \frac{-(b - a^2 - 1) \pm \sqrt{(b - a^2 - 1)^2 - 4a^2}}{2} \tag{2.15}$$

Nullclines: The $\dot{x}$ nullcline is computed by putting, $\dot{x} = 0$, which gives,

$$y = \frac{b+1}{x} - \frac{a}{x^2} \tag{2.16}$$

Similarly, the $\dot{y}$ nullcline is computed by putting, $\dot{y} = 0$, which gives,

$$x = \frac{b}{y} \qquad \& \qquad x = 0 \tag{2.17}$$

For the parameter values $a = 2$ and $b = 5.2$, the nullclines are shown in the Fig. 2.8(d).

Bifurcation analysis: There is no other fixed point apart from the fixed point $(a, b/a)$ in this system. Thus it is reasonable to guess that there will be Hopf bifurcation in this system if the value of the parameters a and b changes. Hopf bifurcation is a local bifurcation in which a fixed point of a dynamical system loses stability, as a pair of complex conjugate eigenvalues of the linearized Jacobian matrix around the fixed point, cross the imaginary axis of the complex plane. Under reasonably generic assumptions about the dynamical system, we can expect to see a small-amplitude limit cycle branching from the fixed point. *Hopf bifurcation theorem* can be stated as follows. For a system given by,

$$\dot{x} = f_\mu(x, y),$$
$$\dot{y} = g_\mu(x, y),$$

where μ is a parameter and the point $(x, y) = (x_o, y_o)$ is the fixed point of the system which can depend on the value of μ. Let the eigenvalues of the linearized system, J, about this fixed point be given by $\lambda(\mu)$ where $\lambda_\pm(\mu) = \alpha(\mu) \pm i\beta(\mu)$. Suppose further that for a certain value of μ, say $\mu = \mu_o$, the following conditions are satisfied,

$$\tau = 0 \text{ and } \Delta > 0,$$
$$\frac{d}{d\mu}\Re(\lambda_+(\mu))\bigg|_{\mu=\mu_o} \neq 0,$$

where, τ and Δ are trace and determinant of J respectively and $\Re(z)$ denote the real part of z. Then a unique curve of periodic solutions bifurcates from point $(x_o(\mu_o), y_o(\mu_o))$. The amplitude of the periodic orbits grows like $\sqrt{\mu - \mu_o}$ and the periods tend to $2\pi/\beta$. The bifurcation is called supercritical if the bifurcating periodic solutions are stable, and subcritical if they are unstable [30].

To do the bifurcation analysis of the above system we fix the value of a and vary b. In our case, $\tau = 0$ for $b = a^2 + 1$ for this value of b, $\Delta = a^2 > 0$. Now $\Re(\lambda_+)$ is $-\tau/2 = (-b + a^2 + 1)/2$ thus,

$$\frac{d}{db}\left(\frac{-b + a^2 + 1}{2}\right)\bigg|_{b=a^2+1} = -\frac{1}{2} \neq 0$$

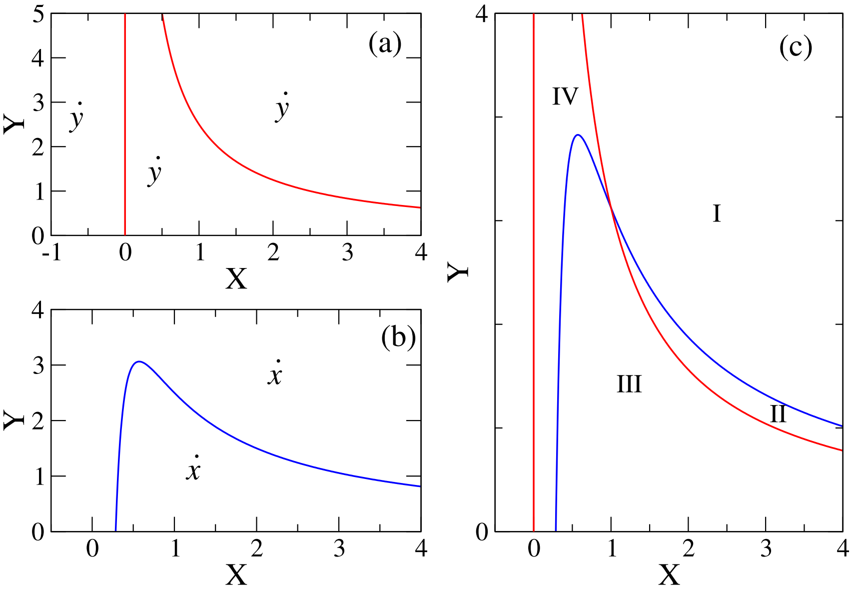

Figure 2.9: Plot showing the nullclines of the Brusselator system. In (a) $\dot{y} = 0$ nullcline defined by Eq. (2.17) and in (b) $\dot{x} = 0$ nullcline defined by Eq. (2.16) is shown. In (c) the intersections of both the nullclines are shown which divide the positive quadrant into four quadrants. Here the parameter values are $a = 1$ and $b = 2.5$.

Hence, in our case Hopf Bifurcation occurs when $b > a^2 + 1$.

Trapping region: From the above bifurcation analysis it is clear that for $b > a^2 + 1$ the fixed point is a repellor and there exist a periodic orbit. We will now construct a trapping region inside which a closed orbit exists according to **Poincaré-Bendixson Theorem**.

The theorem states that for a continuously differentiable vector field $\dot{\mathbf{x}} = f(\mathbf{x})$ on an open set containing **R**, which is a closed, bounded subset of the plane and does not contain any fixed point, there exists a trajectory which starts in **R** and stays in **R** for all future time. This mean that either the trajectory is a closed orbit or it spirals towards the closed orbit as $t \to \infty$ [30].

Now let us consider our system defined by Eq. (2.14). For simplicity, we fixed the value of the parameters $a = 1$ and $b = 2.5$. The nullclines of the system are shown in the Fig. 2.9. First we consider, Fig. 2.9(a), where the $\dot{y} = 0$- nullclines are shown. Clearly, the field $\dot{y} < 0$ for the region left to the $\dot{y}$ nullcline $x = 0$ (in the region $x < 0$) and $\dot{y} < 0$ for the region right of it. Now we consider the other $\dot{y} = 0$ nullcline which is $y = b/x$. We

Region	$\dot{x}$	$\dot{y}$
I	+ve	-ve
II	-ve	-ve
III	-ve	+ve
IV	+ve	+ve

Table 2.1: Table showing the sign of the vector fields in the region defined in Fig. 2.9(c).

take two points $(a, \frac{b}{a} \pm \epsilon)$ where ϵ is very small. Clearly, the location of these two points are above and below the nullcline $y = b/x$. The value of $\dot{y} = x(b - x)$ for point $(a, \frac{b}{a} + \epsilon)$ is,

$$\dot{y} = a\left[b - \left(\frac{b}{a} + \epsilon\right)a\right] = -\epsilon a^2 < 0$$

Thus, the field $\dot{y}$ for the points whose location is above the nullcline is $\dot{y} < 0$ and similarly, $\dot{y} > 0$ for the points which are below the nullcline as shown in the Fig. 2.9(a).

Similarly, the direction of the field $\dot{x}$ can be determined by considering the points $(a \pm \epsilon), b/a$ which are inside and outside the nullcline defined in the Eq. (2.16). For the point $(a + \epsilon, b/a)$, field $\dot{x}$ becomes,

$$\dot{x} = a - (b + 1)(a + \epsilon) + (a + \epsilon)^2 \frac{b}{a} = \epsilon^2 \frac{b}{a} + \epsilon(b - 1) > 0$$

Thus, $\dot{x} > 0$ for the points above the $\dot{x} = 0$ curve and $\dot{x} < 0$ for the points below the curve as shown in the Fig. 2.9(b). The first quadrant separates into four regions by the intersection of x and y nullclines as shown in the Fig. 2.9(c). In all the regions the direction of the vector fields $(\dot{\mathbf{x}}, \dot{\mathbf{y}})$ are different. The sign of the vector fields $\dot{\mathbf{x}}$ and $\dot{\mathbf{y}}$ are tabulated in Table 2.1. Now, we will construct the trapping region as follows. The $\dot{x}$ nullcline intersect the x axis at,

$$0 = a - (b + 1)x + x^2(0) \implies x = \frac{a}{b + 1}$$

also the line $x = a/(b + 1)$ intersect the $\dot{y}$ nullcline $0 = x(b - xy)$ at

$$y = \frac{b(b + 1)}{a}$$

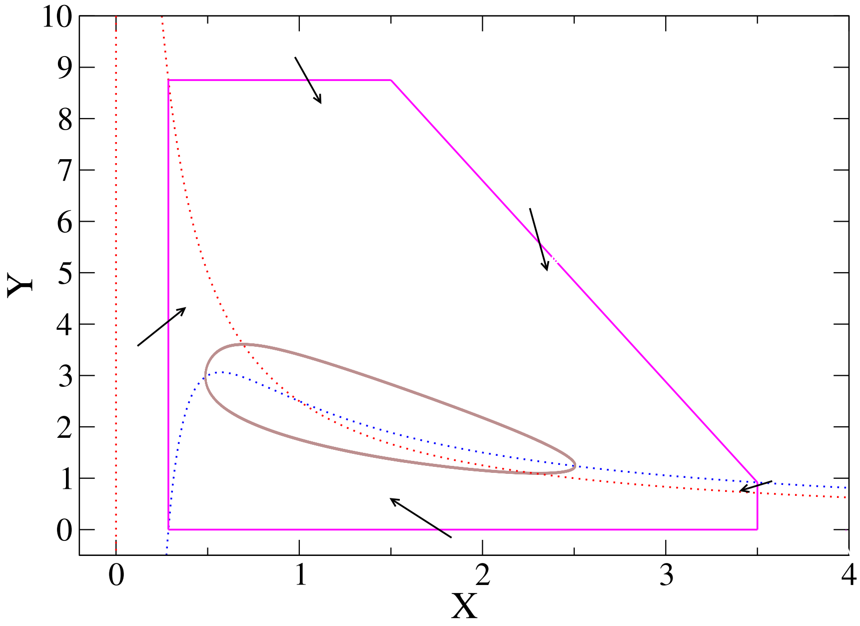

Figure 2.10: Plot the trapping region of the Brusselator system, for the parameter values $a = 1$ and $b = 2.5$, along with some representative vectors showing the direction of the flow. The limit cycle for the system is shown by brown color. The $\dot{x} = 0$ nullcline is shown by blue and $\dot{y} = 0$ is shown by color red.

We join the point $(a/(b+1), 0)$ and $(a/(b+1), b(b+1)/a)$ by line. This will be our left boundary box. Now we move along the line $y = b(b+1)/a$ to a point whose x co-ordinate is l. Now we have to find a line starting from this point and descend down to the x axis, so that its slope is greater than the slope of the vector field $\dot{\mathbf{x}}$ and $\dot{\mathbf{y}}$. Now, the vector field has slope, m, given by,

$$m = \frac{\dot{y}}{\dot{x}} = \frac{bx - x^2y}{a - (b+1)x + x^2y}$$

which can be simplified to,

$$m = -\frac{bx - x^2y}{(bx - x^2y) - (a - x)} < -\frac{bx - x^2y}{bx - x^2y} = -1 \text{ for } x > a$$

Thus, when the line $y = b(b+1)/a$ crosses $x = a$, any line whose slope is greater than -1, can be used as right boundary. The lower boundary of the bounding box will be $y = 0$. A line $x = r$ connects $y = 0$ to $\dot{x} = 0$ nullcline. This will be the trapping region for our system. A trapping region for the representative value of parameters $a = 1$ and $b = 2.5$ is shown in the Fig. 2.10.

The direction of the flow is determined using table 2.1. For region I, $\dot{x} > 0$ and $\dot{y} < 0$ which mean the arrow should point down and to the right. For region II, both $\dot{x}$ and $\dot{y}$ are negative, so the arrow should point down but to the left. Similarly, since in region III, $\dot{x} < 0$ and $\dot{y} > 0$, the arrow should point up and to the left and lastly in region IV, where both $\dot{x}$ and $\dot{x}$ are positive, the arrow should point up and to the right, as shown in the Fig. 2.10.

Now, since we have constructed a trapping region and there are no fixed points apart from the fixed point at the intersection of the nullclines which is a repeller, it is proved from **Poincaré-Bendixson Theorem** that there exists a closed orbit as shown in Fig. 2.10.

In summary, in this Chapter we have discussed models capturing the essential phenomena of neuronal dynamics and chemical oscillations. In the subsequent chapters, we will use these low-dimensional models as the nodal dynamics in our networks and lattices.

Chapter 3

Implications of the imbalance of positive and negative links

In this chapter we will discuss the effect of positive and negative links on spatiotemporal regularity on a network of neurons. As we have discussed in Chapter 1 that the properties and the dynamics of naturally occurring networks are best described by weighted network and few existing studies of weighted random dynamical networks, consider the weights of the connectivity matrix to be drawn from a zero mean gaussian/uniform distribution [5, 105, 54, 55]. So, the interesting scenario of *distributions skewed towards positive or negative weights* has not been adequately addressed. Nor has the dynamical significance of the imbalance of positive-negative links been sufficiently studied. The focus of this chapter here is to address this unexplored problem.

In particular, here we consider *random weighted networks of chaotic maps*, with the nodal dynamics modeling neuronal activity. Namely, we have a network where the dynamical evolution of the state of the nodes is governed by a local nonlinear map modeling neuronal spiking, as well as a local field arising from the interactive web of positive/negative feedbacks from other neurons. We study the most general scenario where the weights of the links of the random network are drawn from distributions with zero, as well as non-zero, mean. This helps us to investigate the effect of the balance/predominance of the positive-negative links, on the time-evolution of the dynamical states of the nodes, as well as on the global characteristics of the evolved network.

The primary questions we focus in this Chapter are:

(i) What are the dynamical consequences of connection weight distributions skewed towards inhibitory or excitatory links? Specifically, is the balance of positive and negative feedback loops conducive to regularity, or is it detrimental?

The motivation for this question arises from a hypothesis to explain the origin of the irregular spiking observed in the cortex, which is a long standing problem in neurobiology [106]. The idea is as follows: in cortical anatomy each neuron has a huge number of synapses [107]. By central limit theorem, these uncorrelated synaptic inputs sum up to a regular total input signal with only small relative fluctuations, thus precluding irregular dynamics. An explanation of the observed irregularity comes from the idea that the excitatory (positive) and inhibitory (negative) inputs to each neuron are balanced and only the fluctuations lead to spikes. Studies on sparse random networks of simple binary model neurons showed that irregularity arose from approximate balance of excitatory and inhibitory inputs [108, 109].

Here we consider a more realistic model of neurons, having a real continuous membrane potential coupled to a recovery current variable. We inspect the validity of the balanced hypothesis for such a model, for different interaction scenarios. We do not confine our investigation to sparse connectivity. Instead we scan the full connectivity space, ranging from dilute connections to global connections, under varying coupling strengths. Further we investigate the effects of system size on regularity, as well as the effects of the variance of connection strengths.

(ii) The second significant question we address is the following: what properties of the connectivity matrix crucially influence the spatiotemporal dynamics? For instance, does size matter?

This is interesting vis-a-vis the May-Wigner condition which gives that stability is inversely proportional to connection strengths, connectivity and size in a random network [105].

In this chapter, we investigate the above issues through extensive numerical simulations, and also provide analysis of the central observations.

3.1 Model

We consider a network of N dynamical elements, with a 2-dimensional map modeling the dynamics of neurons at each node. These neurons interact with each other through a connectivity matrix $\mathbf{J}$. Such a network mimics aspects of the dynamics and architecture of local neuronal populations in the brain.

Here we consider the most general scenario where the matrix of connection strengths $\mathbf{J}$ is asymmetric, random weighted and with different degrees of sparseness, ranging from dilute links to globally coupled scenarios [110, 111]. The entries of the connectivity matrix govern both the *strength* and the *type* of interaction (namely, excitatory vis-a-vis inhibitory) between pairs of neurons. So, the evolution of the state at the nodes in the network is governed by a nonlinear function of the local internal states, as well as an interactive component similar to generalized global coupling. We describe the intrinsic and interactive components of the dynamics in more detail below.

Nodal Dynamics : the dynamics at each node i ($i = 1, \cdots, N$) is described by two continuous state variables $x_n(i)$ and $y_n(i)$ which capture the fast and slow dynamics respectively of the ith model neuron at the time n. The dynamics of a single neuron is mimicked by a two-dimensional map and given by Eq. (2.1) which has already been discussed in Chapter 2. Here the parameters of the map are $a = 0.89$, $b = 0.18$, $c = 0.28$ and $k = 0.03$ for which the map shows chaotic behavior [87].

Interactions : In our model the interaction is given by a coupling matrix $\mathbf{J} = \{J_{\mathrm{ij}}\}$, where J_{ij} determines the coupling between a pair of nodes i and j. It is a sparse $N \times N$ matrix, with density of non-zero links given by connectivity C, i.e. with probability $1 - C$ an element J_{ij} is zero. So, C controls the degree of connectivity in the system, and the effective or average degree is CN. Note that the "self-interaction" terms are zero here, namely the diagonal entries $J_{ij} = 0$, indicating that individual neurons do not contribute to the local interaction field.

The non-zero J_{ij} follow a normal distribution with mean, $\overline{J}$ and variance, σ^2. The magnitude of J_{ij} determines how strongly the nodes are coupled, and the sign determines whether the interactions are inhibitory/excitatory. Positive weights imply strengthening interactions, while negative weights inhibit activity.

The overall evolution of the system is governed by the following set of equations:

$$x_{n+1}(i) = f_1[x_n(i), y_n(i)] + \frac{1}{N}\sum_{j=1}^{N} J_{ij} x_n(j) \tag{3.1a}$$

$$y_{n+1}(i) = f_2[x_n(i), y_n(i)] \tag{3.1b}$$

where, $f_1(x_n, y_n)$ and $f_2(x_n, y_n)$ are given by Eq. (2.1). Clearly, the interactive component of dynamics of the membrane potential of each neuron is influenced by a local field comprised of the weighted sum of the activity of the other neurons. The mean $\overline{J}$ determines the balance of negative and positive interactions, and σ determines the fluctuation in the interaction strengths.

Note that a network with strongly chaotic dynamics at the nodes, is naturally spatiotemporally chaotic in the limit of coupling connections going to zero (namely the uncoupled state comprised of a collection of uncorrelated chaotic dynamics). In such a system coupling plays the regularizing role and is the sole source of synchronicity in the system. So all changes in the spatiotemporal behavior arises from changes in the density of links and the distribution of connection weights.

3.2 Results

First, we simulate the dynamics of this network, and qualitatively investigate its behavior over a wide range of size (i.e. number of nodes, N), connectivity C (i.e. the density of links), and distributions of connection weights (characterized by different mean and variance σ^2). In all our simulations, we leave $10,000$ transient steps, for each run starting from random initial conditions drawn from the interval $[0:1]$.

Further we quantify the degree of synchronization in the network by computing an average error function defined as the mean square deviation of the instantaneous states of the nodes:

$$Z(n) = \frac{1}{N}\sum_{i=1}^{N}\{[x_n(i) - \langle x_n\rangle]^2 + [y_n(i) - \langle y_n\rangle]^2\} \tag{3.2}$$

where, $\langle x_n\rangle = \frac{1}{N}\sum_{i=1}^{N} x_n(i)$ and $\langle y_n\rangle = \frac{1}{N}\sum_{i=1}^{N} y_n(i)$ at time n. This quantity averaged over time n and over different realizations is denoted as $\langle Z\rangle$. When $\langle Z\rangle = 0$, we have complete synchronization. As $\langle Z\rangle$ becomes larger, the degree of synchronization gets lower. The average in the results reported here is typically over 500 time steps, and over 10 different initial network conditions.

We describe below the dynamical features of the emergent network state, with respect to the key coupling parameters, as evident qualitatively through bifurcation diagrams, and quantitatively through the above synchronization measure.

Influence of connectivity C on spatiotemporal regularity:

When connectivity is low, ($C \to 0$), the local chaos is the dominant influence on the overall dynamics, and the fixed point is destabilized in the above system for all $\overline{J}$. Namely, when there are few links per node, all regularity in temporal behavior and spatial synchronization is lost. This is clearly seen from the contrasting temporal and spatial patterns of the Fig. 3.1a, 3.2a, which are for $C = 0.01$ and the other two figures for higher connectivity value in Fig. 3.1, 3.2, which are for $C = 0.5$ and $C = 0.9$. By contrast, when $\overline{J}$ is not close to zero, high connectivity, C, leads the system to a spatiotemporal fixed point (see Fig. 3.3 for representative examples). The qualitative observations from the bifurcation diagrams are corroborated quantitatively through the synchronization error function plotted in Figs. 3.4-3.6. It is clear then, that the nodes have to be coupled to a large number of nodes in the network in order to support a stable steady state. We will later rationalize this through our analysis of the network dynamics.

Influence of mean $\overline{J}$ on spatiotemporal regularity:

As mentioned above, when connectivity C is high, we observe the following: high positive mean (i.e $\overline{J} > 0$), as well as low negative mean (i.e. $\overline{J} < 0$) *stabilizes the fixed point* in the system. This implies that when the links are predominantly positive or predominantly negative the neuronal dynamics goes to a rest state. However when the positive and negative links are well balanced, i.e $\overline{J} \sim 0$ the dynamics becomes irregular across the network and the neurons at the nodes exhibit large irregular spikes in activity. Figs. 3.1,3.3 demonstrates this behavior for a representative set of parameters. Note that the fixed point stabilized for positive $\overline{J}$, x^*_+, is different from that stabilized for negative $\overline{J}$, x^*_-. For largely negative links, one obtains a fixed point close to zero, i.e. the nodes become inactive. For largely positive links, on the other hand, the fixed state is that of some constant activity determined by the value of $\overline{J}$. So, it is evident that a *balance of excitatory and inhibitory interactions is not conducive to a dynamical steady state*. Only when one type of influence dominates the other, stable fixed points are obtained.

Effect of standard deviation, σ:

Figures in Fig. 3.5 display the effect of standard deviation of the connection weights, σ, on the dynamical state of the nodes in the network, for varying mean, $\overline{J}$ of the connection weights. It is observed that for positive mean, $\overline{J} > 0$, increasing the value of σ and number

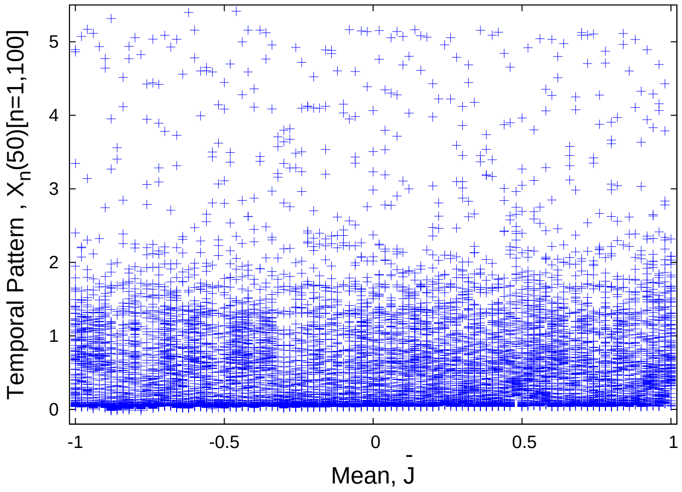

(a) $C = 0.01$

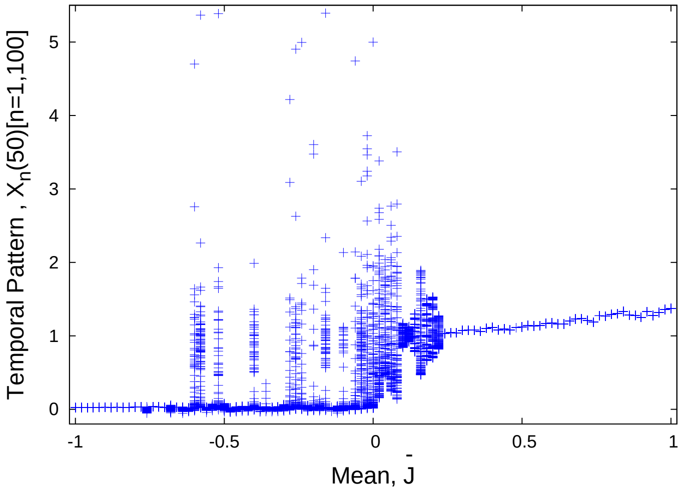

(b) $C = 0.5$

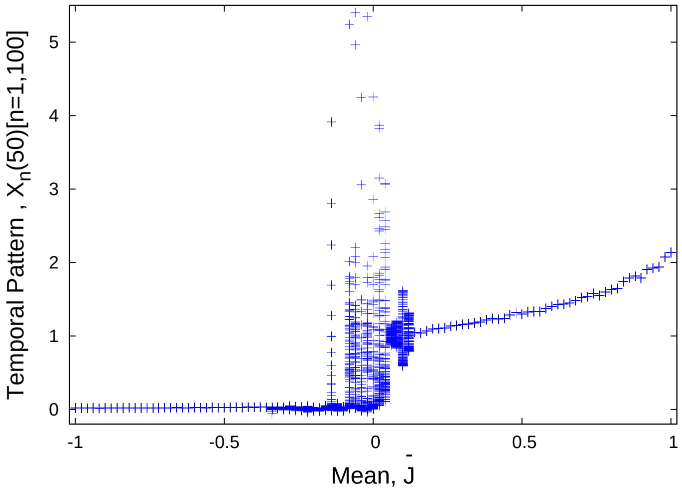

(c) $C = 0.9$

Figure 3.1: Bifurcation diagrams of the temporal pattern in the network with respect to Mean, $\overline{J}$ for various value of connectivity, C. The number of nodes is 100, and the standard deviation, σ is 0.2.

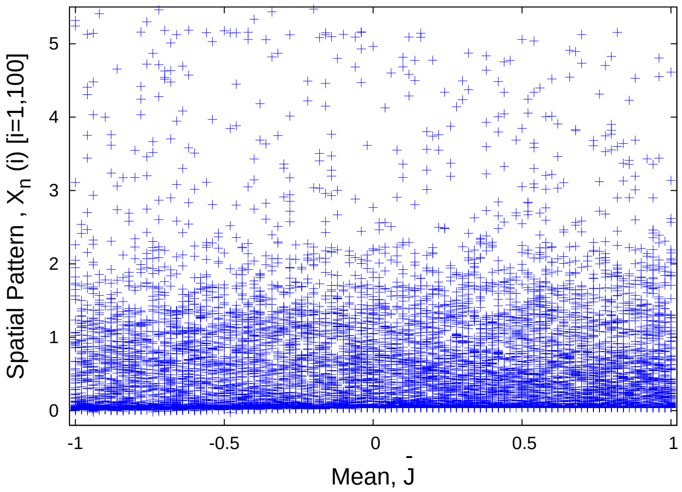

(a) $C = 0.01$

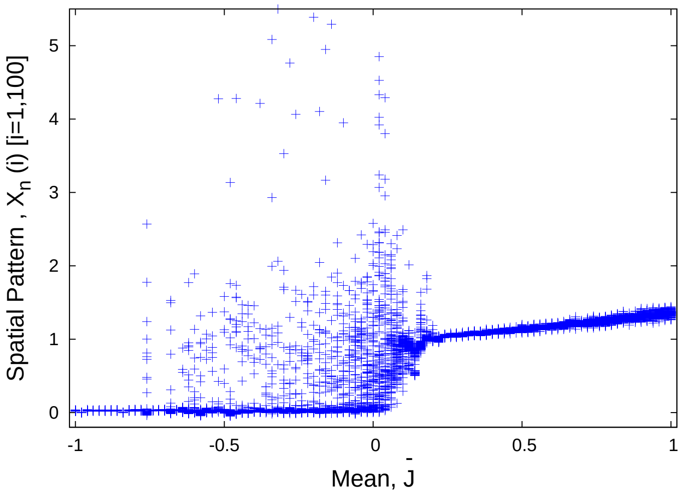

(b) $C = 0.5$

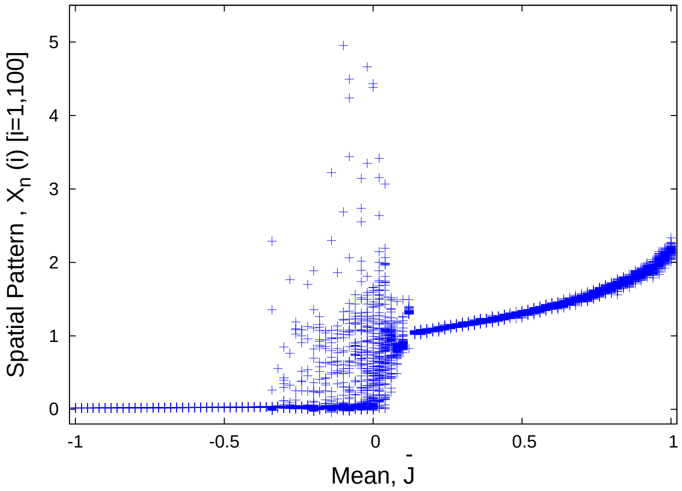

(c) $C = 0.9$

Figure 3.2: Bifurcation diagrams of the spatial pattern of a randomly chosen node in the network with respect to Mean, $\overline{J}$ for various values of connectivity, C. Here, the number of nodes is 100, and the standard deviation σ is 0.2.

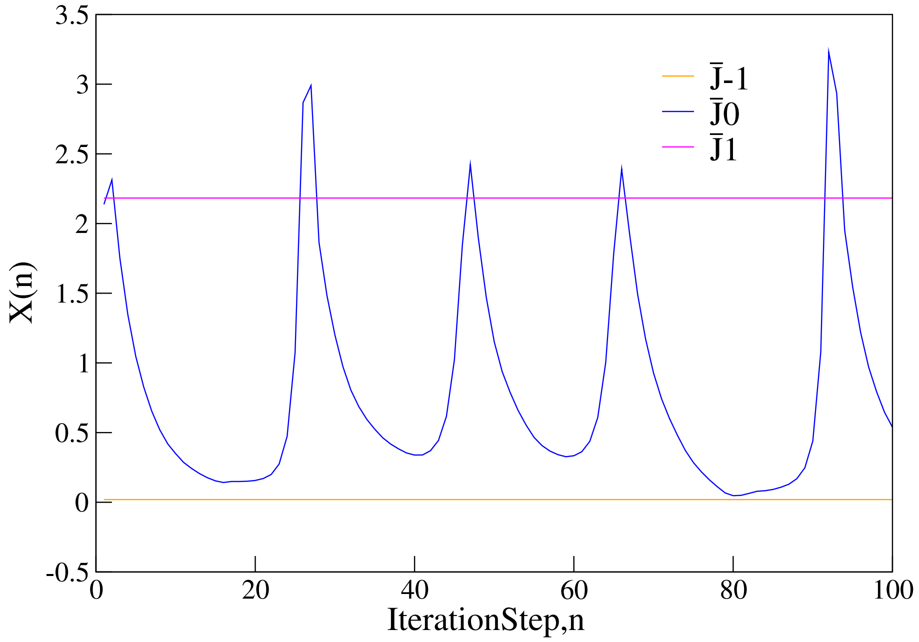

Figure 3.3: Spiking patterns of a representative neuron in a network of size $N = 100$, for mean connection weight $\overline{J} = -1, 0, 1$. Standard deviation, σ, of the connection weights is 0.2. Note the temporal irregularity of the case where the connection weights have zero mean, namely the positive and negative links are balanced.

of nodes N, does not influence spatiotemporal regularity much.

However for low negative mean synchronization depends crucially on both σ and system size N. For example, as shown in Fig. 3.4 a large number of nodes and fairly high connectivity is required for the synchronization of the system for $\overline{J} = -1$. Further when negative links were very predominant, we observed the co-existence of two kinds of dynamics: some initial network states were attracted to the spatiotemporal fixed point close to zero (as seen in Fig. 3.1), while for certain other initial states the nodal dynamics was prone to rapid runaway instability (see Fig. 3.6). This unbounded dynamics is similar to the runaway activity in [112]. This is in contrast to the $\overline{J} \geq 0$ region where the dynamical state displayed in Fig. 3.1 and Fig. 3.3 appeared to be the global attractor of the system.

Effect of System Size:

In the balanced regime where the mean connection weight is close to zero we observe that increasing system size does not affect spatiotemporal dynamics much, especially when connectivity is low. Similar trends occur in the dominantly excitatory region, namely the synchronicity of the dynamics does not depend on network size. This is manifested clearly in Fig. 3.4 and Fig. 3.5, from where it can be seen that for $\overline{J} \geq 0$, the synchronization error does not change with varying network size.

However in the predominantly inhibitory region it is clear that a larger number of nodes in the network, stabilizes the system, and the *runaway unbounded dynamics is strongly suppressed in large networks* in the dominantly inhibitory regime. This is evident through Fig. 3.6 which display the synchronization properties of networks of three different sizes in the $\overline{J} < 0$regime. Further, in general, sparse networks ($C \sim 0$) are much less effected by system size than highly connected ones. This is in concordance with the results in [109].

To check the generality of the above observations we also studied the system,

$$x_{n+1}(i) = f_1[x_n(i) + \frac{1}{N}\sum_{j=1}^{N} J_{ij}x_n(j)], \tag{3.3a}$$

$$y_{n+1}(i) = f_2[x_n(i), y_n(i)]. \tag{3.3b}$$

Qualitatively similar results are obtained here as well. Broadly speaking, the above dynamical rules also involve local chaos and positive/negative interactions. However, in contrast to Eq. (3.1), where the nodes are updated locally and then the interactions alter the nodal state, here the state of the system updates locally after the interactions have altered the nodal state [54, 55]. It was observed that qualitatively similar phenomena emerge with this variation in dynamics as well.

Now, in the section below, we will rationalize these observations through mean field analysis of the network dynamics.

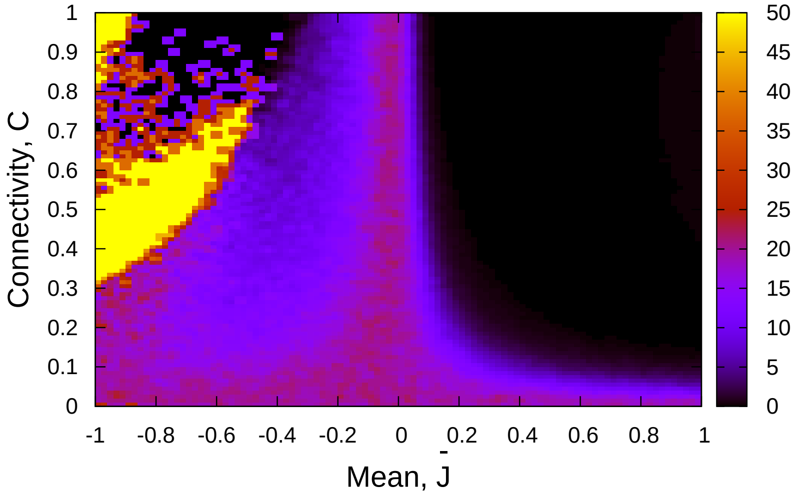

(a) $N = 50$

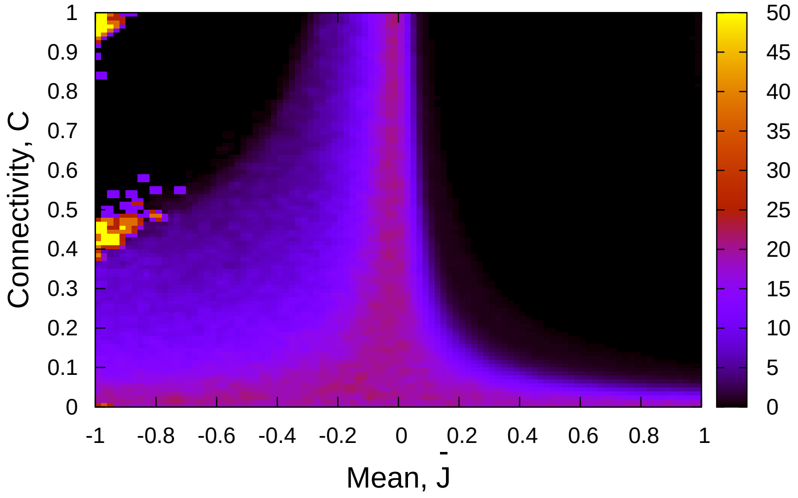

(b) $N = 100$

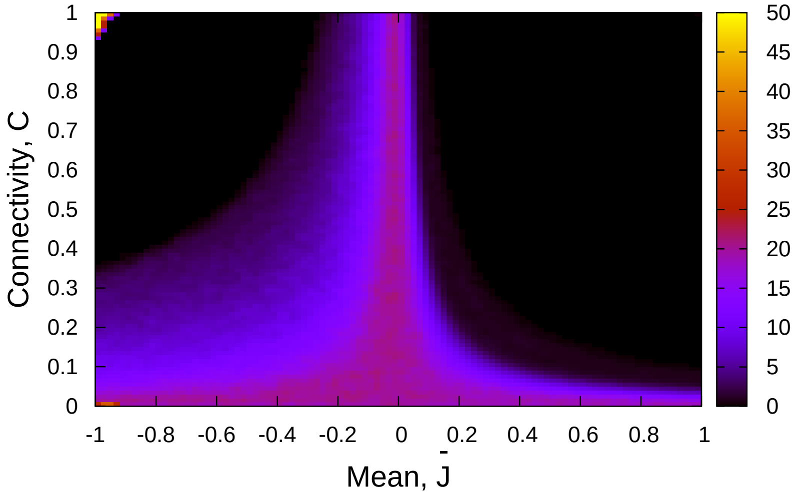

(c) $N = 250$

Figure 3.4: Density plot of the Synchronization Error (defined by Eq. (3.2)) in the parameter space of Mean $\overline{J}$ and Connectivity C, for various system sizes. Here, the standard deviation of the connection weight distribution is 0.2. The yellow region on the density plot indicates unbounded dynamics.

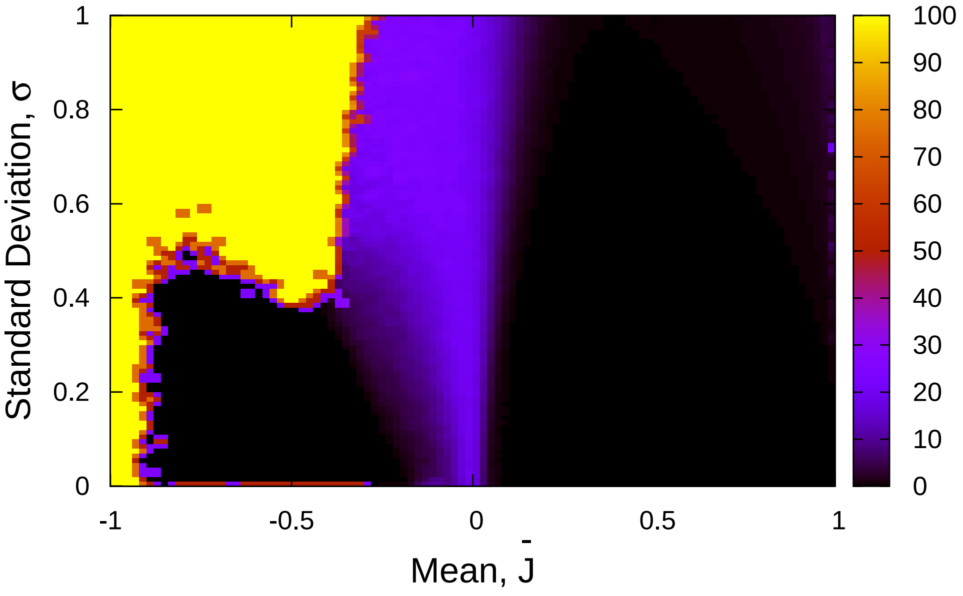

(a) N = 100

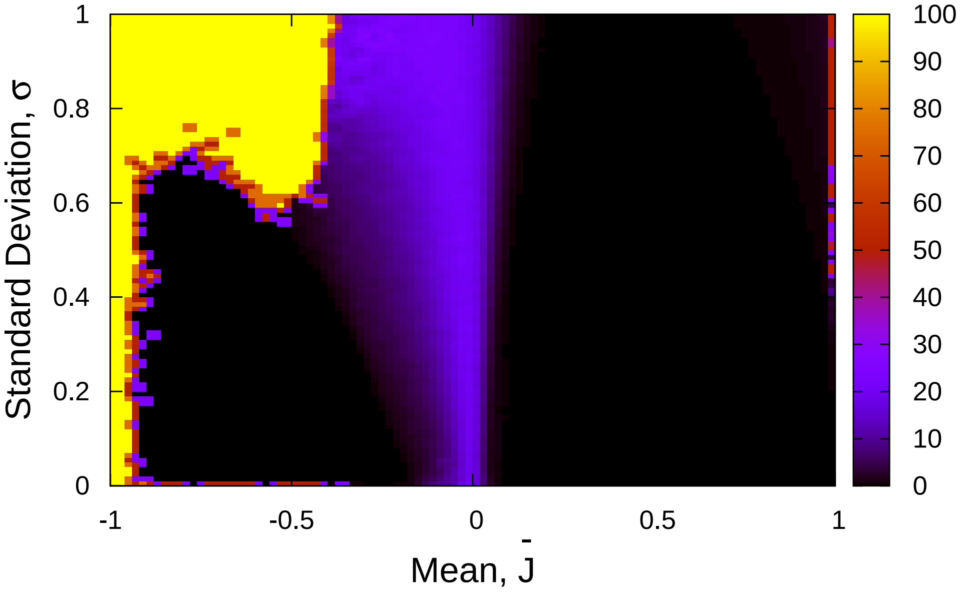

(b) N = 200

Figure 3.5: Density plot of the Synchronization Error (defined by Eq. (3.2)) in the parameter space of Mean $\overline{J}$ and Standard Deviation σ, for two system sizes (a) N: 100 and (b) 200. Here $C = 1$, and an average over 20 different random initial conditions was considered.

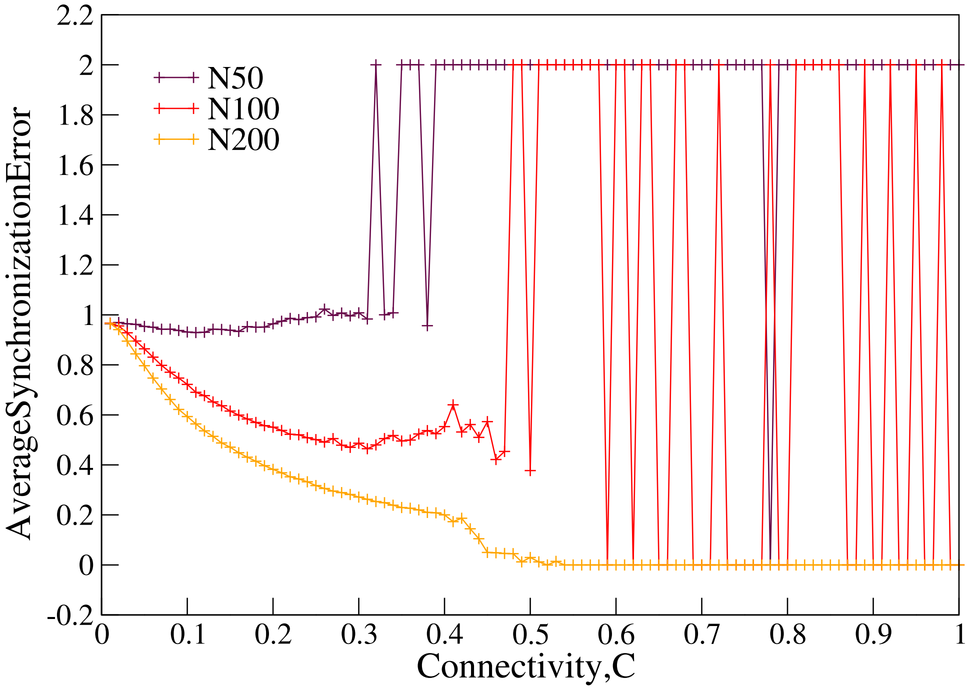

(a) $\overline{J} = -0.5$

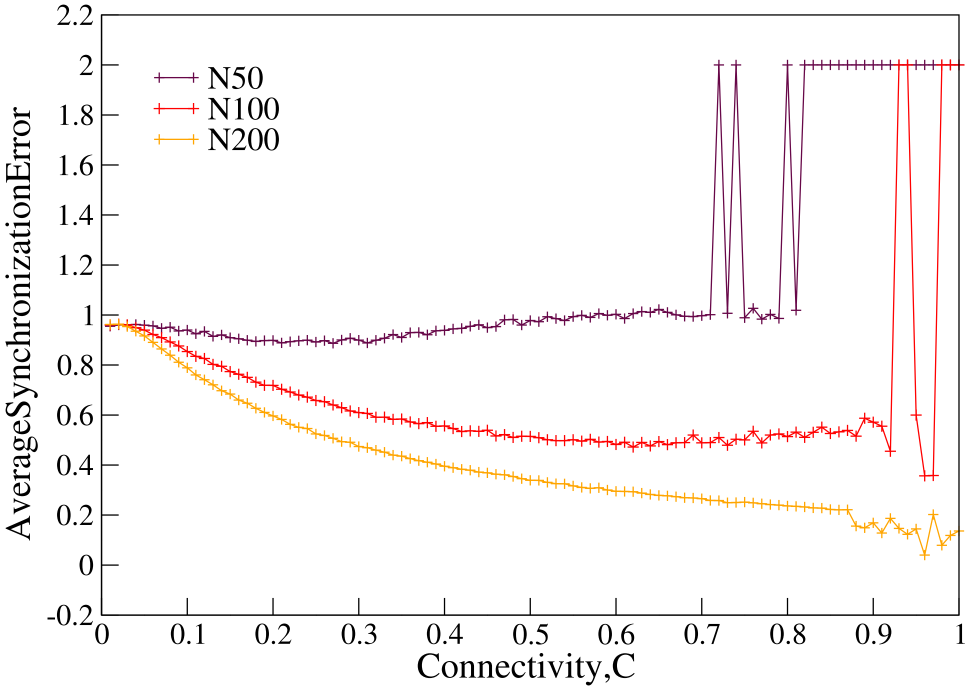

(b) $\overline{J} = -0.8$

Figure 3.6: Average synchronization error vs connectivity C, for a network of three different sizes ($N = 50, 100, 200$). Here the standard deviation of the connection weight distribution $\sigma = 0.5$, and the mean of the non-zero connection weights is $\overline{J} = -0.5$ in (a) and $\overline{J} = -0.8$ (b). The y-axis is truncated at 2, and synchronization errors larger than 2 (which occur for unbounded situations) are shown by points at 2. Clearly, larger size yields more regularity, namely lower synchronization error, and also, runaway instabilities are suppressed in larger networks.

3.3 Analysis of the Network Dynamics

Now we will try to understand the numerical observations above through an approximate mean-field analysis of the network dynamics.

At the spatiotemporal fixed point all $x(i) = x^*$, and so the coupling term,

$$\frac{1}{N}\sum_{j=1}^{N} J_{\mathrm{ij}} x(i) = x^* \frac{1}{N}\sum_{j=1}^{N} J_{ij}.$$

Now, for a very large number of nodes N,

$$\frac{1}{N}\sum_{j=1}^{N} J_{\mathrm{ij}} \sim \overline{J}C$$

as the sum is over the NC non-zero entries J_{ij} (of average value $\overline{J}$) of the coupling matrix.

Using this, our system, when close to a steady state x^*, y^*, can be described approximately as,

$$x_{\mathrm{n+1}}(i) = f_1[x_n(i), y_n(i)] + \overline{J}Cx^*, \tag{3.4a}$$

$$y_{\mathrm{n+1}}(i) = f_2[x_n(i), y_n(i)], \tag{3.4b}$$

where, $f_1(x_n, y_n)$ and $f_2(x_n, y_n)$ are given by Eq. (2.1).

The approximate evolution equation above is obtained in the limit of the number of nodes in the system $N \to \infty$, and $\sigma \to 0$. So in order to be closer to this description of the network dynamics, the network size has to be large and the variance of the connection strengths has to be small.

Now it is immediately clear from Eq. (3.4) that, in the limit $C \to 0$ (namely extremely sparsely connected neurons) and in the limit $\overline{J} \to 0$ (namely when the positive/negative connection weights are balanced) one will obtain spatiotemporal chaos. This follows from the fact that both these limits decouple the neurons, and so the full system becomes a set of uncoupled, thus uncorrelated, chaotic local neurons. This inference is bourne out by numerics (e.g. Fig. 3.1).

We will now analyze the stability of spatiotemporal fixed point in Eq. (3.4), when $\overline{J}C \neq 0$. First, note that the fixed point is given as a solution of following equations,

$$x^* = (x^*)^2 \exp(y^* - x^*) + k + \overline{J}Cx^*, \tag{3.5a}$$

$$y^* = ay^* - bx^* + c. \tag{3.5b}$$

We consider the parameter values $a = 0.89$, $b = 0.18$, $c = 0.28$ and $k = 0.03$, for which a single node is chaotic, as in the numerics.

Simplifying Eq. (3.5), by substituting,

$$y^* = \frac{c - bx^*}{1 - a}$$

we get the following equation,

$$x^* = f(x^*, \overline{J}C) = (x^*)^2 \exp\left(\frac{c - bx^*}{1 - a} - x^*\right) + k + \overline{J}Cx^* \tag{3.6}$$

We use the above effective equation, which reduces the N coupled chaotic neuronal maps to an effective dynamical map describing one neuron in a mean field of coupling interactions, as the starting point of our stability analysis.

Now, the $\overline{J}C$ can have a maximum value of 1 and a minimum value of -1 when the mean $\overline{J}$ is in the range -1 to 1, as the maximum value of C is 1. From Eq. (3.6), it is clear that $f(x, \overline{J}C)$ is always greater than x for $\overline{J}C \geqq 1$. Thus we can only have a real solution for x when $\overline{J}C < 1$.

The solutions of the above, given by the intersection of the $y = x$ (45^0 line) and the $y = x^2 \exp\left(\frac{c-bx}{1-a} - x\right) + k + \overline{J}Cx$ curve, are shown graphically in Figs. 3.7- 3.8. It is clear

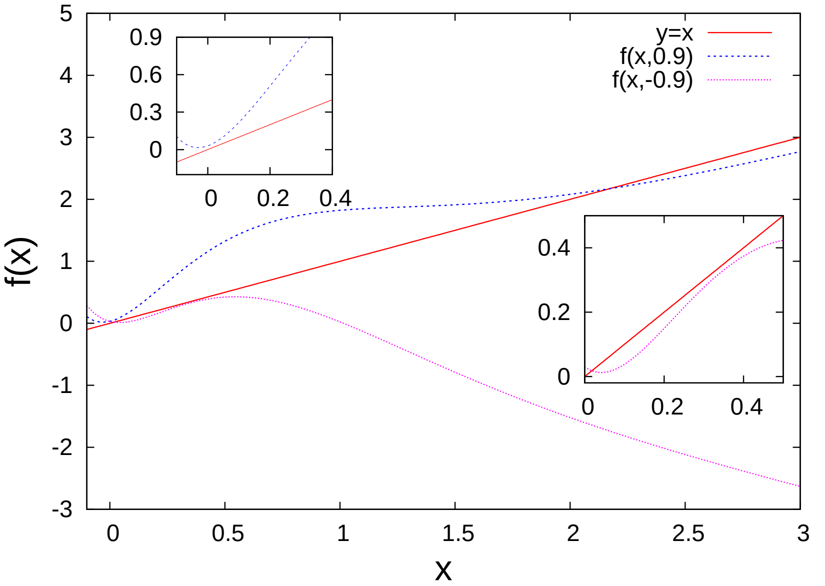

Figure 3.7: Plot of $f(x, \overline{J}C) = x^2 \exp\left(\frac{c-bx}{1-a} - x\right) + k + \overline{J}Cx$ vs. x for $\overline{J}C = 0.9$ and -0.9, namely for highly negatively skewed weights and highly positively skewed weights.

that for very negatively skewed connection weights, for instance, $\overline{J}C \sim -0.9$, there is *one solution close to zero*, namely $x^*_- \sim 0$. For very positively skewed connection weights, for instance,$\overline{J}C \sim 0.9$, there is a solution at high $x^*_+ \sim 2$. This is entirely consistent with the numerically obtained bifurcation diagrams shown in Fig. 3.1. The function $f(x, \overline{J}C)$ can either have one zero or three zeros depending on the parameter value $\overline{J}C$. Graphically it can easily be seen that there is only one solution for Eq. (3.6) from $\overline{J}C = -1$ to $\overline{J}C \sim -0.85$, and from $\overline{J}C \sim -0.15$ to 1. In between these, following a tangency in two different places, there is a transition from one solution to three solutions. One stable solution is close to x^*_+, one stable one close x^*_- and one unstable point in between these two, x^*_{thresh}, which gives a threshold below which x^*_- is stabilized, and above which x^*_+ is attracting.

The stability of the fixed points can be gauged from the eigenvalues of the Jacobian of the effective dynamics of a single node, given by:

$$\mathbf{J} = \begin{bmatrix} exp(y^* - x^*)x^*(2 - x^*) + \overline{J}C & x^{*2}exp(y^* - x^*) \\ -b & a \end{bmatrix} \tag{3.7}$$

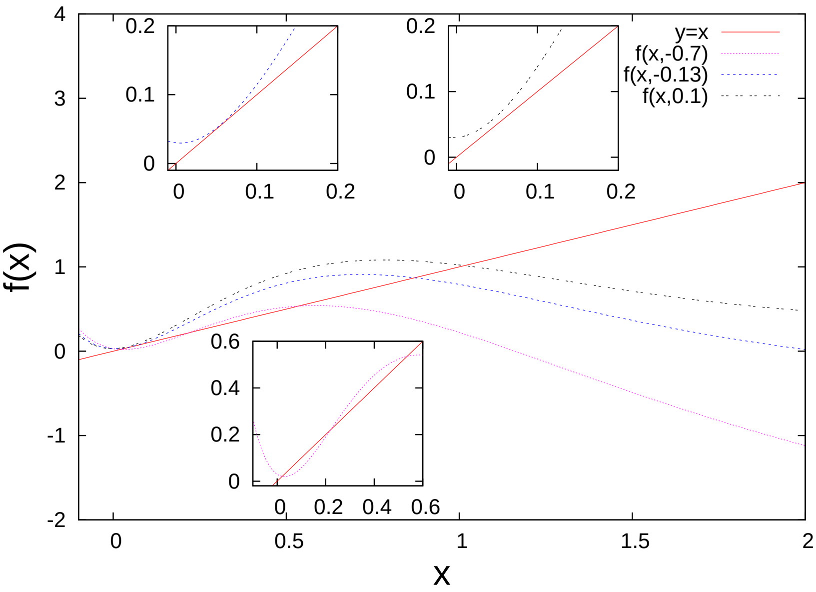

Figure 3.8: Plot of $f(x,\overline{J}C) = x^2 \exp\left(\frac{c-bx}{1-a} - x\right) + k + \overline{J}Cx$ vs. x for $\overline{J}C = -0.7, -0.13, 0.1$. Note the evident tangency, which leads to intermittency in the dynamics.

We compute the stable fixed point for Eq. (3.6) for different values of mean $\overline{J}$ and connectivity C, and finally calculate the eigenvalues of the Jacobian matrix J (for the most stable fixed point in case there is more than one). The magnitude of the largest eigenvalue, thus computed, is shown in Fig. 3.9. From the figure it is seen that for almost all values of $\overline{J}$ and C (except both being equal to 1), the eigenvalues of Jacobian matrix are less than one. So this approximate system supports a stable spatiotemporal fixed point, with varying degrees of stability given by the varying magnitude of the eigenvalues. The color density plot of the eigenvalues in Fig. 3.9 suggests a similarity with the overall stability of the system in Eq. (3.1), such as seen in Figs. 3.1, 3.4-3.6.

The stability of the true dynamics can be gauged by considering the stability of the above approximate system under considerably large random fluctuations. First, the parameters for which eigenvalues are closer to zero will support a more robust spatiotemporal fixed point than those where the eigenvalues are closer to one. This accounts for the enhanced stability of the spatiotemporal fixed point for large positive $\overline{J}C$. That is, when the connections are dense and skewed considerably towards positive links the fixed point x^*+ (which is the only solution of Eq. (3.6)) is stabilized. Fig. 3.9 also suggests that for large C and

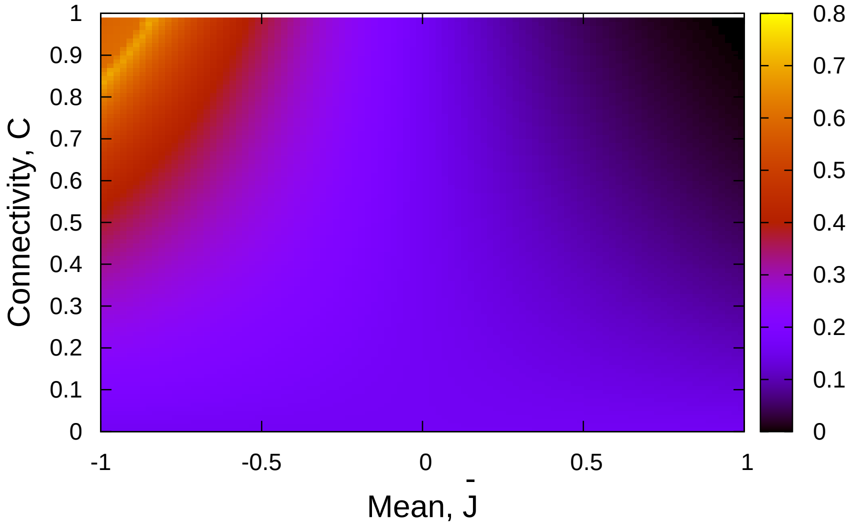

Figure 3.9: Eigenvalues of Jacobian matrix against mean ($\overline{J}$) and Connectivity(C). (See Fig. 3.4 for comparison.)

dominantly negative connection strengths, the eigenvalues approach one. This suggests the observed instabilities encountered when $\overline{J}C \rightarrow -1$ (cf. Figs. 3.5-3.6).

The next feature suggested by the analysis is the following: when there is *one* attracting fixed point, the dynamics is more stable under large fluctuations, as there is no competing sink for the phase flow. However when the negative and positive connection strengths are more balanced, there are *two competing attracting fixed points* separated by an unstable one, giving a “threshold” below which the fixed point closer to zero (namely complete inactivity) is stabilized. Above the “threshold” the large fixed point is attracting. So for a system subject to large fluctuations, the dynamics will swing randomly from around x^*_- (close to zero) to around x^*_+ (which is large).

Lastly, larger N implies smaller fluctuations about the mean field approximation, as the law of large numbers dictates that the mean square deviation of the interaction field term goes as $O(1/N)$. Similar effect occurs for small σ, which implies that the connection weights are clustered closely around the mean value. So for increasing N and decreasing σ the stability is closer to that given by the mean field analysis. This is consistent with our numerical observation that larger network size, and smaller variance, leads to enhanced spatiotemporal regularity.

Lastly, one can also use results from random matrix theory [113], which give the largest eigenvalue of a symmetric random matrix, whose entries are from a normal distribution with mean, $\mu > 0$ and variance, ν to be,

$$\lambda_{max} = N\mu + \frac{\nu}{\mu}. \tag{3.8}$$

In our network, the mean is $\overline{J}C$ and the variance is $\sigma^2 C + \overline{J}^2 C(1 - C)$. So, the maximum eigenvalue of the Jacobian matrix will be [114]

$$\lambda_{max} \sim f'(x^*) + \overline{J}C + \frac{\sigma^2}{\overline{J}N} + \frac{\overline{J}(1 - C)}{N} \tag{3.9}$$

Thus, it is clear that for mean $\overline{J} \to 0$ the maximum eigenvalue of the Jacobian matrix gets very large indeed, indicating strong instability of the spatiotemporal fixed point state. This is completely consistent with the numerical observation that balanced positive and negative links yields spatiotemporal irregularity.

Caveat: We should mention here though, that the generality of these results, vis-a-vis variation in local dynamics, distribution functions, and network types, is an open issue. It is possible that the delicate interplay between the local evolution and the global connections may yield a variety of different spatiotemporal behavior. It is indeed an outstanding problem to gauge what features are universal (if any) in the emergence of collective behavior from the complex interplay of the nodal dynamics and positive/negative feedbacks due to connections.

3.4 Conclusions

We have investigated the effect of the interplay of positive and negative links, on the dynamical regularity of a random weighted network, with neuronal dynamics at the nodes. We investigated how the mean $\overline{J}$ and the variance of the weights of links, influence the spatiotemporal regularity of this dynamical network. We find that when the connections are predominantly positive (i.e. the links are mostly excitatory, with $\overline{J} > 0$) the spatiotemporal fixed point is stable. A similar trend is observed when the connections are predominantly negative (i.e. the links are mostly inhibitory, with $\overline{J} < 0$). However, when the positive and negative feedback is quite balanced, namely when the mean of the connection weights is close to zero) one observes spatiotemporal chaos. So counter-intuitively, it appears that in this random weighted network of neuronal maps, balanced positive and negative feedback leads to the destabilization of the fixed (rest) state, resulting in large irregular spiking. Namely balanced inhibition and excitation leads to spatiotemporal chaos in the neuronal population.

Further we observed that, for non-zero mean, larger network size leads to greater spatiotemporal regularity. Namely, the stability of the fixed state increases with increasing number of coupled neurons. This is interesting vis-a-vis the May-Wigner condition which gives that stability is inversely proportional to size in a random network [5, 105, 54, 55]. We rationalized our observations through mean field analysis of the network dynamics.

Now the origin of the irregular spiking that is observed in the cortex is a long standing problem in neurobiology. Our observations are consistent with the hypothesis that the temporal chaos in the firing of a neuron results from an approximate balance between its excitatory and inhibitory inputs [106, 108, 109].

So in summary, the trends observed in networks where the connection weights are randomly distributed about a non-zero mean, are significantly different from those seen in the commonly studied random weighted networks with zero-mean. Our central result is that, to be stabilized to a inactive state, one needs one type of connection (either excitatory or inhibitory) to dominate. Namely, when the mean of the connection weights is far from zero, the spatiotemporal steady state is obtained.

Chapter 4

Cluster formation in populations of coupled chaotic neurons

In this chapter, we discuss formation of clusters in a populations of coupled chaotic model neurons under homogeneous global coupling, and distance-dependent coupling. In distance-dependent coupling case, the coupling weights between neurons depend on their relative distance. Here, we will explore whether the emergent spatiotemporal patterns are *the dynamical effect of inhomogeneity in the coupling or the result of the influence of the underlying lattice structure*. To understand this problem, we have considered the same system under a coupling scheme where the coupling strength among the nodes are randomly distributed but like distance dependent coupling in the averaged sense.

We have discussed in Chapter 1 that for a system of coupled maps, which is commonly used to model the spatiotemporal dynamics of extended chaotic systems [31, 39, 111], the dynamics consists of two components: (i) a local nonlinear mapping, which is a source of local instability and on-site complex behavior; (ii) interactions with subsets of other elements. The coupling promotes synchronization in the evolution of the elements, while the local dynamics tends to destroy this coherence. The balance between these two trends accounts for rich pattern formation in such systems, such as stable clusters or condensate of elements [42, 43]. Synchronization [18, 19] is an emergent property in such networks of interacting dynamical elements. So, it is also vital to try and understand the routes of transition from incoherent dynamical elements to synchronized groups.

4.1 Population of Interactive Neurons

Now, we describe our model of a population of interactive neurons. It is comprised of local neuronal dynamics, coupled through varying forms of interaction. The nodal dynamics gives rise to the complexity in dynamics through the strong non linearity. The interactions induce coherence in varying degrees, yielding different clustering patterns in the population.

Nodal Dynamics: The local dynamics in the network is described by a two-dimensional Chialvo map [87], which mimic the dynamics of a single neuron, and given by Eq. (2.1). The parameters of the map are $a = 0.89,\ b = 0.18,\ c = 0.28$ and $k = 0.03$ for which the map shows chaotic behavior as discussed in Chapter 2.

Coupling interactions: First we consider homogeneous diffusive *global* coupling that involves all elements weighted equally, with the overall dynamics is given by,

$$x^i_{n+1} = f_1(x^i_n, y^i_n) + \frac{\epsilon}{N}\sum_{j=1}^{N}(x^j_n - x^i_n), \tag{4.1a}$$

$$y^i_{n+1} = f_2(x^i_n, y^i_n), \tag{4.1b}$$

where, ϵ is the coupling strength, $i = 1, \cdots, N$ is the site index, N is the total number of nodes in the lattice, n is iteration steps and $f_1(x_n, y_n)$ and $f_2(x_n, y_n)$ are given by Eq. (2.1).

Next, we consider *distance dependent coupling* with the neurons in a ring-like lattice. Here the coupling is weighted inhomogeneously, and depends on the relative distance between the nodes. Unlike the homogeneous global coupling case above, the *structure* of the network now influences the dynamics, with the evolution equations given as,

$$x^i_{n+1} = f_1(x^i_n, y^i_n) + \frac{\epsilon}{N}\sum_{j=1}^{N}\left(1 - \frac{\tau_{ij}}{N}\right)x^j_n, \tag{4.2a}$$

$$y^i_{n+1} = f_2(x^i_n, y^i_n), \tag{4.2b}$$

where, $\tau_{ij} = |i - j|$, is the smallest distance between the two nodes i and j. Clearly, the strength of the coupling between two elements varies in the interval $(0, \epsilon/2]$ such that the strength of link decreases linearly with the increase in distance between the two nodes. So, while the coupling is global here as well, as every node is influenced by all elements, it is not homogeneous as in Eq. (4.1).

At last, we consider randomly distributed inhomogeneity in the coupling strength for the lattice where the distribution is such that the coupling between the nodes is like the distance dependent case above, in an averaged sense. First, we study a system where the coupling of node i to node j is randomly chosen from a set of $N/2$ coupling strengths: $(1 - i/N)\epsilon$, with $i = 1, \ldots, N/2$. We also considered the case, where the coupling strength between two nodes i and j are randomly drawn from an uniform distribution between $[0 : \epsilon/2]$. So, for both these types of inhomogeneous coupling, each site, on an average has an uniform spread of coupling strengths from 0 and $\epsilon/2$, just as in the distance dependent coupling scenario. However, unlike distance dependent coupling, there is no regularity in the value of coupling strength, and there is no sense of an underlying lattice structure.

4.2 Phenomenology

We explore the spatiotemporal patterns that emerge in this system under varying strengths and forms of coupling. In particular, we focus on the emergence of clusters or condensates of model neurons in the population.

When coupling is homogeneous and global, the route to complete synchronization for this

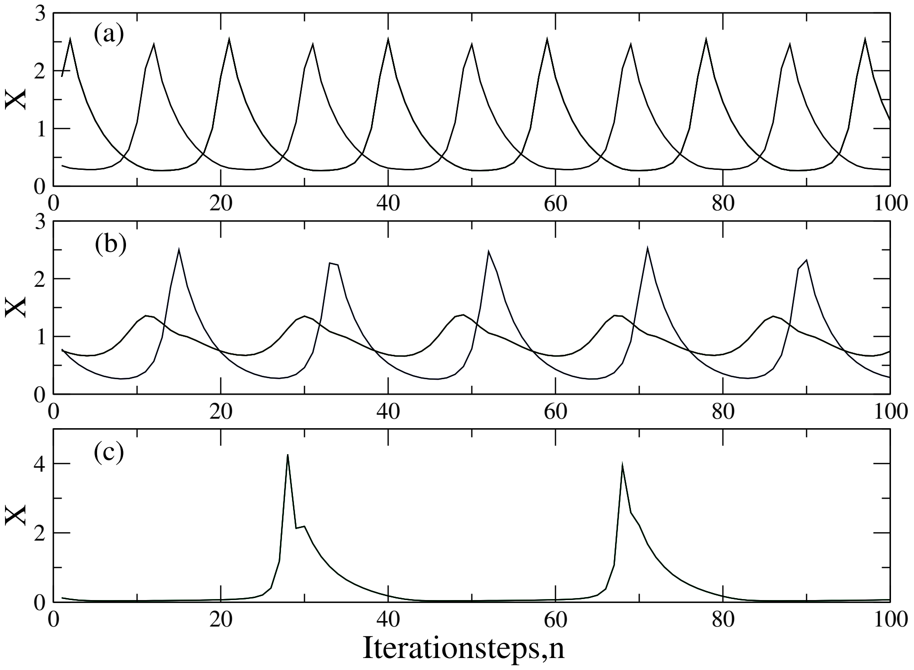

Figure 4.1: Time series of the population showing (a) two anti-phase clusters for $\epsilon = 0.04$, (b) two clusters, in arbitrary phase relation with each other for $\epsilon = 0.1$, (c) one synchronized cluster for $\epsilon = 0.12$, in a system with homogeneous global coupling. The total population consists of 200 model neurons, with each neuron in the chaotic regime. Here the dynamics of all the neurons are superimposed.

network is as follows:

(i) For very small coupling strengths all the elements are desynchronized.

(ii) For coupling strength ϵ in the range $0.04 - 0.05$, the neuronal population splits into two subgroups. All neurons have the same amplitude, but the neurons in different sub-groups have different phases, with the phase difference being approximately π. We term this *anti-phase cluster* or *phase flip cluster*, as the two subgroups are in opposite phase, as is evident from Fig. 4.1(a). The number of elements in each cluster, is the same, for this state.

(iii) Further increase in the value of ϵ leads to desynchronization among the two subgroups.

(iv) The desynchronization window above is followed by a range of coupling, $\epsilon \in$

0.09 − 0.10, where the neuronal population again divides into two synchronized subgroups. Here each subgroup has different amplitude and different phase of oscillation as shown in Fig. 4.1(b). Unlike the clusters in (ii) above, the elements are not equipartitioned into the two clusters. Rather, the number of elements in the large amplitude group is greater than those in the small amplitude group.

(v) Lastly, for $\epsilon > 0.11$, we obtain complete synchronization among the group as shown in Fig. 4.1(c). Namely, when coupling strength is larger than a critical value ~ 0.11, we get $x_j = x$, for all $j = 1, \ldots, N$, i.e. all the elements in the system behave as one.

In order to quantify the degree of synchronization in the network, we compute an average error function defined as the mean square deviation of the instantaneous states of the nodes:

$$Z_n = \frac{1}{N}\sum_{i=1}^{N}\{[x_n^i - \langle x_n\rangle]^2 + [y_n^i - \langle y_n\rangle]^2\}, \tag{4.3}$$

where, $\langle x_n\rangle$ and $\langle y_n\rangle$ are the space averages of the fast and slow variables at time n. This quantity averaged over time n, and over different realizations, is denoted as Z. When $Z = 0$, we have complete synchronization.

The variation of synchronization error with respect to global coupling strength ϵ is displayed in the Fig. 4.2. Clearly, $Z \to 0$ for $\epsilon > 0.11$. Further note that system size does not influence synchronization properties.

In summary, for homogeneous global coupling we find three types of clusters: *phase flip cluster*, *two state cluster* and *one synchronized cluster*, as global coupling strength is varied.

Now we describe the spatiotemporal patterns arising from distance dependent coupling. As coupling strength increases, we observe the following:

(i) For very small value of coupling strength the lattice is desynchronized.

(ii) With increasing coupling strength, namely in the ϵ-range $0.03 - 0.04$, the population

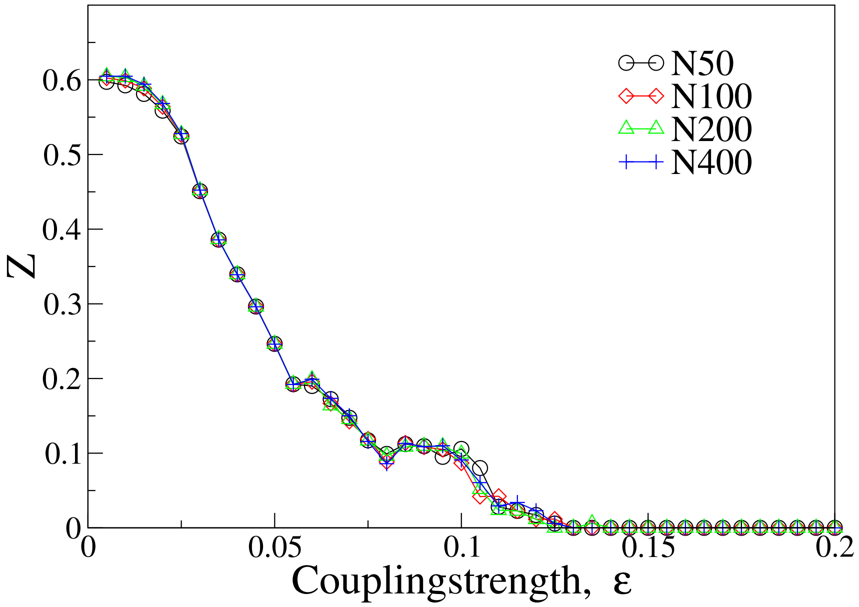

Figure 4.2: Plot of the synchronization error, Z (defined by Eq. (4.3)) vs. coupling strength ϵ, for coupled chaotic neurons. Results for different system sizes N are displayed. Here the synchronization error is computed by averaging over 1000 iterations after transience, and a further average over 10 initial conditions. Clearly, system size does not affect synchronization properties.

splits into two groups, whose phase difference appears to be equal to π. The time series and phase space plot of this anti-phase clustered state is shown in Figs. 4.3(a) and 4.4(a), respectively. The number of elements in each synchronized cluster is again the same.

(iii) Further increase in the value of coupling strength, ϵ, leads to desynchronization among the elements first, followed by formation of clusters. In the ϵ range $0.05 - 0.055$, we find that the lattice split into *three clusters*, as shown in the Figs. 4.3(b) and 4.4(b). In this clustered state, two subgroups contain synchronized elements having different amplitude, as well as different phase relation with respect to the other group. The third subgroup is desynchronized and incoherent, and co-exists with the two synchronized groups. *Notice, that homogeneous global coupling did not yield this class of clustered states.*

(iv) The novel three cluster state reduces to a two clusters with increasing coupling

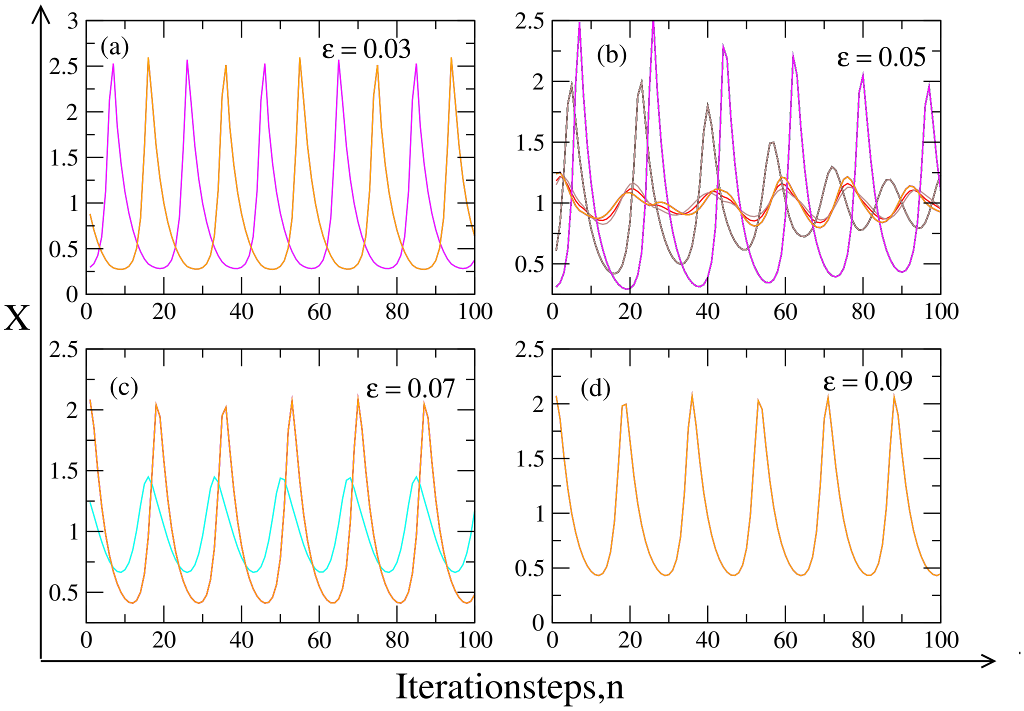

Figure 4.3: Time evolution of state space of model neurons under distance dependent coupling. The total number of nodes in the lattice is $N = 200$ and each node is in the chaotic regime. In each plot the dynamics of all the neurons are superimposed.

strength, namely in the ϵ range $0.06 - 0.075$. A representative time series of this is shown in the Fig. 4.3(c). The phase diagram shown in Fig. 4.4 (c) displays the two limit cycles of different amplitude. The number of elements in large amplitude cluster is greater than that in the small amplitude cluster.

(v) For $\epsilon > 0.075$, we find that the group is fully synchronized in both amplitude and phase as seen in Fig. 4.3(d).

(vi) As the value of the coupling strength increases further, the system goes to a fixed point, which is stable for $\epsilon > 0.12$. This will be shown analytically in the section (4.3). But, it can be seen from the Fig. 4.4, that the size of limit cycle decreases as the strength of the coupling is increased. Thus, for larger coupling strength all the elements will settle to a fixed point.

We also find co-existence of different dynamics in small ranges of ϵ, near the transition

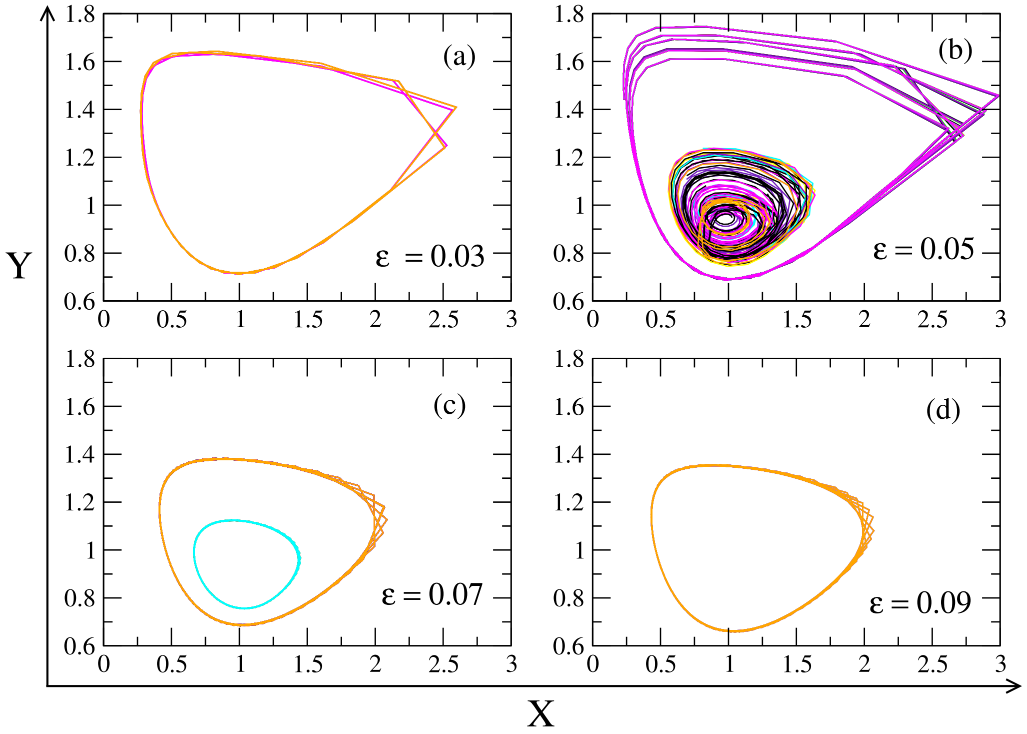

Figure 4.4: Phase space plots of the model neurons under distance dependent coupling. The total number of nodes in the lattice is $N = 200$ and each node is in the chaotic regime. In each plot the dynamics of all the neurons are superimposed

point. For instance, we find desynchronized dynamics along with the three cluster state near $\epsilon = 0.05$ for certain initial conditions. Other than at these transition points, the dynamical states are quite robust and most likely global attractors.

The phenomena of different types of clustering in this system can also be visualized by using the Poincaré section. To construct the Poincaré section, we have recorded the value of the slow variable y_n, whenever the value of the fast variable x_n is equal to 1 for each neuron. Also, we have considered only those values of y_n for which, $(x_{n+1} - x_{n-1}) > 0$. Using this, we obtain the bifurcation diagram of the Poincaré section of this system with respect to coupling strength ϵ, as displayed in Fig. 4.5.

The time series results are completely consistent with the bifurcation diagram shown in Fig. 4.5. Here, anti-phase cluster and synchronized cluster are represented by a single point in the diagram. For the two cluster state we get two points, as they have two distinct

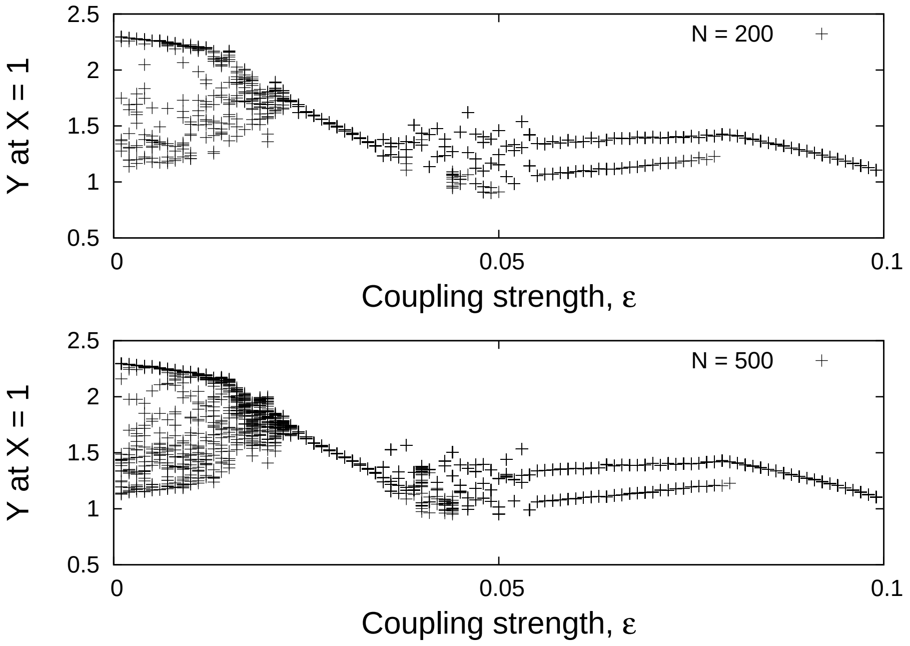

Figure 4.5: Poincaré section of the model neurons with respect to coupling strength ϵ for system size $N = 200$ and $N = 500$. Note that system size does not influence the emergent dynamical properties.

limit cycles. For the three cluster state, the amplitude of the limit cycles vary (as evident in Fig. 4.4(c)), and so we get a scatter of points in the poincaré section in this regime. The coexistence of different dynamics for a small range of ϵ, at transition points, is also evident.

In summary, for distance dependent coupling, we have all the clustering patterns found in systems with homogeneous global coupling. Additionally, we have a distinct clustering behavior, the three cluster state, where the population splits into three groups, namely two synchronized groups and one incoherent group.

Lastly, we try to address the following question: do the spatiotemporal patterns observed in distance dependent coupling arise from the inhomogeneity of coupling strengths due to their distance dependence, or is it a result of the sensitivity of distance dependent coupling to the underlying lattice structure.

To understand this issue, we study inhomogeneity in the coupling strength, ϵ. First we

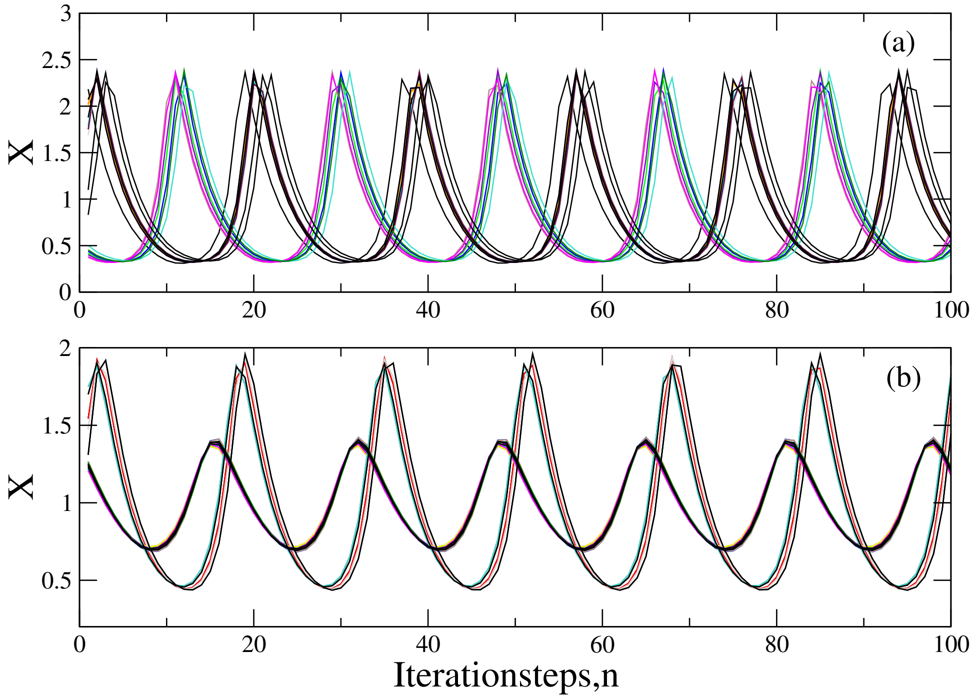

Figure 4.6: Time Series of the population with inhomogeneous coupling strengths, depicting (a) fuzzy phase flip clusters for $\epsilon = 0.055$ and (b) fuzzy two-state clusters for $\epsilon = 0.11$. Here, the dynamics of all the neurons are superimposed.

consider the coupling strengths randomly distributed among the same set of strengths that would rise in distance dependent coupling, namely, $(1 - i/N)\epsilon$, with $i = 1, \dots, N/2$. For this class of inhomogeneous coupling, the three state cluster is not found. However, fuzzy phase flip and two-state cluster arise, and a representative time series of these are shown in Fig. 4.6. For larger values of ϵ, all nodes settled down to fixed points.

We also considered the case, where the coupling strength between two nodes i and j are given by a connectivity matrix C, where the elements of the matrix are taken from uniform random distribution between $[0 : \epsilon/2]$, and $C_{ii} = 0$ for all i. For this class of coupling, we found that all the elements are desynchronized for small value of coupling strength ϵ, and settle to a fixed point for larger values of ϵ.

Clearly, the special pattern found in distance dependent coupling, namely the three state cluster, is the dynamical effect of the lattice structure imposed by distance dependent coupling and not due to inhomogeneity alone.

4.3 Stability Analysis for Distance Dependent Coupling

Finally, we analyze some aspects of the dynamical patterns arising in the extensive numerical simulations reported above. Now, the stability of the fixed point for distance dependent coupling can be gauged by eigenvalues of the Jacobian matrix. For the fixed point solution we have,

$$x^i_{n+1} = x^i_n = x \; \& \; y^i_{n+1} = y^i_n = y \; \forall \; i.$$

Solving Eq. (2.1) for the slow variable and substituting back in the Eq. (4.2) we get,

$$x = x^2 exp\left(\frac{c - bx}{1 - a} - x\right) + k + x\frac{\epsilon}{N}\sum_{j=1}^{N}\left(1 - \frac{\tau_{ij}}{N}\right), \tag{4.4}$$

which can be simplified for even N, and we have,

$$x\left[1 - \epsilon\left(\frac{3}{4} - \frac{1}{N}\right)\right] = x^2 exp\left(\frac{c - bx}{1 - a} - x\right) + k \tag{4.5}$$

Clearly, the right hand side is always positive. Hence the solution will exist only when, $\epsilon < \frac{4N}{3N-4} \sim 1.33$. Now the Jacobian matrix, $\mathbf{J}$, for the system is a $2N \times 2N$ circulant matrix [115] and can be written as,

$$\mathbf{J} = \text{circ}\left(a_0, a_1, \cdots, a_{N/2}, \cdots, a_2, a_1\right), \tag{4.6}$$

where, a_i for $i = 0, 1, \cdots, N/2$ are 2×2 matrices and defined as,

$$a_0 = \begin{pmatrix} a_{01} & a_{02} \\ a_{03} & a_{04} \end{pmatrix} \tag{4.7}$$

with,

$$a_{01} = \frac{\partial f_1(x,y)}{\partial x}, \; a_{02} = \frac{\partial f_1(x,y)}{\partial y}, \; a_{03} = \frac{\partial f_2(x,y)}{\partial x}, \; a_{04} = \frac{\partial f_2(x,y)}{\partial y} \tag{4.8}$$

and for $i \neq 0$, we have,

$$a_i = \begin{pmatrix} \frac{\epsilon}{N}\left(1 - \frac{i}{N}\right) & 0 \\ 0 & 0 \end{pmatrix} \tag{4.9}$$

$\forall\ i = 1, \ldots, N/2$. The Jacobian matrix defined in Eq. (4.6) is a block-circulant matrix and can be set into a block-diagonal form by a unitary transformation. The unitary matrix which affects the block diagonalization is a direct product of Fourier matrices of sizes $N \times N$ and 2×2, the entries of which are roots of unity, independent of the matrix being diagonalized [115, 116].

In the block diagonal form the above matrix can be written as,

$$\mathbf{BD} = diag(D_0, D_1, \cdots, D_{N-1}), \tag{4.10}$$

where, the matrix D_r; for $r = 0, 1, \cdots, N-1$ are 2×2 matrix, are given as, $D_r = a_0 + \omega_r a_1 + \cdots + \omega_r^{N/2} a_{N/2} + \cdots + \omega_r^{N-1} a_1$, where $\omega_r = e^{i\theta_r}$ and $\theta_r = 2\pi r/N$.

Hence, to check the eigenvalues at the fixed point for the whole range of θ i.e. from $\theta = 0$ to $\theta = 2\pi$, it is enough to check the eigenvalues for $\theta = 0$ and $\theta = \pi$. Clearly, $\theta = 0$ also covers $r = 0$. Now for the $\theta = 0$, the matrix D_r for $r = 0, 1, .., N-1$, can be written as,

$$D_r(\theta = 0) = \begin{pmatrix} a_{01} + \epsilon(\frac{3}{4} - \frac{1}{N}) & a_{02} \\ a_{03} & a_{04} \end{pmatrix} \tag{4.11}$$

and for $\theta = \pi$ and $r = 1, 2, .., N-1$ we have,

$$D_r(\theta = \pi) = \begin{pmatrix} a_{01} + \frac{\epsilon}{N^2} & a_{02} \\ a_{03} & a_{04} \end{pmatrix} \tag{4.12}$$

Clearly, if the magnitude of the eigenvalues of the above two matrices is less than one, the fixed point is stable. The fixed point is calculated by bisection method for the Eq. (4.5) in the ϵ range $[0, 0.1]$, and by the iteration method for $\epsilon > 0.1$. Considering these values of the fixed point solution, and calculating the eigenvalues of the matrix D_r for $\theta = 0$ and $\theta = \pi$, we find that for $\epsilon > 0.12$ the fixed points are stable. This is consistent with our numerical observation.

4.4 Conclusions

We have investigated the effect of distance dependent coupling vis-a-vis homogeneous global coupling on cluster formation in a population of chaotic neurons. For global diffusive coupling, we found three types of coherent clusters: *anti-phase cluster*, *two state cluster* and *one synchronized cluster*. For distance dependent coupling, apart from these three coherent clusters we found a new type of clustering where the population splits into three subgroups, with two subgroups synchronized within themselves while the third subgroup has incoherent elements. This three state cluster reduced to a two state cluster with increasing coupling strength. We also considered randomly distributed inhomogeneity in the coupling strength, where the distribution is such that the coupling between the nodes is like the distance dependent case, in an averaged sense. But, the three state cluster is not found which indicates not only the inhomogeneity but also a particular type of architecture in the coupling strength is needed to observe this clustered state. So, in summary, a rich variety of cluster formation emerged in this population of chaotic neurons, yielding different routes to complete synchronization under varying coupling forms.

Chapter 5

Emergent patterns in interacting neuronal sub-populations

In this Chapter, we consider interacting populations of model neurons, where the coupling asymmetry arises due to the interacting groups being in different dynamical domains. Such a network is motivated by the fact that the brain, broadly speaking, is a system of interacting neural groups which can be in different dynamical domains.

Our primary motivation is to understand how groups can induce synchronization in other dynamically distinct groups. We look for phenomena analogous to event-related oscillatory response in models of the brain, termed as *Event-Related Synchronization* (ERS) or *Desynchronization* (ERD). Typically ERD occurs when a small group of oscillators separate themselves from the larger synchronized group due to an *event* [117, 118]. This phenomena is relevant, for instance, in *Attention Deficit/Hyperactivity Disorder* (ADHD), where ERD was observed in the alpha band and ERS in the beta band [119].

Now, the event could be a dynamic signal from outside the system, or it may be from a different region in the same system that is characteristically different from the rest of the system, like in the case, where sensory stimuli from the other parts of the body desynchronizes the synchronized delta oscillations during light anesthesia [120, 121]. Further, synchronized clusters play a central role in many brain related phenomena, such as in epileptic networks, determining seizure onset and propagation [122]. So, it is vital to study the formation of clusters due to interaction of one synchronized group with the other synchronized group where each group can be characteristically different in their sizes and their intrinsic behaviors.

Specifically here, we explore the dependence of the synchrony of a sub-population on inter/intra-group coupling strengths, relative size of the groups and their intrinsic behaviors. The principal question we address is this:

(i) Does a group have to be a majority group in order to influence another dynamically different one?

(ii) What kind of intrinsic dynamical behavior is most amenable to influence by another group, and what behavior wields most influence?

In this chapter, we will show that, counter-intuitively, certain minority groups can be very effective in inducing synchronization in a dynamically different majority group. We will also report the range of clustering behavior induced by inter-group coupling, ranging from two synchronized groups and anti-phase clusters.

5.1 Interacting Populations of Model Neurons

The local dynamics at each node i where $i = 1, \ldots, N$ in this network, models neuronal dynamics through a two-dimensional Chialvo map [87] with two state variables, $x_n(i)$ and $y_n(i)$, which are described by Eq. (2.1). We consider the parameter values, $a = 0.89$, $c = 0.28$ and $k = 0.03$, and vary the parameter b in order to model nodes with oscillatory dynamics (for $b = 0.6$) and aperiodic bursting, namely chaotic, behavior (for $b = 0.18$).

In our model, we have two populations denoted by (**A** and **B**). The parameters of the local map modeling the neurons in each group can be chosen such the neurons are either periodic or chaotic. The intra-group and inter-group coupling strengths are ϵ_1 and ϵ_2 respectively. So the dynamics of the interactive system of **A** and **B** dynamical groups is given as,

$$x_{n+1}^{(A)}(i) = f_1[x_n^{(A)}(i), y_n^{(A)}(i)] + \frac{\epsilon_1}{N}\sum_{j=1}^{N_1}(x_n^{(A)}(j) - x_n^{(A)}(i)) + \frac{\epsilon_2}{N}\sum_{j=N_1+1}^{N}(x_n^{(B)}(j) - x_n^{(A)}(i)); \quad (5.1a)$$

$$y_{n+1}^{(A)}(i) = f_2[x_n^{(A)}(i), y_n^{(A)}(i)], \quad (5.1b)$$

$$x_{n+1}^{(B)}(i) = f_1[x_n^{(B)}(i), y_n^{(B)}(i)] + \frac{\epsilon_1}{N}\sum_{j=N_1+1}^{N}(x_n^{(B)}(j) - x_n^{(B)}(i)) + \frac{\epsilon_2}{N}\sum_{j=1}^{N_1}(x_n^{(A)}(j) - x_n^{(B)}(i)); \quad (5.1c)$$

$$y_{n+1}^{(B)}(i) = f_2[x_n^{(B)}(i), y_n^{(B)}(i)]. \quad (5.1d)$$

Thus, the dynamics of the membrane potential of each neuron is influenced by a local field comprised of sum of the activity of all neurons, with different coupling weights, depending on whether the neuron is in same group or not. So, we have each group responding to a "dynamic signal" from a different group, which may or may not be in the same dynamical regime as itself. We study the type of clusters arising under this interaction, for different dynamical behavior and population sizes of the groups, under varying inter-coupling strengths.

We consider the system under three qualitatively different partitions:

(i) *Equipartitioning*, namely the case where the sub-populations **A** and **B** have same number of elements

(ii) **A** is the majority sub-population and **B** is the minority, namely the number of elements in **A** is significantly more than that in **B**. For instance, when the full system size $N = 200$, group **A** has 150 elements, and group **B** has only 50.

(iii) **B** is the majority sub-population and **A** is the minority, namely the number of elements in **B** is significantly more than that in **A**. For instance, when the full system size $N = 200$, group **B** has 150 elements, and group **A** has only 50.

We now present the types of spatiotemporal patterns which emerges from such inter-group interactions, for different intrinsic dynamics and relative sizes of the sub-groups, under varying coupling strengths.

5.2 Cluster Formation Patterns

In order to quantify the degree of synchronization in the system we compute an average error function defined as the mean square deviation of the instantaneous states of the nodes,

$$Z_n = \frac{1}{N} \sum_{i=1}^{N} \{[x_n(i) - \langle x_n \rangle]^2 + [y_n(i) - \langle y_n \rangle]^2\} \tag{5.2}$$

where, $\langle x_n \rangle$ and $\langle y_n \rangle$ are averages of fast and slow variables of all the elements at time n. This quantity averaged over time n, and over different realizations, is denoted as Z. For $Z = 0$, we have complete synchronization.

In our study we consider the intra-group coupling strength ϵ_1 to be 0.15. At this coupling strength, a homogeneous group of periodic neurons, as well as a homogeneous group of chaotic neurons, would be synchronized, as evident from Fig. 5.1. We then vary the inter-group coupling strength, ϵ_2, in the range 0 to 0.15.

Interacting groups in different dynamical regimes:

First we consider the sub-populations **A** and **B** to have different dynamical behaviors, namely: neurons in one group are chaotic, while those in the other are in the periodic regime. We denote the number of elements in the chaotic group as N_c and the size of the periodic group as $N_p = N - N_c$.

Fig. 5.2 shows the evolution of the neurons in the chaotic and periodic sub-populations, for representative cases. The periodic group, which has a very low synchronization threshold, always remains synchronized. However, notice the variation in the synchronization properties of the chaotic group. When the chaotic group is small, coupling with the large

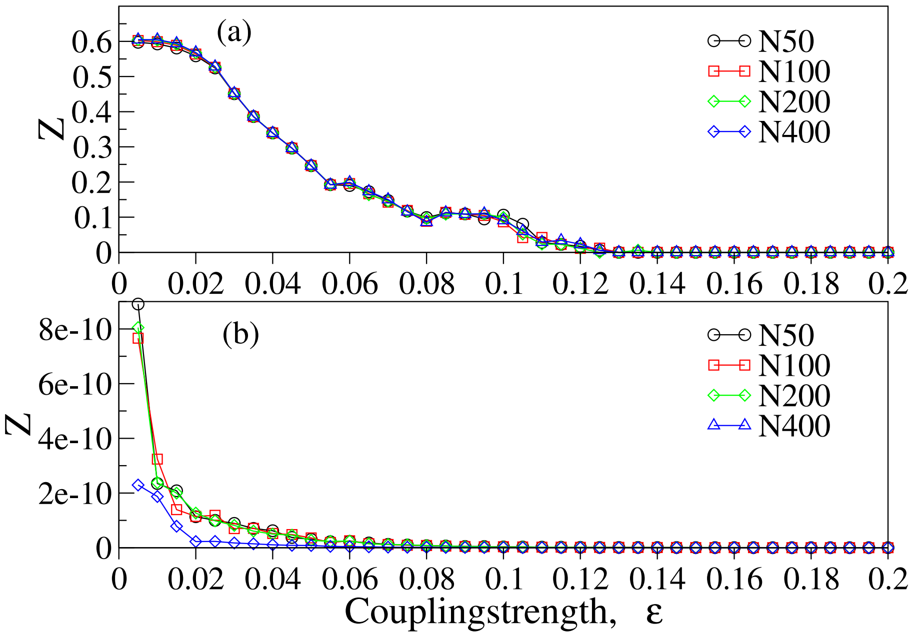

Figure 5.1: Plot of Synchronization error, Z, (defined by Eq. (5.2)) vs. coupling strength ϵ for the case where groups **A** and **B** are in the same dynamical domain, and the strength of intra and inter group coupling is the same (namely global coupling) i.e., $\epsilon_1 = \epsilon_2 = \epsilon$. The case of the groups of neurons in the (a) chaotic regime, (b) periodic regime, for various system sizes N, are displayed. Here the synchronization error is obtained by averaging over 1000 iterations after transience, and then further averaged over 10 realizations.

periodic group does not induce synchrony, and the chaotic neurons remain desynchronized. Also their temporal behavior is chaotic with Lyapunov exponents similar to that of an uncoupled single chaotic neuron. As the chaotic group grows bigger, synchronization sets in, and one obtains various clusters of synchronized elements. Finally, when the chaotic group is in a clear majority and is coupled to a small periodic group, we get complete synchronization. Further, the temporal behavior of the chaotic neurons gets more regular as the chaotic group grows larger and the periodic group grows smaller, with the Lyapunov exponents of typical elements in the chaotic group being closer to zero when $N_c > N_p$.

Interestingly then, the synchronized periodic population has a de-synchronizing effect on the chaotic group, when it is in the majority, as mentioned above. However, when the periodic group is in a minority, the coupled chaotic group synchronizes. This is demonstrated quantitatively through the synchronization error parameter Z, displayed in Fig. 5.3.

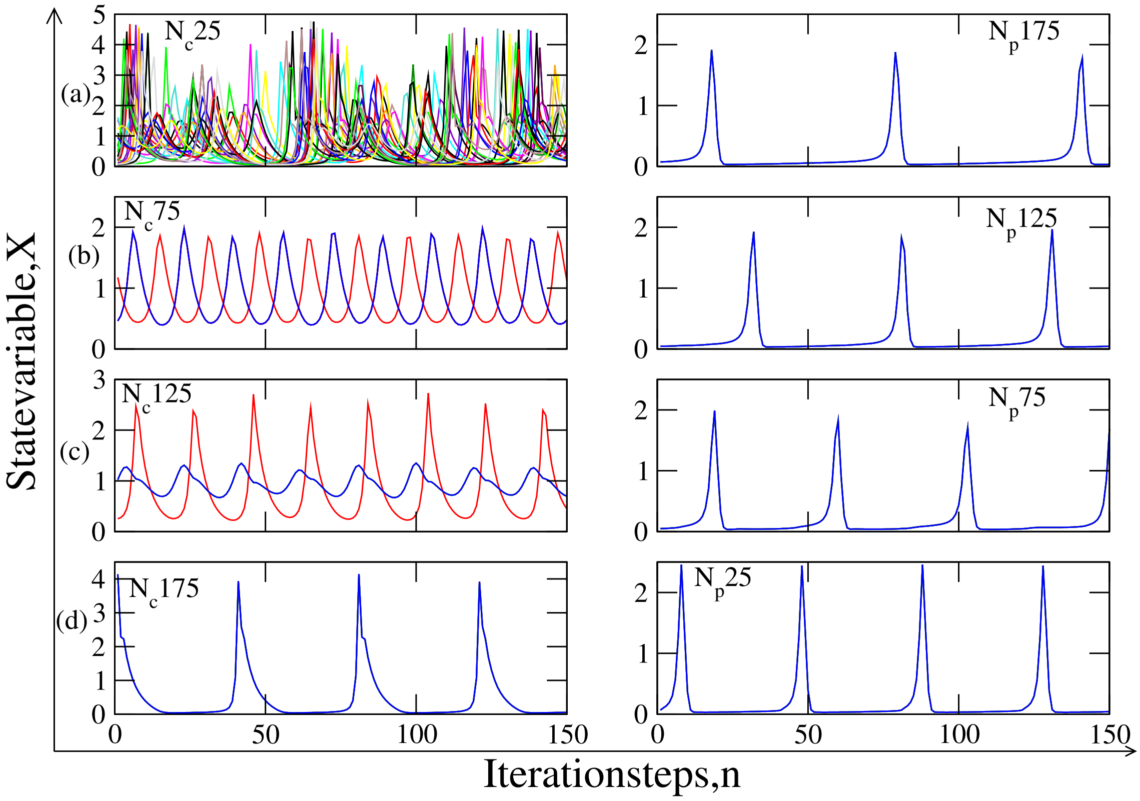

Figure 5.2: Time series of two interacting populations: one chaotic (shown in left column) and the other periodic (shown in the right column), displaying different levels of synchronization in the chaotic group, for (a) $N_c = 25$, $N_p = 175$ (b) $N_c = 75$, $N_p = 125$ (c) $N_c = 125$, $N_p = 75$ and (d) $N_c = 175$, $N_p = 25$, where N_c is the number of elements of the chaotic group and N_p is the number of elements in the periodic group. Here the inter-group coupling strength ϵ_2 is 0.01, and the intra-group coupling strength ϵ_1 is 0.15.

So, synchronization is crucially dependent on the relative sizes of the interacting subpopulations. Importantly, small periodic groups coupled to large chaotic groups yield complete synchronization within the groups, while a majority periodic group when coupled strongly to a chaotic minority group desynchronizes it.

Notice that the chaotic group, when un-synchronized, evolves to three qualitatively different clustering patterns. First, we have anti-phase clusters, as shown in Fig. 5.2(b) where the group splits into two subgroups that appear to be in opposite phase with respect to each other. This cluster is found only when the chaotic elements are in a minority. Further, one can define the strength or intensity of synchronization as the number of oscillators in the largest synchronized cluster [72, 118]. In the case of anti-phase clusters we have this

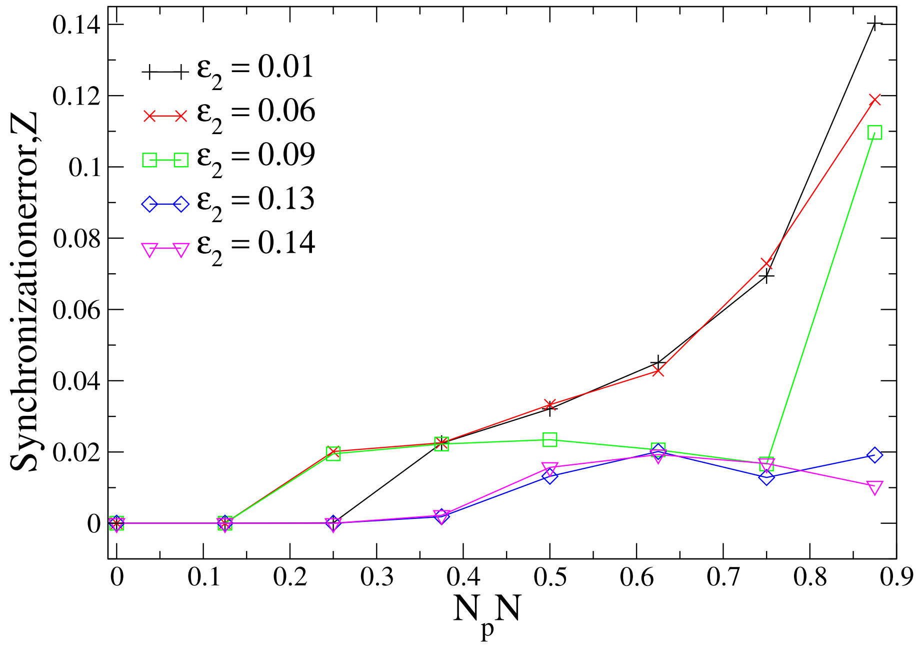

Figure 5.3: Synchronization Error Z of the chaotic sub-population of N_c elements, coupled to a periodic group of size N_p (where $N_c + N_p = N$), with respect to the fraction N_p/N. Here the intra-group coupling strength, ϵ_1 is equal to 0.15. Note that the chaotic sub-population synchronizes when coupled to a minority periodic group. However, counter-intuitively, a large periodic group cannot induce synchronization in a small chaotic group.

intensity roughly equal to 0.5

The other type of clustering observed in the chaotic group, is shown in Fig. 5.2(c). It too has two subgroups. But the amplitude and phase of the subgroups have no particular relation. This cluster is found when the size of the chaotic group is larger than the periodic group. For such two-state clusters, the intensity of synchronization is observed to be roughly 0.66 – 0.75.

Lastly, there is the fully synchronized cluster shown in Fig. 5.2(d). Here all the elements in the sub-groups are synchronized within their groups. Such a state is found for large inter-group coupling strengths ϵ_2, as well as for relatively large chaotic sub-populations, namely when N_c is much larger than N_p.

Interacting groups in the same dynamical regime:

Now we consider the case where the interacting sub-populations **A** and **B** have qualita-

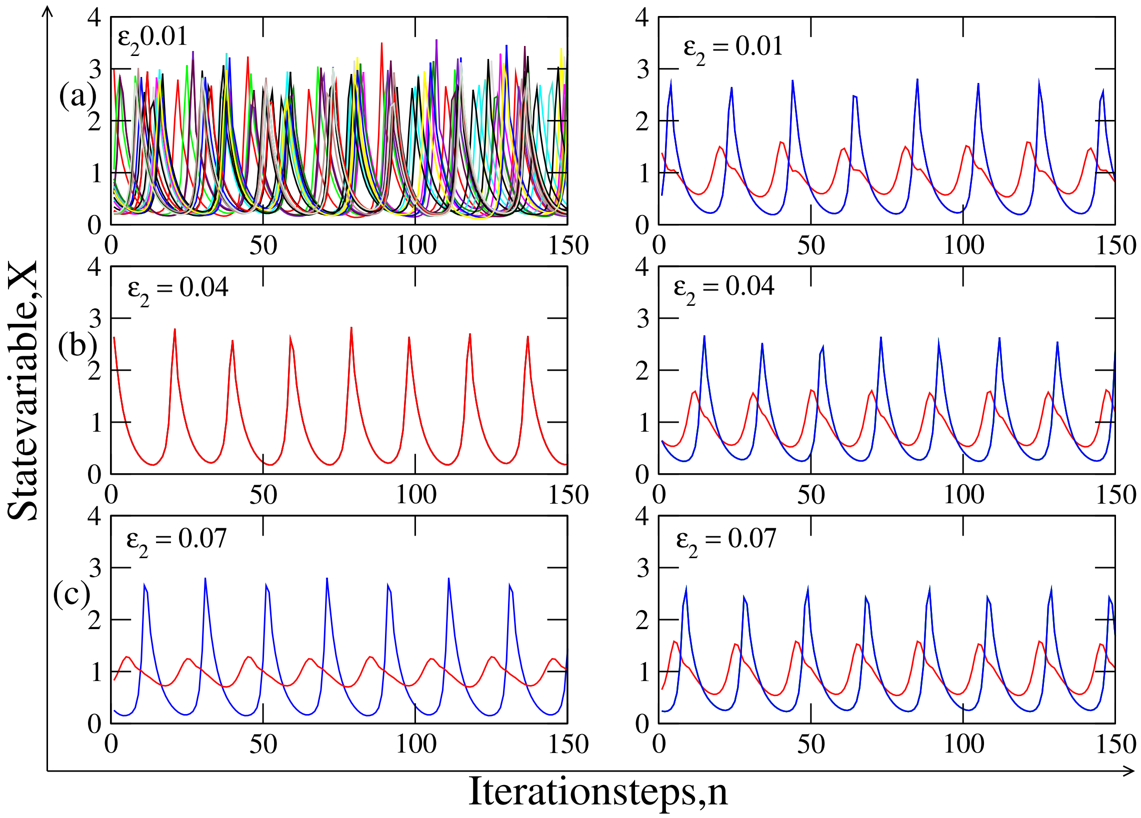

Figure 5.4: Time series of the two interacting chaotic populations for various inter-group coupling strength, ϵ_2, displaying different clusters in each group. The dynamics of the elements in the minority group (size 25) are shown in the left column, while those of the majority group (size 175) are shown in the right column. Here $\epsilon_1 = 0.15$.

tively same intrinsic dynamics, namely both groups are chaotic, or both are periodic. The only difference between the groups is that the initial states of the two groups lie in different bands. [1] Again, the intra-group coupling strength ϵ_1 is fixed at 0.15, and we vary the sizes of the two groups and their inter-group coupling strength, ϵ_2, in the range $0 - 0.15$.

Chaotic (A) and Chaotic (B):

We start with the case where one group has 25 elements, and the other 175, namely the minority group is much smaller than the majority group, i.e. the partitioning of the population is very imbalanced. Here we observe the following: For very small inter-group coupling strength ϵ_2, the minority group gets desynchronized, while the majority group

---

[1] For group **A**, we have taken the initial condition from a uniform distribution [0, 2.5] for the fast variable x and [0.7, 1.55] for the slow recovery variable y. Similarly, for the group **B**, the initial condition are drawn from a uniform distribution [2.5, 5] for the fast variable x and [1.55, 2.4] for the slow recovery variable y, thus covering the whole phase space of the chaotic regime.

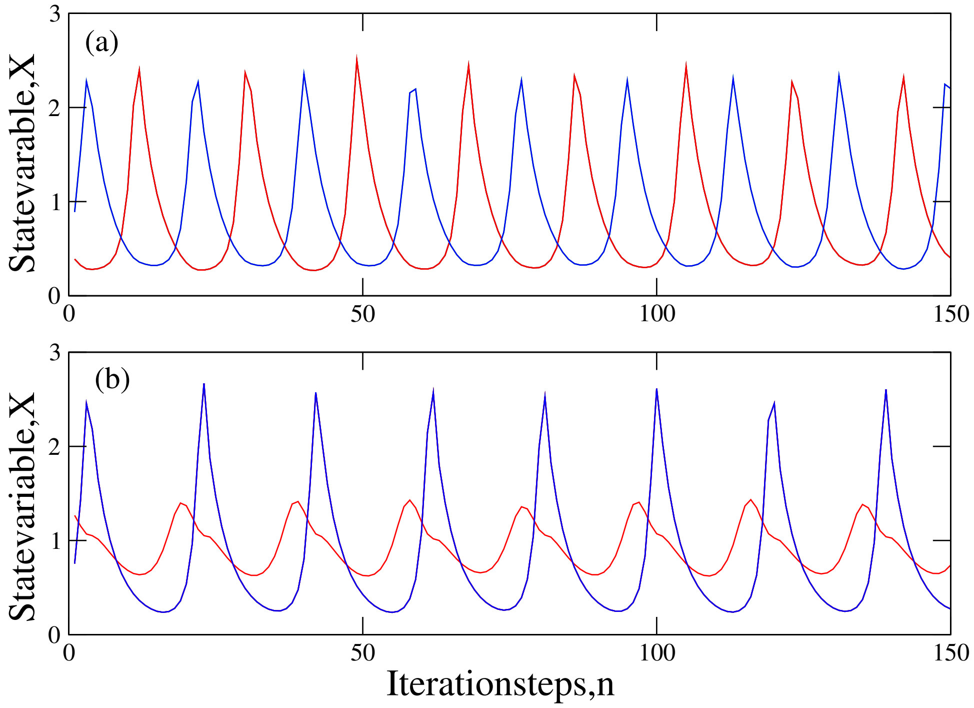

Figure 5.5: Time series of neurons in two interacting chaotic populations, for inter-group coupling strength, $\epsilon_2 = 0.01$, showing (a) anti-phase clusters in the minority population (size 50), and (b) a two state cluster in the majority population (size 150). Here $\epsilon_1 = 0.15$.

splits into two subgroups as shown in Fig. 5.4(a). Further increase in the value of ϵ_2 does not effect the larger group, but the smaller group first synchronizes within itself and then also splits into two subgroups, as shown in the Fig. 5.4(b) and Fig. 5.4(c). Finally, for $\epsilon_2 > 0.1$, the two groups are completely synchronized, as anticipated from Fig. 5.1(a).

Now we consider the population partitioned into minority and majority groups, but with less imbalance in the size of the groups, for instance, when the two groups have 50 and 150 elements respectively. In such an interactive ensemble we observe that for small inter-group coupling strength, ϵ_2, the smaller group splits into two subgroups as displayed in Fig. 5.5, with the two sub-groups being in opposite phase. The larger group also splits into two sub-groups with differing amplitude and phase (but with no clear relation between the phases of the two clusters).

Increasing the inter-group coupling strength between the two sub-populations leads to synchronization in the smaller group, while the larger group again splits into two sub-

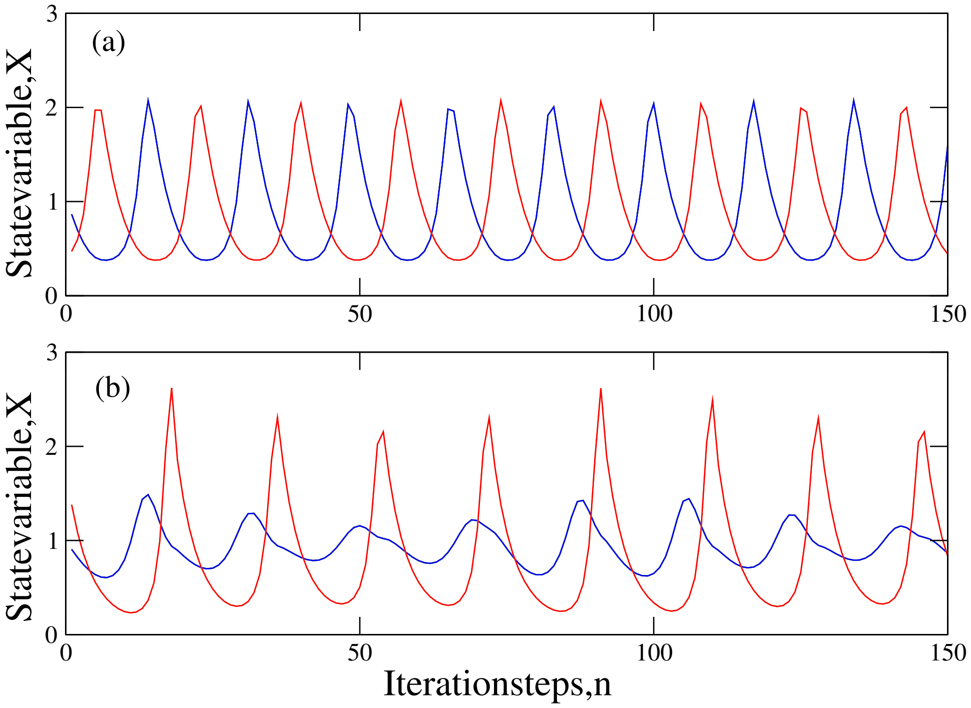

Figure 5.6: Time series of the two equipartitioned chaotic populations displaying different clusters for the inter-group coupling strength, (a) $\epsilon_2 = 0.01$, (b) $\epsilon_2 = 0.09$. Here, $N = 200$ and $\epsilon_1 = 0.14$.

groups. Further increase in ϵ_2 shows the same route of synchrony among the two groups, as found in the strongly imbalanced case above.

When the chaotic groups are equipartitioned, each group synchronizes within itself. However, the two groups are out-of-phase with respect to each other for low coupling strength. For instance for $\epsilon_2 = 0.01$ the two groups are approximately anti-phase, and for larger inter-group coupling such as $\epsilon_2 = 0.09$ the groups get closer in phase, while still remaining distinct. Further note that the amplitude of the two groups get increasingly different, as ϵ_2 increases, i.e. one group oscillates with high amplitude while the other has low amplitude. The representative of above features can be seen in Fig. 5.6. Lastly, for sufficiently high ϵ_2 one obtains complete synchronization, as is anticipated from Fig. 5.1(a).

Periodic (A) and Periodic (B): For this case, we have only one cluster, namely synchronized cluster, as the periodic group synchronizes at very low global coupling strengths.

5.3 Conclusion

In summary, we studied the spatiotemporal dynamics of coupled groups of neurons, where the groups have varying sizes and possess different intrinsic dynamics, ranging from periodic to chaotic. Here the inter-group coupling interaction is effectively like a dynamic signal from a dynamically different sub-population. We observe that this coupled system yields a wide variety of clustering patterns, ranging from different distinct groups of synchronized clusters to anti-phase clusters, determined by the interplay of the relative sizes and dynamics of the interacting groups.

Interestingly, we found that, when a large periodic group couples to a small chaotic group, it induces desynchronization in the chaotic minority, while coupling to a small group of periodic elements can lead to synchronization within the chaotic majority group. So, our results suggest that a small periodic group can be very effective in inducing synchrony within a large chaotic group. This is reminiscent of event-related synchronization/desynchronization in complex networks, which underlies biological phenomena ranging from Attention Deficit/Hyperactivity Disorder to desynchronization of delta oscillations during light anesthesia.

Chapter 6

Enhancement of diversity induced coherence under dynamic random links

In this chapter, we study the effect of diversity and random connections on the temporal regularity in spike events of the model neurons in a coupled neuronal populations. Here we are addressing the two complexity classes together, namely, *parametric heterogeneity* and *network evolution*.

Naturally, in an spatially extended system the constituent elements may differ from each other. So, many studies have been devoted to study the constructive role of parametric heterogeneity which is present at the nodal level. For example, it is found that the spatiotemporal chaos in an array of coupled pendulums can be tamed by optimal magnitude of disorder, induced by disparity in pendulum lengths [76, 77]. This type of heterogeneity can be considered as a noise which is quenched in time. It is also found that the emerging phenomena in these systems are quite similar to noise induced resonance phenomena [38, 79], in a spatially extended system. For example, Tessone *et. al.* have found that different sources of diversity, such as those represented by quenched disorder or noise, can induce a resonant collective behavior in an ensemble of coupled bistable or excitable systems [78]. This resonance like behavior is termed as diversity induced resonance. Thus, diversity is playing a role similar to that of the noise.

Also, in various naturally occurring network topologies, the coupling between the nodes in the network may change over time [73, 74, 75], especially in social and biological networks. The constructive effects of noise has been considered for these networks. For example, for diffusively coupled FitzHugh-Nagumo model neurons, coherence resonance is induced by rewiring [123]. Also, fast random rewiring and strong connectivity is found to impair sub-threshold signal detection in excitable networks [124].

In this chapter, we aim to study the effect of both random connections and diversity on resonant collective behavior for an extended system. Specifically, we consider a one dimensional coupled map lattice (**CML**) with neuronal dynamics at its node and some degree of randomness in spatial coupling. CML is chosen as it not only captures the essential features of an extended system [31] but also is computationally more efficient. Previously, diversity-induced coherence resonance is found for a coupled map based neuron system [125]. Also, the noise- and topology-induced resonance phenomena in two-dimensional map-based neural networks have been also reported [126, 127]. As discussed earlier, diversity plays a similar role to that of noise, it will be interesting to study its effect on coherent motion of spikes in a lattice which have some degree of randomness in spatial coupling. Now, the link between two randomly chosen sites in a network can be either static or dynamic. The static links are invariant throughout the system evolution whereas the dynamic links imply that the random links are switched throughout the evolution [75]. We will investigate the effect of both types of random connections and the diversity of elements in the lattice on the temporal order in firing of the coupled neurons.

Our principal question is the following:

(i) do random links enhance diversity-induced temporal coherence in neuronal networks?

(ii) is there any significant distinction in temporal coherence for a network with dynamic (switched) random connections and one where the random links are quenched (or static)?

In this chapter we will first describe the mathematical model and the order parameter for the system, which measures the temporal regularity in spiking of model neurons in the network. After this we will present the numerical results and at last, we summarize our findings.

6.1 Model and method

We consider networks of diffusively coupled elements with the nodal dynamics given by a map, which is introduced by Rulkov [88]. This map captures all the essential feature of neuronal dynamics ranging from regular spiking to self-sustained chaotic bursting as discussed in Chapter 2. Temporal evolution of these coupled elements are described by the following sets of equations,

$$x_{n+1}(i) = f_\alpha[x_n(i), x_{n-1}(i), y_n(i) + \beta_n(i)], \tag{6.1a}$$

$$y_{n+1}(i) = y_n(i) - \mu(x_n(i) + 1) + \mu\sigma(i), \tag{6.1b}$$

where, i $(= 1, \ldots, N)$ is the cite index, N is the total number of elements in the lattice, and n is the discrete time index. Also, $x_n(i)$ is a fast variable which represents membrane potential and $y_n(i)$ is a slow variable. $\beta_n(i)$ represent external input. $f_\alpha(x, x', y + \beta)$ is a piecewise nonlinear function which is designed to shape spiking oscillations in fast subsystems. It contains three intervals which can be described as follows,

$$f_\alpha(x, x', y + \beta) = \begin{cases} \frac{\alpha}{1-x} + y & \text{for} \quad x \leq 0 \text{ and } x' \leq 0, \\ \alpha + y & \text{for} \quad 0 < x < \alpha + y \text{ and } x' \leq 0, \\ -1 & \text{for} \quad x \geq \alpha + y \text{ and } x' > 0. \end{cases} \tag{6.2}$$

α and σ are the control parameter of the map. As discussed in Chapter 2, in the absence of external input, i.e., for $\beta = 0$, the map generates spikes, if $\sigma > \sigma_{th} = 2 - \sqrt{\alpha}$, for the α value less than 4.0, else stays in a silent state. For $\alpha > 4$ we have bursts of spikes including both periodic and chaotic bursting. In this work, the value of α is fixed and diversity in the lattice is introduced through the parameter σ. The values of $\sigma(i)$ for the cite i is taken from a Gaussian distribution with mean σ_0 and variance D^2. Thus, D measures the diversity in the system. It is prevalent to study the excitable systems in such a parameter regime which is close to a bifurcation point. So, through diversity the system can be pushed from above or below the threshold [78].

The external signal or coupling term for this network is,

$$\beta_n(i) = \frac{\epsilon}{2}[x_n(\xi) + x_n(\eta) - 2x_n(i)], \tag{6.3}$$

where, ϵ is the strength of diffusive coupling. $\xi = (i + 1)$ and $\eta = (i - 1)$ for the nearest neighbor coupling (with periodic boundary conditions). For random connections, we consider the situation where a fraction, p, of randomly chosen sites in this lattice are coupled to other random sites, instead of their nearest neighbors, i.e., ξ and η are random sites. Clearly, the topology of the network can be changed by adjusting rewiring probability parameter, p. For regular networks (nearest neighbor coupling), $p = 0$ and for completely random network, $p = 1$. Further, we consider two cases: (i) *static random connections*, where the random links in the system are *quenched* and do not change over time; (ii) *dynamic random connections* where the random links can switch at the time scale of the local map updates, namely the connectivity matrix changes at each instant n.

The temporal coherence of firing of neurons in the networks is usually measured by the distribution of the pulse interval, $S_k(i)$. For example, see Ref. [128, 129, 130]. The pulse interval is defined as, $S_k(i) = \tau_{k+1}(i) - \tau_k(i)$, where, $\tau_k(i)$ is the time of the kth spike in the ith neuron. The sharpness of the distribution is given by,

$$Z = \frac{\langle S_k(i)\rangle}{\sqrt{\langle [S_k(i)]^2\rangle - [\langle S_k(i)\rangle]^2}} \tag{6.4a}$$

$$\text{with, } [S_k(i)]^n = \frac{\sum_{i=1}^{N}\sum_{k=1}^{k_i}[S_k(i)]^n}{\sum_{i=1}^{N} k_i}, \tag{6.4b}$$

which, is the ratio of the average and the standard deviation of inter-spike interval and is a measure of coherence of spike events. Biologically, it is related to the timing precision of the information processing [128, 129, 130]. Larger values of Z imply a better temporal regularity of spikes. Also, Z is considered to be zero if all the neurons are in the silent state.

In this work, we investigate the effect of quenched and dynamic random links on the temporal regularity of spiking, under increasing diversity, in a network composed of inhomogeneous neurons. Now, the individual neurons will generate spikes if the value of the parameter $\sigma(i)$ is equal to or greater than the threshold value, $\sigma_{th} = 2 - \sqrt{\alpha}$. Here the parameter α of the nodal map is chosen to be 3.0, and so $\sigma_{th} \sim 0.268$. With no loss of generality, we consider a network of size $N = 500$, and in the network, σ_i of the constituent neurons is randomly distributed about an average value σ_0 with variance D^2, with $\sigma_0 = 0.25 < \sigma_{th}$. Since there are several neurons with $\sigma_i < \sigma_{th}$, an adequate level of diversity D is necessary in order to enable the active elements in the network to induce spiking behavior in the sub-threshold neurons.

In particular, we study the quantitative measure of temporal coherence Z, with respect to the following important parameters: (a) *measure of diversity*, D, (b) *coupling strength*, ϵ, and (c) *fraction of sites*, p with random (quenched or dynamic) links. Note that the value of Z is obtained by averaging over 100 different initial conditions. For each initial condition, the first 10^5 iterations (transience) are discarded and the subsequent 10^5 iterations are used for calculating Z.

6.2 Diversity-Induced Coherence

Representative cases of the temporal coherence of neuronal spikes for increasing diversity D, are shown in Figs. 6.1, 6.2 and 6.3. In all cases, it is clearly evident that temporal coherence in spiking increases with diversity up to an optimal level of diversity D =

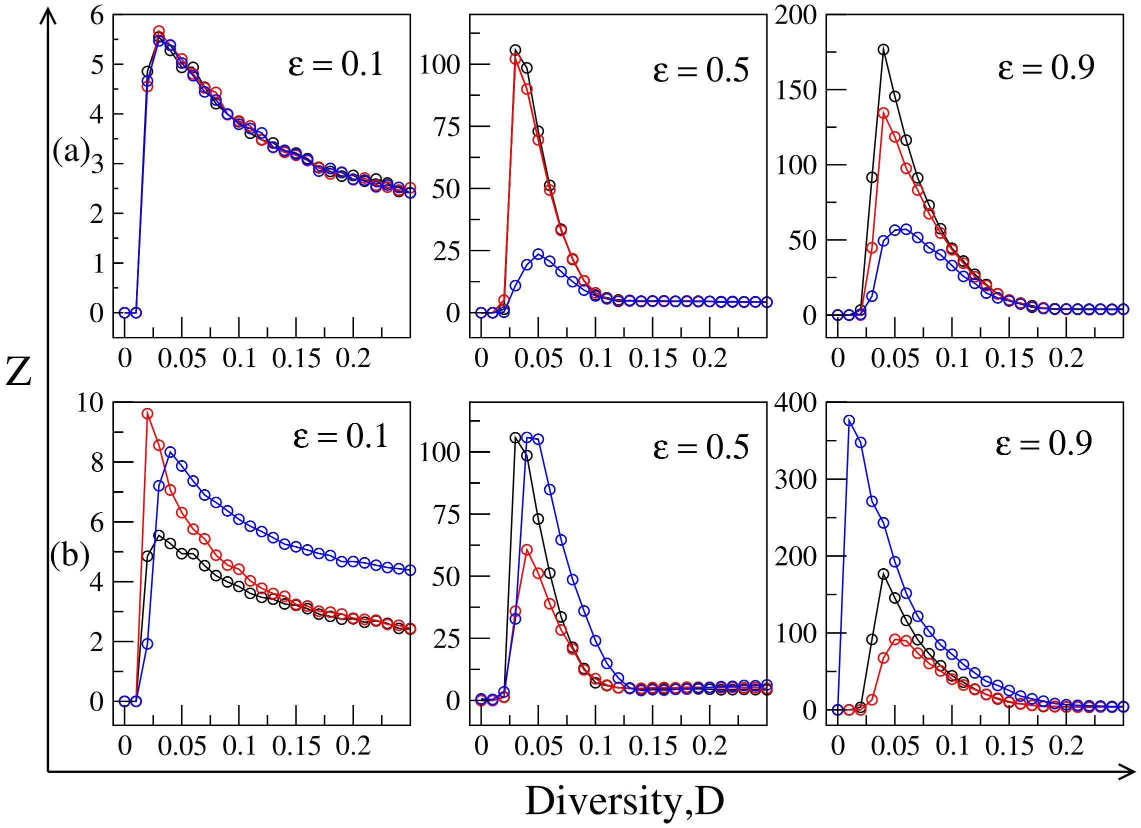

Figure 6.1: Temporal coherence, Z (defined by Eq. (6.4)) vs. Diversity, D, for different values of coupling strength, ϵ. Here the black curve represents regular nearest neighbor coupling, i.e., $p = 0$ case, while the red and the blue curves show results from networks with quenched and dynamics random links respectively, for the case of (top panels) $p = 1/N = 1/500$, and (bottom panels) $p = 0.9$. The other parameters are $N = 500$, $\alpha = 3.0$ and $\sigma_0 = 0.25$.

D_{opt}, where one attains the maximum coherence Z_{max}. After that, increasing diversity has a detrimental effect on coherence, and increasing D decreases the value of Z. This indicates that a moderate level of diversity is most conducive for temporal coherence in spike events. *This diversity induced coherence holds true in all kinds of coupling topologies, ranging from a one-dimensional ring to networks with varying fractions of quenched and dynamic random links.*

Also notice, when coupling is weak, regular coupling yields the highest degree of coherence. However when coupling is strong, larger fraction of random links enhance diversity induced coherence. Additionally, dynamic random links yield significantly higher levels of temporal coherence than quenched random connections. *So, our results demonstrate*

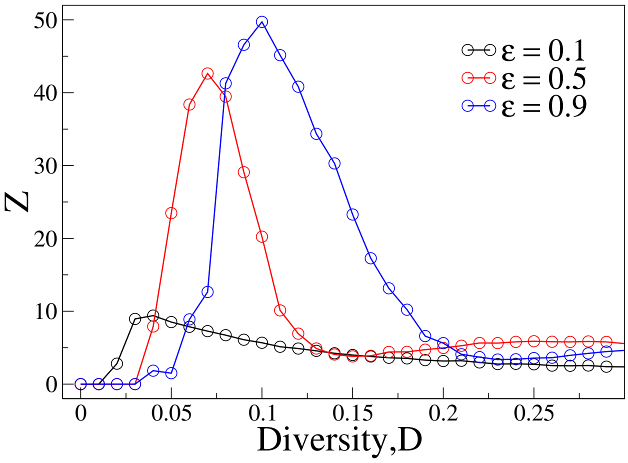

(a) Quenched random links

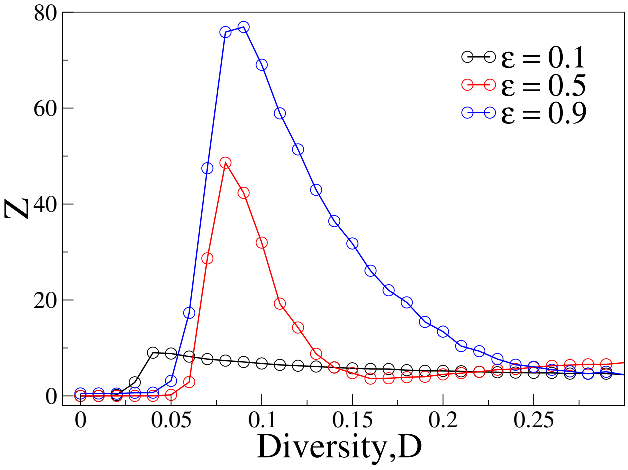

(b) Dynamic random links

Figure 6.2: Temporal coherence, Z vs Diversity, D, for (a) quenched random links and (b) dynamic random links, for different values of coupling strength ϵ. The rewiring probability, $p = 0.5$ for both cases, while the other parameters are $N = 500$, $\alpha = 3.0$ and $\sigma_0 = 0.25$

that the largest coherence in the spike events emerge when the coupling strength is high, and the underlying connections are mostly random and dynamically changing.

Further, Fig. 6.2 shows that more diversity is needed for optimal coherence when coupling is stronger. Namely, D_{opt} is larger for larger coupling strength ϵ. On the other hand, higher degree of randomness in connection entails that the diversity needed for maximal coherence is smaller. This is evident from Fig. 6.3, which shows decreasing D_{opt} with increasing p.

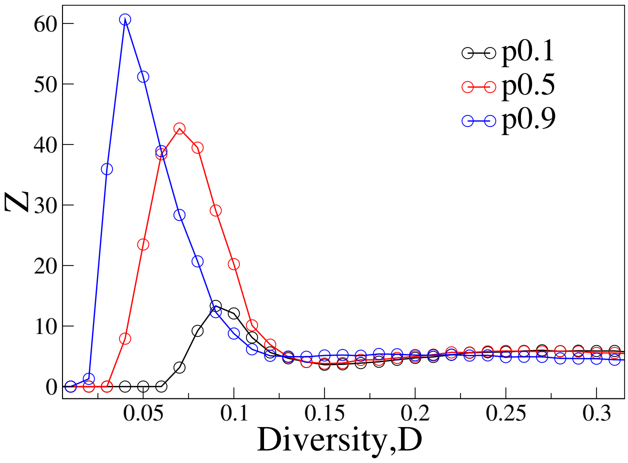

(a) Quenched random links

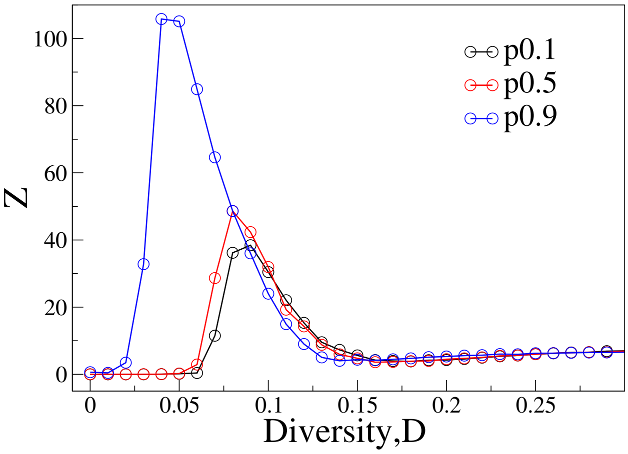

(b) Dynamic random links

Figure 6.3: Temporal coherence Z vs Diversity D, for (a) quenched random links and (b) dynamic random links, for different values of random rewiring probability p. Here, the coupling strength, $\epsilon = 0.5$ for both cases, and the other parameters are $N = 500$, $\alpha = 3.0$ and $\sigma_0 = 0.25$.

Now we investigate the value of Z_{max}, averaged over 10^2 realizations, for varying coupling strengths ϵ and fraction of random links p. This *quantitatively* captures the trends evident in the figures above.

The broad trend evident from Figs. 6.4 and 6.5 is that the maximal coherence that can be induced by diversity increases with increasing coupling strength ϵ and increasing degree of randomness in spatial connections. This implies that, for the optimal diversity, larger coupling strength and a more random network, helps the spiking neurons to induce activity in the silent neurons, enhancing temporal coherence in the system. Furthermore,

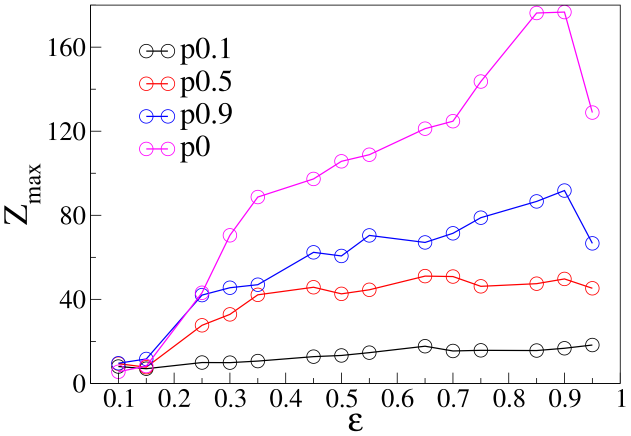

(a) Quenched Random Links

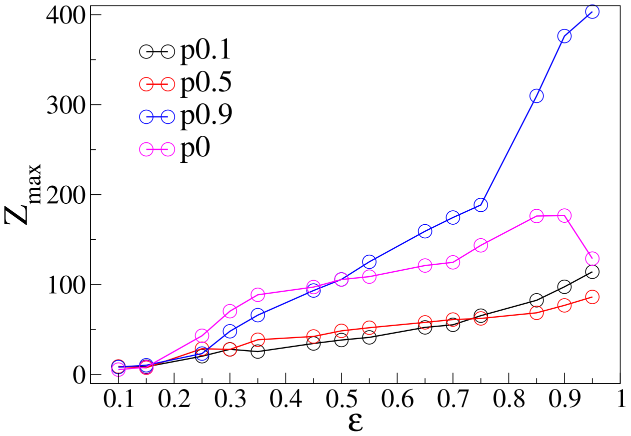

(b) Dynamic Random Links

Figure 6.4: Maximum temporal coherence, Z_{max} (see text) vs. coupling strength, ϵ, for the case of: (a) quenched random links and (b) dynamic random links. Here the $p = 0$ case, namely regular nearest neighbor coupling, is shown in both figures, for reference. The other parameters are $N = 500$, $\alpha = 3.0$ and $\sigma_0 = 0.25$.

comparing the values of Z_{max} clearly shows that *dynamic links are significantly more conducive to temporal coherence than quenched random links*. Namely, there is a marked increase in the temporal coherence of spikes in strongly coupled systems, with large number of random links. Specifically, the optimal coherence that can be achieved, i.e., Z_{max}, is *quadrupled* for dynamic links, as compared with quenched connections, for large rewiring probability, p and coupling strength, ϵ.

Lastly, for quenched random links, the dependence of the maximum temporal coherence on p, differs from the case of dynamic links for high p. Now the value of Z_{max} increases to an optimal value (e.g. $p \sim 0.85$ for $\epsilon = 0.9$, as seen in Fig. 6.5a), and then decreases as the

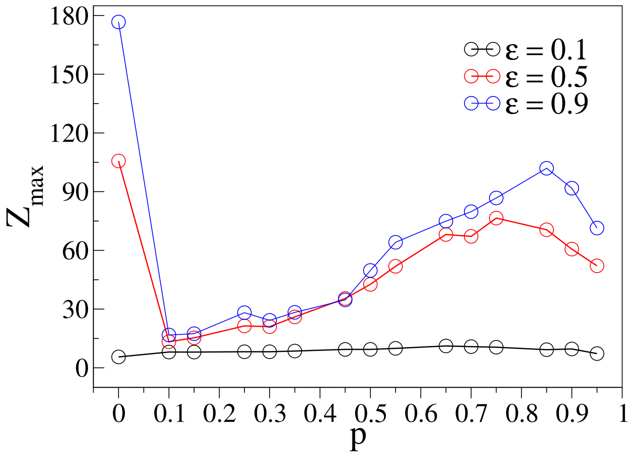

(a) Quenched Random Links

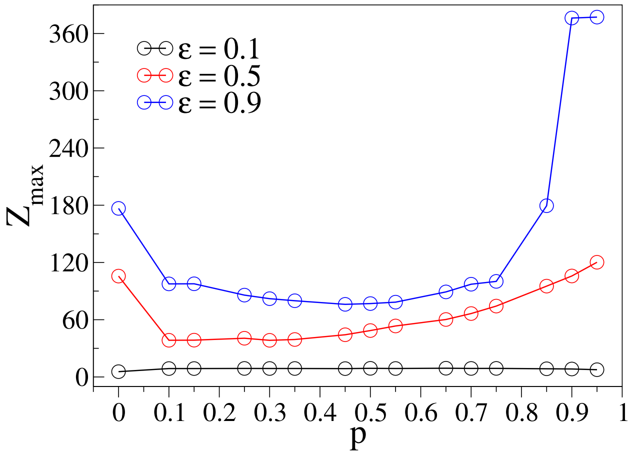

(b) Dynamic Random Links

Figure 6.5: Maximum temporal coherence Z_{max} (see text) vs. random rewiring probability, p, for different values of coupling strength, ϵ, for the case of (a) quenched random links and (b) dynamic random links. The points for $p = 0$ represents the value of Z_{max} for each ϵ in nearest neighbor coupling and are included for the reference. The other parameters are $N = 500$, $\alpha = 3.0$, and $\sigma_0 = 0.25$.

value of p increases further. This non-monotonic dependence of Z_{max} indicates that too many quenched random links actually hinder coherent spiking. This is unlike dynamic links, where increasing the fraction of random links continues to aid coherence.

6.3 Summary

In conclusion, we investigated the effect of diversity and random connections on the behavior of a spatially extended system, which is locally modeled by a non-linear map mimicking neuronal dynamics. We find diversity induced coherence in the spike events, with an optimal amount of parametric heterogeneity at the nodal level yielding the greatest regularity in the spike train. Further, we investigate the system under random spatial connections, where the links are both dynamic and quenched, and in all cases we observe diversity induced coherence. We quantitatively find the effect of coupling strength, and random rewiring probability, on the optimal coherence that can be achieved under diversity. Our results indicate that the largest coherence in the spike events emerge when the coupling strength is high, and the underlying connections are mostly random and dynamically changing.

Chapter 7

Pattern formation in arrays of chemical oscillators

In this Chapter, we will describe a simple model mimicking diffusively coupled chemical micro-oscillators. Here, our aim is to characterize the rich variety of dynamical states or spatiotemporal patterns which emerge from the model under variation of time delay in coupling, coupling strength and boundary conditions.

As we have discussed in Chapter 3 that a population of coupled nonlinear oscillators have been used to describe a broad class of self-organizing phenomena, ranging from biological systems such as groups of fireflies [20], to chemical and physical systems such as coupled oscillatory chemically reacting cells [21] and Josephson junction circuits [26]. An ensemble of identical oscillators can generate a variety of spatiotemporal patterns under varying coupling connections and different constituent oscillators. The new rhythms generated by these ensembles can differ in time period as well as in the phase relations among the constituent oscillators [18, 19].

Apart from these rhythms, we can also have coupling dependent quenching of oscillation. These come under the two classes: Oscillation Death (**OD**) and Amplitude Death (**AD**). OD was first found in two identical Brusselators coupled via a slow recovery variable by

Prigogine and Lefever [103]. In this system, the interactions break the symmetry and we have stable InHomogeneous Steady States (**IHSS**), i.e., the steady states for oscillators are not identical and hence the name IHSS [131, 132, 133, 134, 135]. It was found that this phenomenon is model independent and occurs in several other models of diffusively coupled chemical [132, 136, 137] and biological oscillators [138]. The important thing to note here is that OD is always accompanied by a stable synchronous solution [133, 137].

Amplitude Death (AD) results in a Homogeneous Steady State, where all oscillators go to identical steady states [139, 140]. Therefore, these two are different from each other, as one emerges from symmetry breaking phenomenon, while the other preserves symmetry. AD was found to be stable under delayed coupling as well [141, 142].

Now, time-delay is both natural and inevitable when considering interactions among systems that are spatially separated. From a mathematical point of view, time-delay makes the dynamical system effectively infinite-dimensional: this can open up a range of timescales, interactions, and novel dynamical behavior such as amplitude death [141, 142] and the phase-flip bifurcation [143, 144].

In phase flip, for suitable values of system parameters and delay, the relative phase between the oscillators changes abruptly from zero to π or vice versa. This is also accompanied by a discontinuous change in the frequency of the synchronized oscillators, as well as in the spectrum of Lyapunov exponents. In addition, delay offers an additional parameter that can be varied, and if exogenous, can provide a suitable means of effecting control.

Our study here draws its motivation from experiments of diffusively coupled chemical oscillators in micro-fluidic assemblies [145, 146, 147]. These experiments have nanoliter volume aqueous drops containing reactants of the oscillating reaction, separated by gaps containing typically octane. A variety of dynamics was observed in such systems, most notably in-phase and anti-phase synchronization [148, 17].

Motivated by these recent experiments, here we seek a simple model capable of showing the observed spatiotemporal patterns. In our model the physical gap between the "droplets" of chemical oscillators gives rise to a delay in the coupling interaction between them. So we mimic the micro-fluidic array by a delay-coupled array of oscillatory chemical systems. Our basic aim is to understand the patterns in time and space that arises in such arrays under varying forms of coupling.

The organization of this chapter is as follows: First, we discuss the model and describe the different forms of coupling and different boundary conditions for the array. Then we go on to show how in-phase and anti-phase oscillations can result from a delay in the coupling, which is proportional to the size of the gaps between the chemical reaction droplets.

7.1 Array of brusselator cells

Most chemical and biological processes are best described by relaxation oscillators with a strong nonlinear vector field [149, 150, 151, 152, 153]. Here we choose a brusselator to model the chemical reaction in the beads. The principal motivation to choose the Brusselator is that it originates from the description of a realistic chemical reaction [98]. A single cell Brusselator is described by the Eq. (2.14). In this work, we have taken $a = 2.0$ and $b = 5.5$. For these parameter values, we are in the periodic regime as discussed in Chapter 2.

We will now study N identical coupled brusselators in an array, forming a reaction-diffusion system. At first we assume that there is only nearest neighbor coupling and it is bidirectional in nature. The coupling between the two oscillators is directly proportional to the difference between the concentration of their respective species. The diffusion constant of the first species, x, is very small compared to the second species, y, and hence taken to be zero. This assumption is justified for the relaxation systems, as inhomogeneous solutions are destroyed by coupling through the fast variable thus affecting the most sensitive slow part of the cycle [134, 133, 154].

Like most natural systems the mass of chemical species is transmitted from one site to another with finite velocity, which makes delay coupling appropriate in this system. When all the assumptions mentioned above are taken into account, the dynamics of an array comprising of N droplets is given by $2N$ differential equations:

$$\begin{aligned} \dot{x}_i &= f_1(x_i, y_i), \\ \dot{y}_i &= f_2(x_i, y_i) + \frac{\epsilon}{2}(y_{i+1}(\tau) + y_{i-1}(\tau) - 2y_i), \end{aligned} \tag{7.1}$$

for $i = 1, \cdots, N$. Here ϵ is the coupling strength. The function $f_1(x, y)$ and $f_2(x, y)$ are given by Eq. (2.14). The value of y_0 and y_{N+1} will depend on the boundary condition. Here, $y_i(\tau)$ is the concentration of the ith cell at the delayed instant $(t - \tau)$.

We consider the following different boundary conditions and coupling forms for the array:

(i) $y_0 = 0$ and $y_{N+1} = 0$ for all times t, namely, constant concentration boundary conditions

(ii) $y_1 - y_0 = 0$ and $y_N - y_{N+1} = 0$ for all times t, namely, zero flux boundary conditions

(iii) Boundary cells are coupled to their own delayed species concentration

(iv) Periodic boundary condition

In this chapter, we investigate this system through extensive numerics. First, we study the array under diffusive coupling without delay,namely $\tau = 0$. Then, we go on to study the effects of delay in the coupling. Here, the total number of cells in the system is taken to be 12. At last, we will study the IHSS for a system with a smaller number of cells.

7.2 Coupling without Delay

We now describe below the phenomenology of an array of brusselator cells coupled without delay, under different boundary conditions.

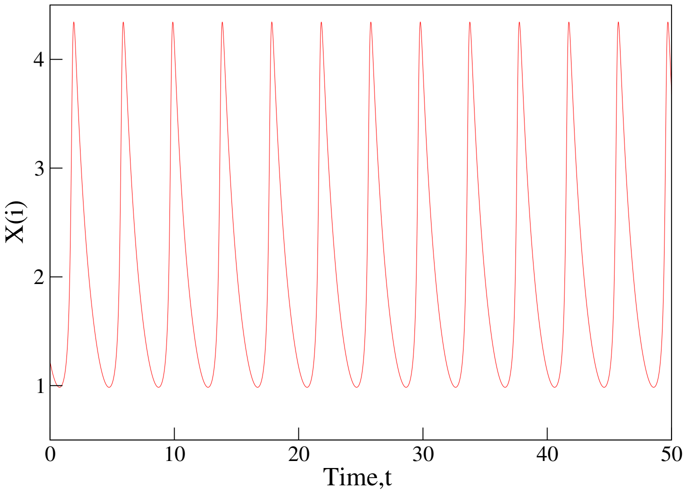

(a) Time series of Fast variable for $\epsilon = 0.05$

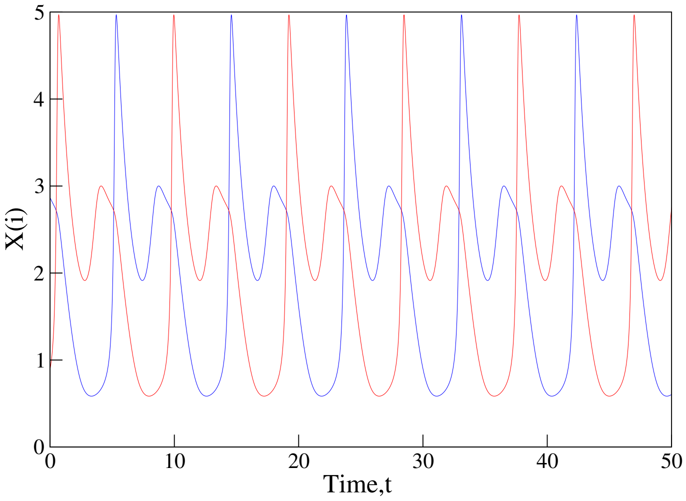

(b) Time series of Fast variable for $\epsilon = 0.2$

Figure 7.1: Plots showing synchronization and synchronized clusters in the system for zero flux boundary condition.

7.2.1 Zero flux Boundary Conditions

At first, we consider Zero flux boundary conditions. Here, under weak coupling, for instance $\epsilon = 0.05$, there is synchrony among all the cells in the array. An increase in the value of coupling strength ϵ leads first to desynchronization of all the cells and finally, for $\epsilon \sim 0.2$ the array evolves to *two synchronized clusters* as shown in the Fig. 7.1.

Further increase in the coupling leads first to desynchronization of the clusters, and then to oscillation death at $\epsilon \sim 0.4$. In the OD regime the whole array goes to *inhomogeneous*

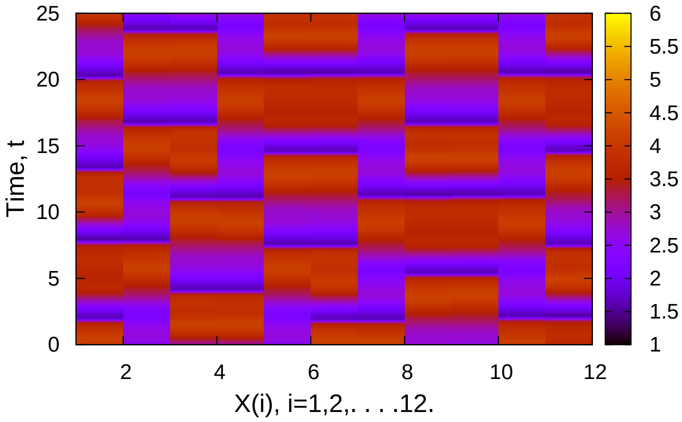

(a) Space time Plot of Fast variable, $\epsilon = 0.30$

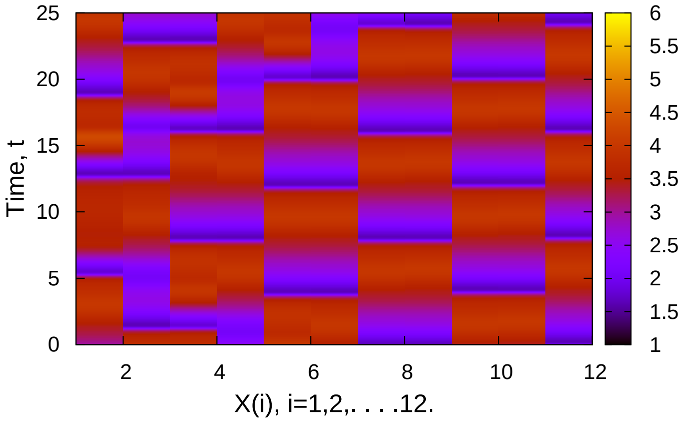

(b) Space time Plot of Fast variable, $\epsilon = 0.35$

Figure 7.2: Plots showing the process of desynchronization for zero flux boundary condition.

fixed points (IHSS), and the number of distinct IHSS depends on coupling strength. For instance, we have two IHSS for $\epsilon = 0.4$, four IHSS for $\epsilon = 0.45$ and six IHSS for $\epsilon = 0.50 - 0.55$.

In the process of desynchronization almost all the cells oscillate very differently from each other, displaying both large amplitude oscillations (visible as yellow in Fig. 7.2) and small amplitude oscillations (visible as red in the same figure). As coupling strength increases these differences get more pronounced.

For $\epsilon = 0.6$, we have complex dynamics, which we describe as *Mixed Dynamics*. Here the dynamical behavior of the different cells is quite different: some cells in the array oscillate (with varying amplitudes and frequencies), while the others experience oscillation death

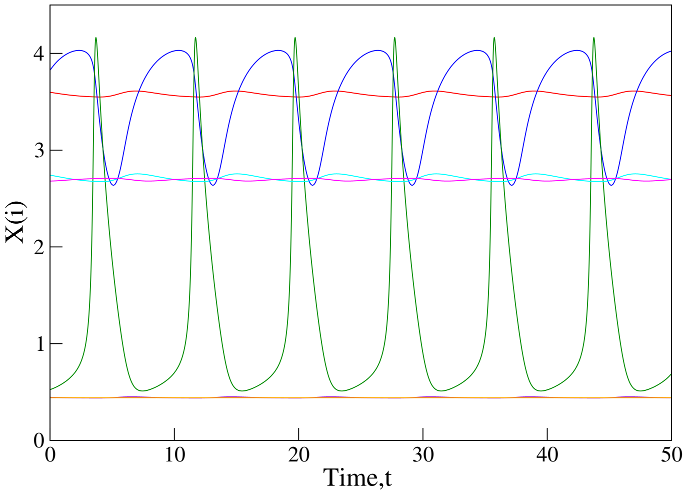

(a) Time series of Fast variable, $\epsilon = 0.6$

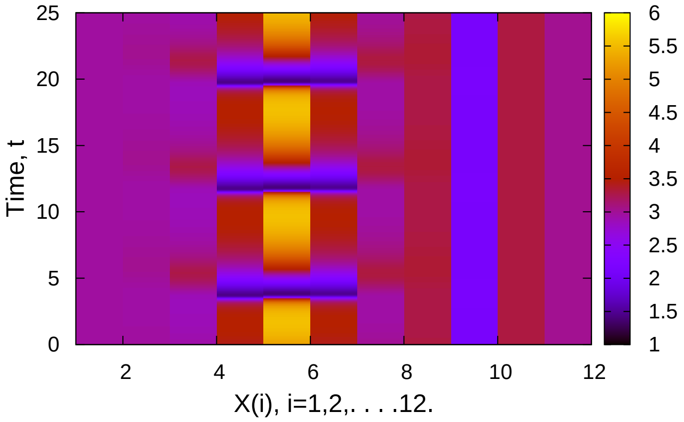

(b) Space-Time Plot of Fast variable, $\epsilon = 0.6$

Figure 7.3: Plots showing Oscillation Death and Mixed Oscillation in the system for zero flux boundary condition.

and settle down to fixed points. Both time series and spatiotemporal plot of the fast variable in this dynamical regime, are shown in Fig. 7.3.

For coupling strengths greater than 0.65 all the cells settle down to fixed points. The number of distinct fixed points depends on the value of ϵ again. For instance, in the ϵ range $0.70 - 0.80$ we have two fixed points, while for $\epsilon = 0.85$ we have seven fixed points.

In summary, we have oscillation death in the ϵ range $0.40 - 0.55$ and $0.67 - 1.0$. For ϵ value in between these two ranges we have complex mixed behavior, combining fixed points and oscillations of varying amplitudes and frequencies.

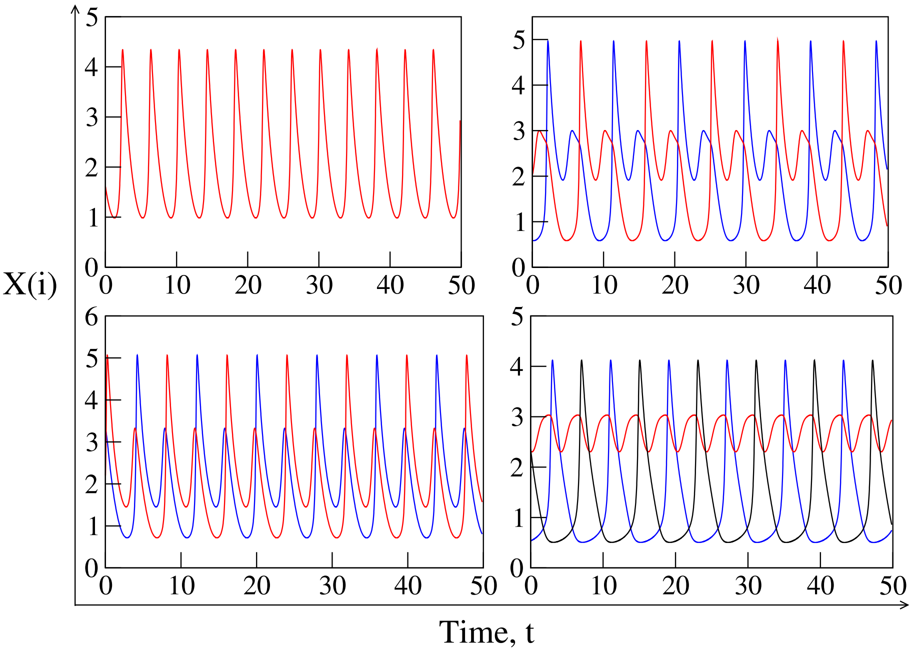

Figure 7.4: Space time plots for $\epsilon = 0.05$ (top left), $\epsilon = 0.10$ (bottom left), $\epsilon = 0.20$ (top right) and $\epsilon = 0.35$ (bottom right) showing the route from synchronization to formation of clusters as the value of ϵ is increased, for Periodic Boundary condition.

7.2.2 Periodic Boundary Conditions

Here, for low coupling all the cells are in synchrony, as can be seen in Fig. 7.4 (top left). As the value of coupling strength ϵ is increased, the cells show high amplitude oscillation followed by small amplitude oscillation. This leads to clustering of the cells into two anti-phase clusters as shown in Fig. 7.4 (bottom left), with adjacent cells in the array being roughly 180^0 out of phase.

With increase in the value of ϵ, cells in these clusters start to desynchronize, and the low amplitude stretch of the oscillation reduces. Further increase in ϵ leads these desynchronized cells again into two clusters with the same pattern i.e. alternate cells are in the same cluster. There is again a constant phase relationship ($\sim 180^0$) between the two clusters, as evident in Fig. 7.4 (top right).

As for zero flux boundary conditions, for higher value of ϵ, the cells start to desynchronize from each other and for $\epsilon > 0.4$ we have oscillation death. In this regime, along with oscillation death, we also find mixed oscillations, where some cells are oscillating while

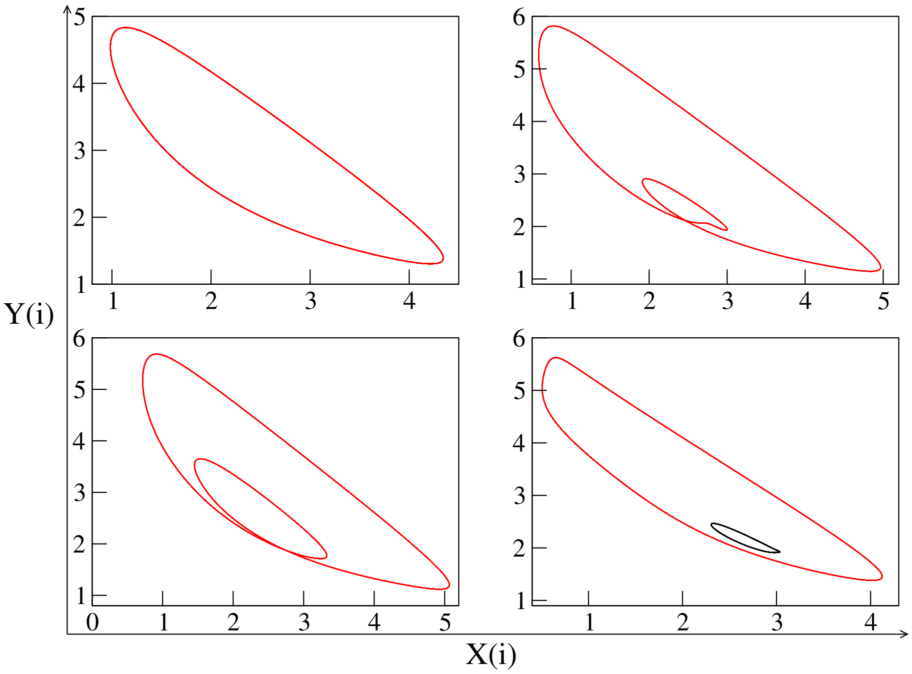

Figure 7.5: Phase space plots for $\epsilon = 0.05$ (top left), $\epsilon = 0.10$ (bottom left), $\epsilon = 0.20$ (top right) and $\epsilon = 0.35$ (bottom right) showing the route from synchronization to formation of clusters as the value of ϵ is increased, for Periodic Boundary condition.

the other are attracted to fixed points.

Interestingly we observed that the number of distinct inhomogeneous steady states (IHSS) that emerge are a divisor of 12 *and have same number of cells are attracted to each distinct IHSS.*

Another interesting phenomena that we observed for the ring of brusselators was the following: there exists three clusters in the second desynchronization regime i.e. for ϵ values in the range $(0.35 - 0.38)$. A representative time series is shown in the Fig. 7.4 (bottom right). Further, it was seen that each cluster had an equal number of cells.

The whole sequence of synchronization to clustering of cells can be viewed in phase space as follows: for small values of ϵ we have one limit cycle, as seen in Fig. 7.5 (top left). As we increase the value of coupling the shape of this limit cycle changes and a small amplitude loop appears, as can be seen in the Fig. 7.5 (bottom left) and (top right). In the case where we have three clusters we find that this loop breaks off and we have two distinct limit cycles as shown in Fig. 7.5 (bottom right).

7.2.3 Constant Concentration Boundary Conditions

For this boundary conditions, we find that all the cells are desynchronized for weak coupling. For intermediate values of coupling strength, we find that the boundary cells oscillate with smaller amplitude and frequency than the rest of the array. The amplitude of oscillation of the cells depend on its relative distance from the boundary. The farther they are from edge, the greater their amplitude. For strong coupling the system settles down to fixed points and we have oscillation death.

7.3 Delay-Coupled Array of Chemical Oscillators

Now we consider this array with delay in the coupling. As motivated earlier, time-delay is both natural and inevitable when considering interactions among systems that are spatially separated. From a mathematical point of view, time-delay makes the dynamical system effectively infinite- dimensional: this can open up a range of time-scales, interactions, and novel dynamical behavior such as amplitude death and the phase-flip bifurcation. For the case of delay, we have integrated the system using the Runge-Kutta fourth order scheme with integration step $\Delta t = 0.01$.

We have also checked these numerics with low step-sizes, but, there is no significant qualitative or quantitative changes.

7.3.1 Zero flux Boundary Conditions

For delay $\tau = 0.5$ to $\tau = 1.0$ we have complete synchrony among all the cells in the array, for all values of coupling strength ϵ. As coupling strength increases, the frequency of the synchronous oscillations get smaller. As we increase the delay time to 1.5, we get a phase flip for $\epsilon = 0.05$, as shown in Fig. 7.6. Further increase in the value of ϵ, first leads to desynchronization, and then complete synchrony of all cells. Also note that the

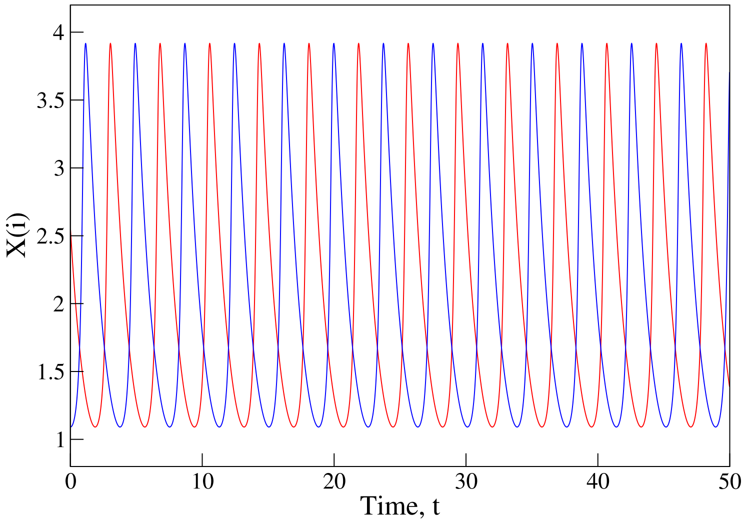

(a) Time series of Fast variable

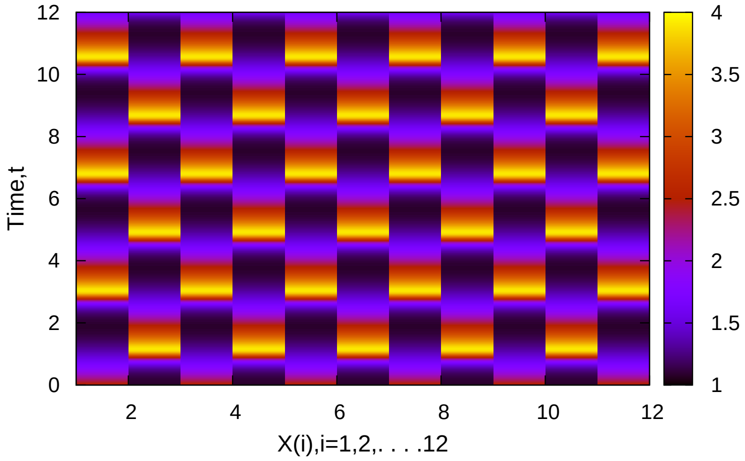

(b) Space-Time Plot of Fast variable

Figure 7.6: Plots showing phase flip in the system for $\tau = 1.5$ and $\epsilon = 0.05$ for zero flux boundary condition.

frequency of oscillation decreases with increasing coupling strength. This trend continues upto delay time $\tau = 2.0$.

At $\tau = 2.5$, we have clustering after phase flip which leads to synchronization of all cells as we increase coupling. For delay time $\tau = 3.0$, we have phase flip at a slightly higher value of coupling, namely $\epsilon = 0.15$. After this phase flip increase in ϵ leads to decrease in the frequency of the synchronous oscillations of the cells.

There are only quantitative changes as we increase the value of delay time τ. As the delay is increased the phase flip is found at higher coupling. For example, the phase flip is found

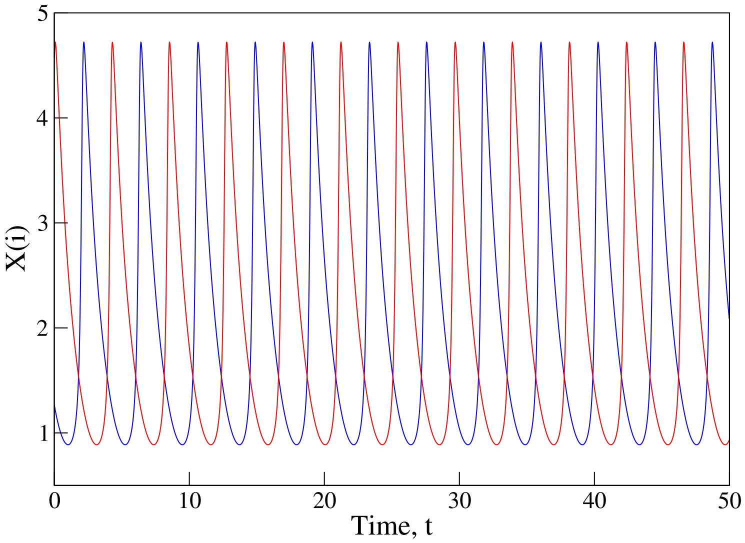

(a) Time series of Fast variable

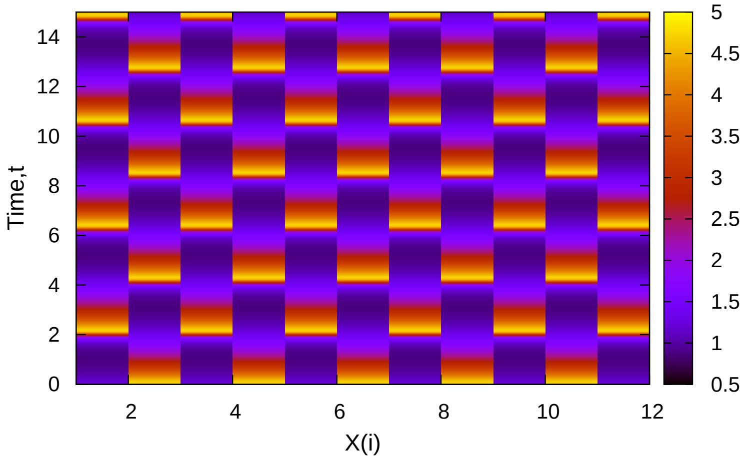

(b) Space-Time Plot of Fast variable

Figure 7.7: Plots showing phase flip in the system for $\tau = 2.5$ and $\epsilon = 0.05$ and for periodic boundary condition.

in the ϵ range $0.10 - 0.15$ for $\tau = 3.0$, $0.15 - 0.20$ for $\tau = 4.0$, $0.15 - 0.25$ for $\tau = 4.5$ and $0.20 - 0.25$ for $\tau = 5.0$. There is also change in the shape of the attractor in phase space for increasing delay τ and coupling ϵ, with the attractor becoming more triangular than elliptical.

7.3.2 Periodic Boundary Conditions

When the cells are in a ring we observe that for small delay time we have synchrony among all the cells. Increasing coupling leads to higher amplitude and smaller frequency synchronous oscillations. As the delay increases we observe different phenomena under increasing coupling. For instance, for $\tau = 1.5 - 2.0$, we have fast desynchronized oscillations for $\epsilon = 0.05$. Increasing the value of ϵ leads to two clusters in this delay range. But as ϵ is increased further beyond ~ 0.15, we have synchronous behavior again.

Phase flips in this system is found in various ranges of delay, for different coupling strengths. For instance, we have phase flips for $\tau = 2.5$ with $\epsilon = 0.05$, for $\tau = 3.5$ with ϵ in the range $0.10 - 0.20$, for $\tau = 4.0$ with ϵ in the range $0.15 - 0.20$, for $\tau = 4.5$ with ϵ in the range $0.15 - 0.25$ and $\tau = 5.0$ with ϵ in the range $0.20 - 0.25$. One representative phase flip is shown in Fig. 7.7.

The next interesting thing here is the *formation of spatial anti-phase patterns* as observed earlier as well. These are found for $\epsilon = 0.1$ in τ range $1.5 - 2.0$, and before the phase flip for higher values of delay. One representative case is shown in the Fig. 7.8. An interesting feature here is that a larger number of loops appear, vis-a-vis Fig. 7.5.

After the phase flip, for almost all values of coupling strength, ϵ, the cells in the array are in synchrony for all values of delay. This is different from what was observed when the cells were coupled without delay where we obtained oscillation death. It is evident that delay coupling makes the IHSS unstable.

7.3.3 Self delayed Coupled Boundary Cells

In this boundary condition, the boundary cells are coupled to their delayed concentration. The qualitative features of spatiotemporal patterns are the same as that are found in periodic boundary conditions with delay. The main difference between the two cases is phase

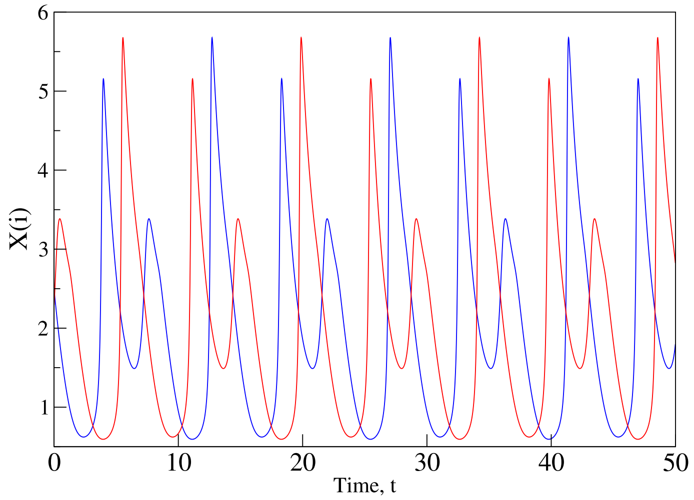

(a) Time series of Fast variable

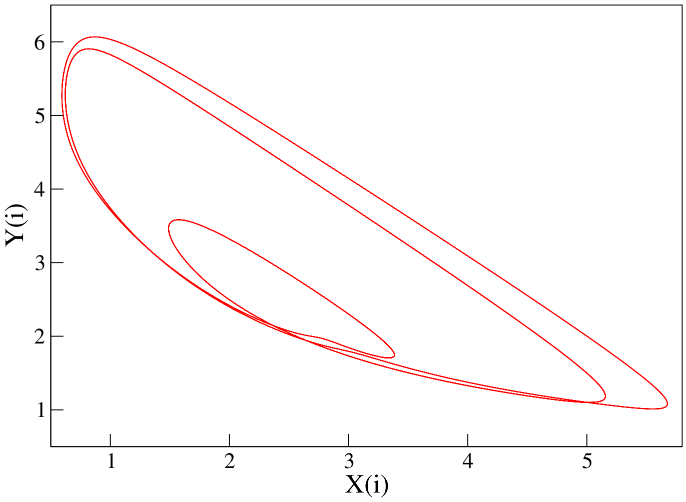

(b) Phase space plot

Figure 7.8: Spatial antiphase pattern in periodic boundary condition for $\epsilon = 1.5$ and $\tau = 3.0$.

flip. The boundary cells, as they are coupled to their respective time-delayed state, do not participate in phase flip. A representative of the time series and phase space plot for such a case is shown in the Fig. 7.9. It is clear that the dynamical attractor of the boundary cells are different from the rest of the array.

For this case also we have change in the shape of the limit cycle as we increase the value of ϵ. A representative of both time series and phase space are shown in Fig. 7.10. These time series and phase space shapes are identical to what we get for periodic boundary condition with delay and for large coupling strength, ϵ.

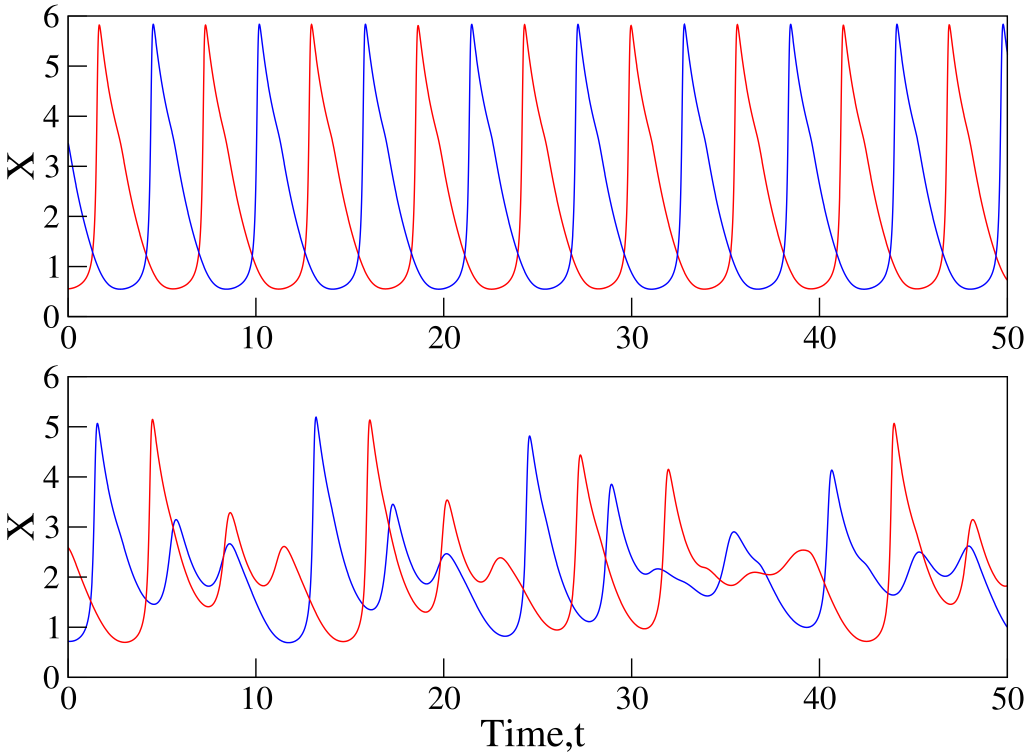

(a) Time series of the end cells (bottom) and rest of the cells (top)

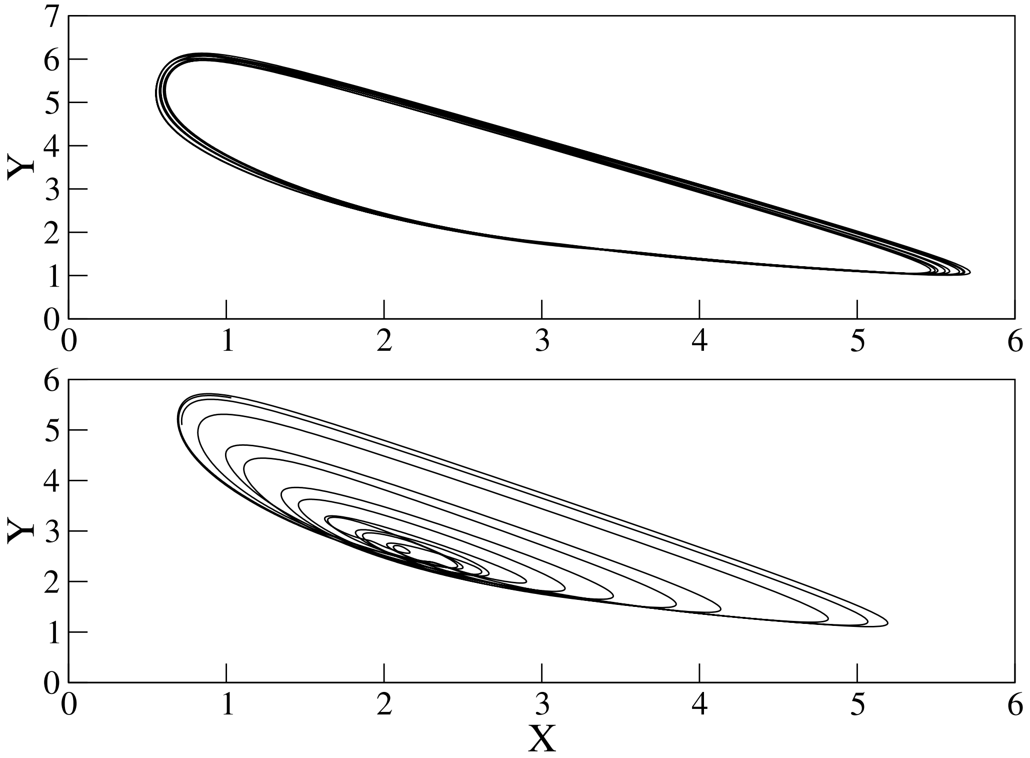

(b) Phase space plot of the end cells (bottom) and rest of the cells (top)

Figure 7.9: Figure showing phase flip in Self delayed coupled boundary condition. Here $\tau = 4.0$ and $\epsilon = 0.25$

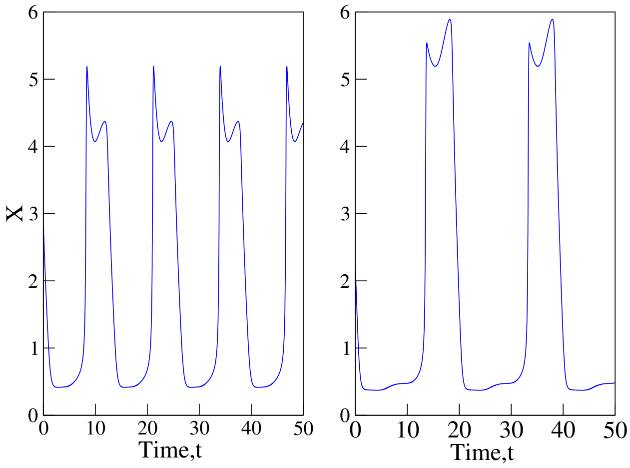

(a) Time series of fast variable

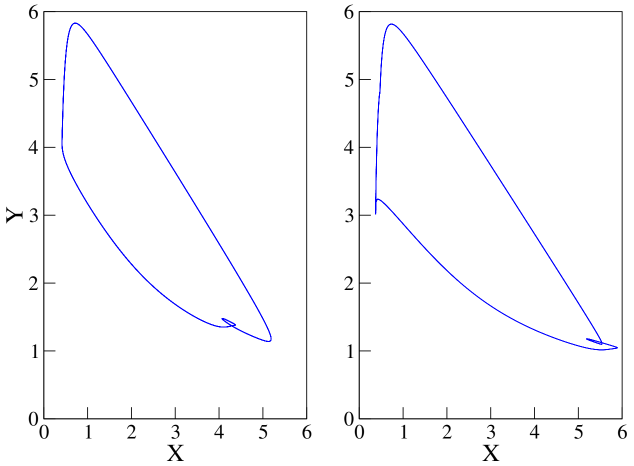

(b) Phase space plot

Figure 7.10: Triangular shaped phase space and small frequency oscillation of fast variable in self delayed coupled boundary condition for $\tau = 4.0$ and $\epsilon = 0.55$ (left) and for $\tau = 5$ and $\epsilon = 0.85$ (right) in both figures.

7.3.4 Constant Concentration Boundary Conditions

Under this boundary condition, the spatiotemporal dynamics is qualitatively similar to the case of coupling without delay. The only difference arises for strong coupling when delay time τ increases, which yields mixed dynamics. Here we have some cells oscillating, while the others go to fixed points. Barring the boundary cells, one observes near phase flip and near synchrony among the cells.

7.4 InHomogeneous Steady States for the array of Brusselator cells

At first, we consider two identical cell with slow variable , y, of one cell is coupled to the other cell. The overall dynamics of the system is given by,

$$\begin{aligned} \dot{x}_{1,2} &= f_1(x_{1,2}, y_{1,2}) \\ \dot{y}_{1,2} &= f_1(x_{1,2}, y_{1,2}) + \frac{\epsilon}{2}(y_{2,1} - y_{1,2}) \end{aligned} \tag{7.2}$$

where, the function $f_1(x, y)$ and $f_2(x, y)$ are given by Eq. (2.14). Following, Tyson and Kauffman [131], the existence and number of IHSS for these two coupled Brusselator cells are summarized in Table (7.1).

One IHSS	Two Distinct IHSS
$\epsilon > \dfrac{4a^2}{b^2 + 2b + 1}$	$\dfrac{4a^2}{b^2 + 2b + 1} \leq \epsilon < \dfrac{a^2}{2(b-1)}$

Table 7.1: Condition for Existence of IHSS

In our case, $a = 2$ and $b = 5.5$. Thus, we will have one distinct IHSS in $\epsilon > 0.378698$ and two distinct IHSS in the ϵ range $0.378698 - 0.444444$.

Now we will discuss the fixed points of the array of Brusselator cells for all boundary conditions:

1. For fixed points in periodic boundary condition we consider, $S(t) = x_1(t) + \cdots + x_N(t)$ and $\Sigma(t) = y_1(t) + \cdots + y_N(t)$, for the array. Hence, we have,

$$\begin{aligned} \dot{S} &= Na - (b+1)S + \sum_{i=1}^{N} x_i^2 y_i \\ \dot{\Sigma} &= bS - \sum_{i=1}^{N} x_i^2 y_i \end{aligned} \tag{7.3}$$

Solving these for fixed point solution we get the following sum condition for fixed

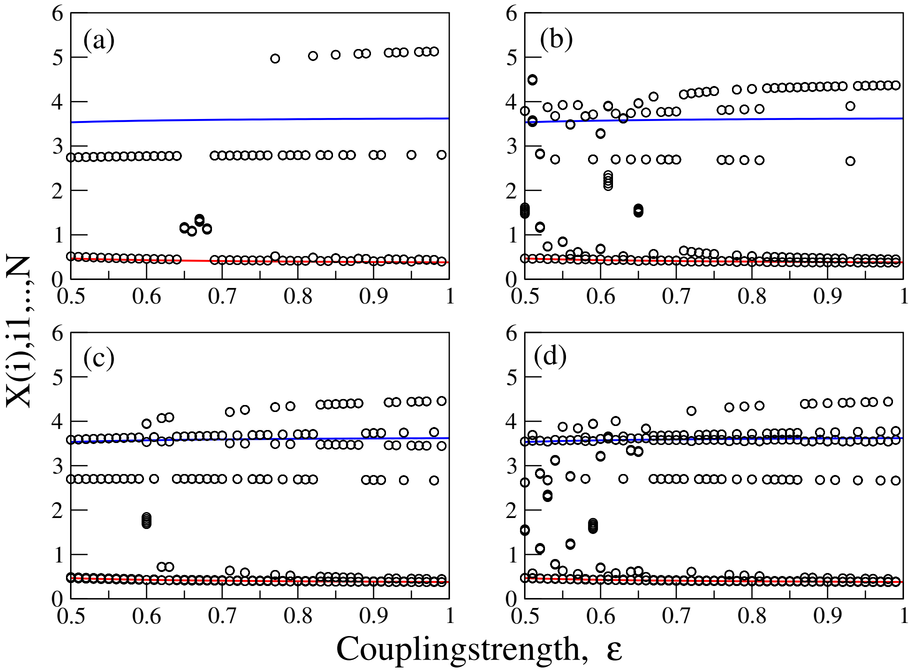

Figure 7.11: Bifurcation diagrams for periodic boundary condition. Here in (a) $N = 3$, (b) $N = 5$, (c) $N = 7$, (d) $N = 9$

points,

$$S = aN \tag{7.4}$$

where, N is the total number of cells in the array. In Fig. 7.11 and Fig. 7.12, we have plotted the IHSS for different values of ϵ. Here, the blue and red line are the two IHSS obtained for two cells. Clearly, for odd number of cells there are more fixed points when the number of cells are increased. But, for even number of cells we found that, the two IHSS obtained for two cell system are quite stable in large region of coupling strength, ϵ. An increase in number of cells in the system leads to more fixed point which satisfy the sum condition given by Eq. (7.4).

2. For zero flux boundary condition, the fixed points also satisfy the condition given by Eq. (7.4). Here, we found that up to $\epsilon = 0.7$, we have mixed dynamics for both even and odd number of total cells. The bifurcation digram of IHSS against ϵ is shown in Fig. 7.13 and Fig. 7.14 with the two IHSS that we have obtained for two cell system (shown in blue and red color). We find that the lower branch of fixed

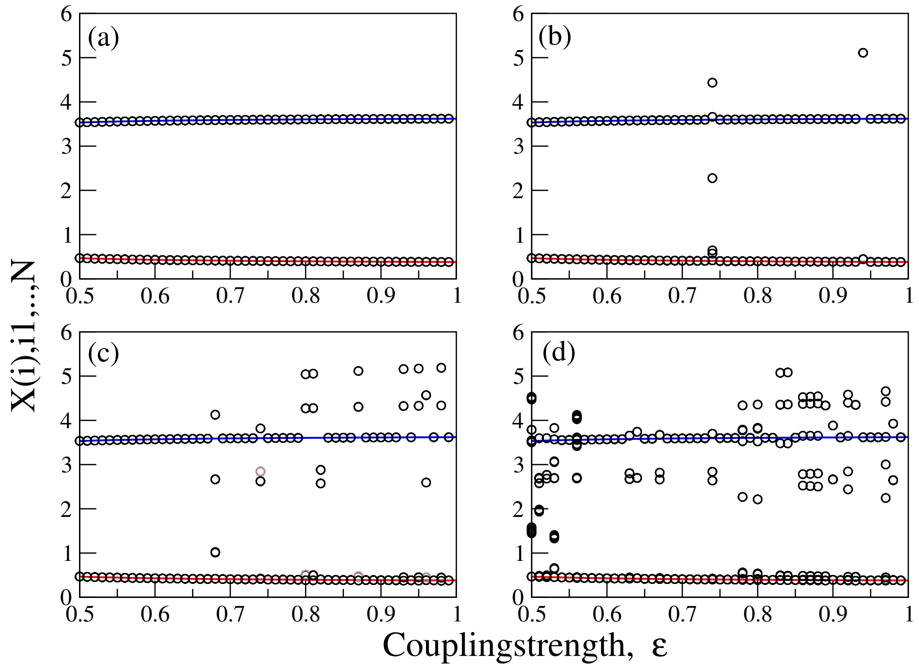

Figure 7.12: Bifurcation diagrams showing spatial profile of all the cell with respect to coupling strength, ϵ, for periodic boundary condition. Here in (a) $N = 4$, (b) $N = 6$, (c) $N = 8$, (d) $N = 10$

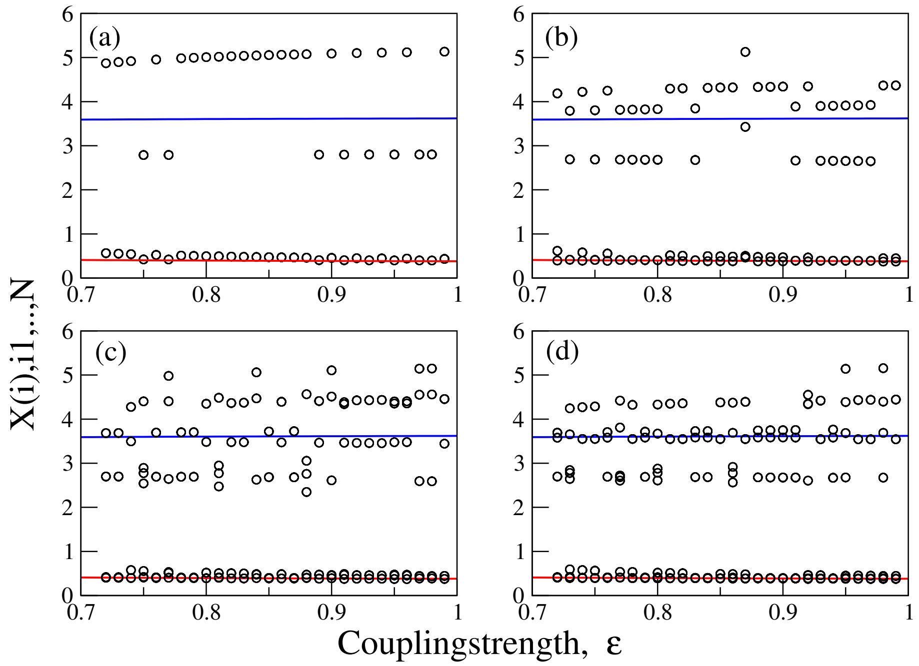

Figure 7.13: Bifurcation diagrams showing spatial profile of all the cell with respect to coupling strength, ϵ, for zero flux boundary condition. Here in (a) $N = 3$, (b) $N = 5$, (c) $N = 7$, (d) $N = 9$

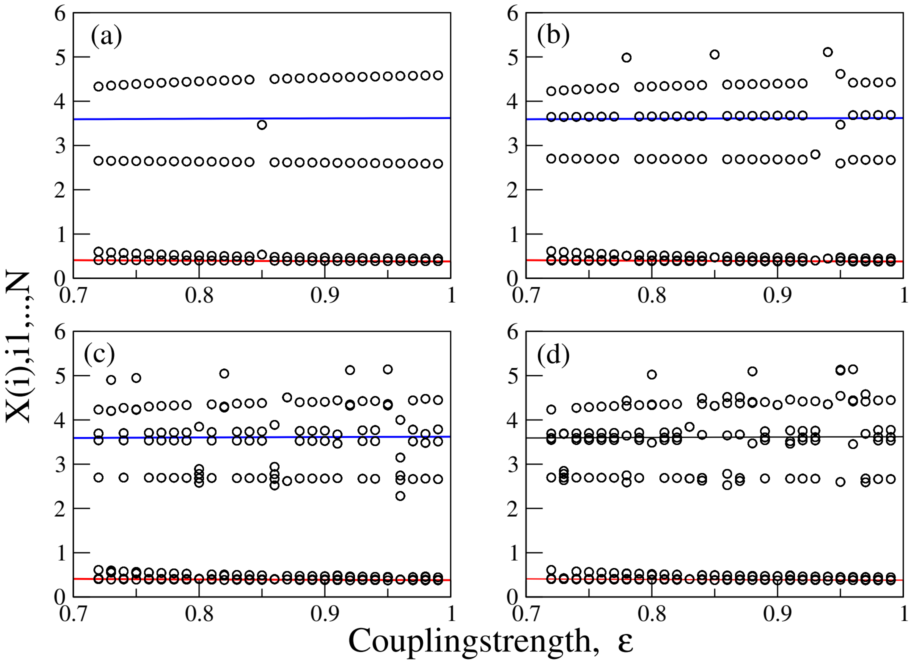

Figure 7.14: Bifurcation diagrams showing spatial profile of all the cell with respect to coupling strength, ϵ, for zero flux boundary condition. Here in (a) $N = 4$, (b) $N = 6$, (c) $N = 8$, (d) $N = 10$

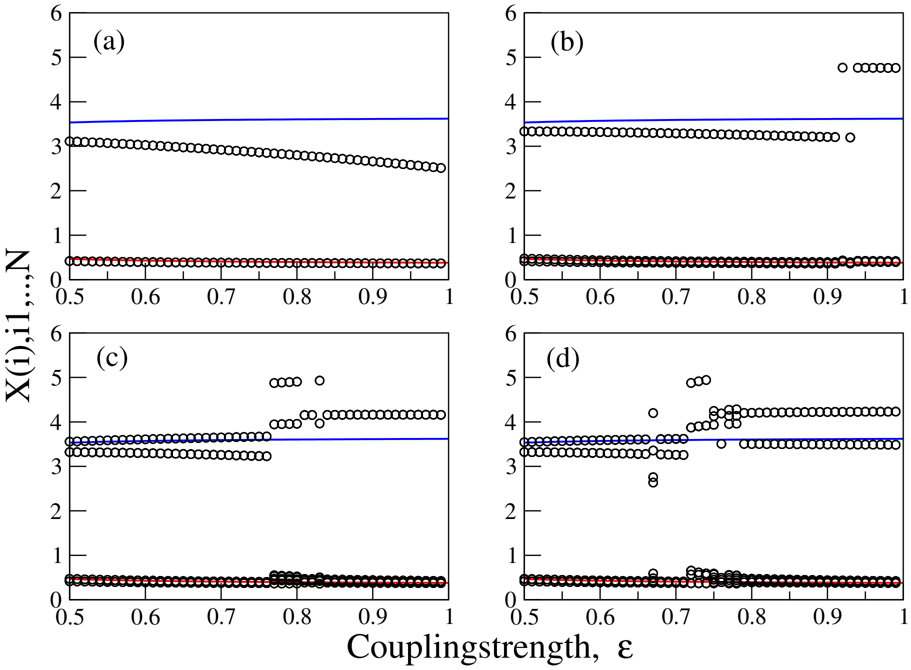

Figure 7.15: Bifurcation diagrams showing spatial profile of all the cell with respect to coupling strength, ϵ, for constant concentration boundary condition. Here in (a) $N = 3$, (b) $N = 5$, (c) $N = 7$, (d) $N = 9$

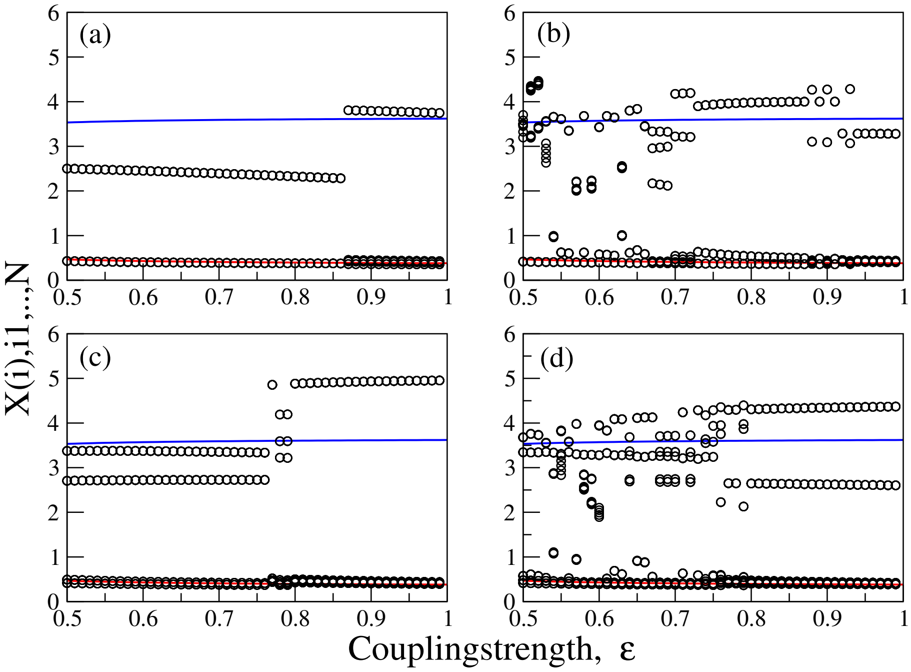

Figure 7.16: Bifurcation diagrams showing spatial profile of all the cell with respect to coupling strength, ϵ, for constant concentration boundary condition. Here in (a) $N = 4$, (b) $N = 6$, (c) $N = 8$, (d) $N = 10$

point for the two cell system is quite stable in this boundary condition for both odd and even number of cells. Clearly, most of cells settle to the lower branch as the fixed point solution is constrained by the sum condition (Eq. (7.4)). Here also, as the number of cells in the system increases, the number of IHSS also increase.

3. In constant concentration boundary condition, we find that for small number of cells there are two fixed points and as the number of cells increases the number of fixed points also increase. We also observed that the end cells start oscillating as we increase the number of cell in the system for small value of ϵ. This can be seen in the Fig. 7.15 and in Fig. 7.16. Here also the blue and red lines are the two IHSS which are obtained for two cell system.

7.5 Conclusion

We studied the phenomenology of an array of coupled brusselator cells with and without delay, under various boundary conditions. We obtain synchronized clusters and mixed dynamics, for both the zero flux and periodic boundary conditions, when there is no delay in the coupling term, over a range of coupling strengths. Also, under constant concentration boundary conditions, we find that the amplitude and frequency of the oscillation of the cells depend on their relative distance from the end cells. Further, we discuss the route from synchronization to formation of clusters, under periodic boundary conditions.

The presence of delay in the coupling yields phase flip, under zero flux and periodic boundary conditions. For self-delayed coupling at the edge and constant concentration boundary conditions, we also find phase flip among the cells, except the boundary cells. Under increasing coupling strengths, we first obtain synchronization. Then the cells undergo phase flip bifurcation, after which there is desynchronization and finally complete synchronization again. This trend is observed in both periodic and zero flux boundary conditions, the only difference being in the critical coupling strength for which the phase flip attractor becomes stable as a function of delay time τ.

In summary, we have modeled a system of diffusively coupled chemical oscillators under a range of coupling schemes and boundary conditions. We obtain a range of spatiotemporal patterns from our models, and these patterns are consistent with the variety of behavior observed in experimental situations [145, 146, 147].

Chapter 8

Conclusion

In this thesis, we have investigated the spatiotemporal dynamics or patterns of the complex system using the framework of coupled map lattices and coupled oscillator chains. These patterns emerge from the interplay of local dynamics, coupling architecture and strength of coupling. The emergent patterns in a complex system are hard to understand due to various level of complications inherent in it. So, in order to gain a better understanding of these systems, we have suppressed certain complications while highlighting the others in our model equations. Thereafter, we characterize the emergent patterns or spatiotemporal dynamics of the system. In this way, we can determine the role of a particular class of complexity on the emergent patterns of the complex system. Now we present the principle conclusions of this thesis.

In Chapter 3, we have considered a network of coupled chaotic neurons whose mean connection weights are skewed towards positive and negative side which represents excitatory and inhibitory connections respectively. Here we have asked the question that which type of connections are more conducive for the dynamical regularity of the neurons. We found that when the connections are predominantly positive, the spatiotemporal fixed points are stable. We found similar trend when the connections in the network are predominantly negative. But, when the connections are quite balanced or when the mean connection weight is zero in the network, we found spatiotemporal chaos. This implies that, when the positive and negative feedback are *balanced*, the spatiotemporal fixed point of the system loses stability which results in the irregular spiking in the system. This observation is consistent with the hypothesis which was given for the observed irregular spiking of neurons in the cortex. This hypothesis states that the temporal chaos in firing of neurons is due to approximate balance between excitatory and inhibitory connections. Along with this, we also observed that for a predominantly negative connection the spatiotemporal fixed point is stable when the number of nodes in the network is large.

In Chapter 4, we have discussed the effect of coupling heterogeneity in the formation of clusters in a coupled neuronal lattice. In here, we have considered a distance dependent coupling in the lattice where the coupling weight between the two nodes depend on their distance in the lattice. Our primary objective was to explore that whether the emergent patterns in this system are the result of coupling heterogeneity or due to underlying lattice structure. To address this issue we have considered the same system under a different coupling scheme where the coupling weight is randomly distributed and is same as that of the distance dependent case in the average sense. We observed a rich variety of spatiotemporal patterns and different routes to synchronization in this system for different coupling schemes. We also found that not only the coupling heterogeneity but also a particular type of coupling architecture is needed for a particular pattern. Hence, the emergent patterns of a heterogeneously coupled system depends on the coupling architecture.

In Chapter 5, we have introduced coupling heterogeneity in a coupled neuronal population through group interaction. Specifically, in this system we have two populations which may or may not be in the same dynamical regime. This system is motivated by the phenomena of *Event Related Synchronization/Desynchronization* (ERD/ERS). Both ERD and ERS are event related response of the brain. Here, an event is a dynamic signal which induces synchrony (ERS) or desynchronization (ERD) in the brain. Here we asked that how does synchrony of a subpopulation depends on inter/intra-group connection weights, relative size of the groups and their intrinsic dynamical behavior. We observed that, the synchronized periodic population has a de-synchronizing effect on the chaotic group, when it is in the majority. However, when the periodic group is in a minority, the coupled chaotic group synchronizes. So, synchronization is crucially dependent on the relative sizes of the interacting sub-populations. We also found wide variety of clustering patterns ranging from different distinct groups of synchronized clusters to anti-phase clusters, determined by the interplay of the relative sizes and intrinsic dynamics of the interacting groups in this coupled system.

In Chapter 6, we studied the temporal regularity of spikes events due to parametric heterogeneity present at the nodal level and the random connections in a coupled neuronal population. In here, we have also considered the case where the random links are dynamic and are switched throughout the evolution. Our primary objective was to explore that whether the addition of random links in the lattice is conducive for the temporal regularity of spike events or not. The other objective was to study the effect of dynamic random links on the temporal regularity of spike events in this system. We observed that for an optimal value of diversity the temporal coherence in the spike events is maximum for regular nearest neighbor coupling and also for both the cases of random connections, namely, quenched random connections where the links are static throughout the evolution and dynamic random connections where the links are dynamic throughout the evolution. This indicates that the temporal coherence in the system is due to diversity or disparity in the characteristic parameter of model neuron. We further observed that the temporal coherence decreases when few random links are added. Also, the largest coherence in the spike events emerge when the coupling strength is large, and the underlying connections are mostly random and dynamically changing.

In Chapter 7, we described a simple model mimicking diffusively coupled chemical micro-oscillators. Our study here draws its motivation from experiments of diffusively coupled chemical oscillators in micro-fluidic assemblies. These experiments have nanoliter volume aqueous drops containing reactants of the oscillating reaction, separated by gaps containing typically octane. A variety of dynamics was observed in such systems, most notably in-phase and anti-phase synchronization. So, we seek a simple model capable of showing the observed spatiotemporal patterns. In our model the physical gap between the "droplets" of chemical oscillators gives rise to a delay in the coupling interaction between them. So, we mimic the micro-fluidic array by a delay-coupled array of oscillatory chemical systems. Our basic aim is to understand the patterns in time and space that arises in such arrays under varying forms of coupling. We observed rich variety of dynamical states emerging from the model under variation of time delay in coupling, coupling strength and boundary conditions. The spatiotemporal patterns obtained include clustering, mixed dynamics, inhomogeneous steady states and amplitude death. Further, under delay in coupling the model yields transitions from phase to anti-phase oscillations, reminiscent of that observed in experiments.

In summary, in the work described in this thesis, we have examined various kinds of complexity classes, which occur naturally in complex systems. We have analysed these in the framework of coupled maps and coupled oscillator chains, and we have determined the interesting, and often constructive role played by complexity in pattern formation. We expect that our results will provide helpful insights into the spatiotemporal dynamics of complex systems in general, and dynamical networks in particular.

Bibliography

[1] L. A. Amaral and J. M. Ottino, “Complex networks,” *The European Physical Journal B-Condensed Matter and Complex Systems*, vol. 38, no. 2, pp. 147–162, 2004.

[2] S. H. Strogatz, “Exploring complex networks,” *Nature*, vol. 410, no. 6825, pp. 268–276, 2001.

[3] M. E. Newman, “The structure and function of complex networks,” *SIAM review*, vol. 45, no. 2, pp. 167–256, 2003.

[4] R. J. Williams and N. D. Martinez, “Simple rules yield complex food webs,” *Nature*, vol. 404, no. 6774, pp. 180–183, 2000.

[5] R. M. May, *Stability and complexity in model ecosystems*, vol. 6. Princeton University Press, 2001.

[6] M. A. Arbib, *The handbook of brain theory and neural networks*. Bradford Book, 2003.

[7] R. Albert, I. Albert, and G. L. Nakarado, “Structural vulnerability of the north american power grid,” *Physical Review E*, vol. 69, no. 2, p. 025103, 2004.

[8] M. Girvan and M. E. Newman, “Community structure in social and biological networks,” *Proceedings of the National Academy of Sciences*, vol. 99, no. 12, pp. 7821–7826, 2002.

[9] A. Arenas, L. Danon, A. Diaz-Guilera, P. M. Gleiser, and R. Guimera, "Community analysis in social networks," *The European Physical Journal B-Condensed Matter and Complex Systems*, vol. 38, no. 2, pp. 373–380, 2004.

[10] V. Latora and M. Marchiori, "Economic small-world behavior in weighted networks," *The European Physical Journal B-Condensed Matter and Complex Systems*, vol. 32, no. 2, pp. 249–263, 2003.

[11] S. Redner, "How popular is your paper? an empirical study of the citation distribution," *The European Physical Journal B-Condensed Matter and Complex Systems*, vol. 4, no. 2, pp. 131–134, 1998.

[12] M. E. Newman, "The structure of scientific collaboration networks," *Proceedings of the National Academy of Sciences*, vol. 98, no. 2, pp. 404–409, 2001.

[13] H. Jeong, B. Tombor, R. Albert, Z. N. Oltvai, and A.-L. Barabási, "The large-scale organization of metabolic networks," *Nature*, vol. 407, no. 6804, pp. 651–654, 2000.

[14] K. R. Sreenivasan, "Fluid turbulence," *Reviews of Modern Physics*, vol. 71, no. 2, pp. S383–S395, 1999.

[15] A. Koch and H. Meinhardt, "Biological pattern formation: from basic mechanisms to complex structures," *Reviews of Modern Physics*, vol. 66, no. 4, p. 1481, 1994.

[16] Y. Kuramoto, *Chemical oscillations, waves, and turbulence*. Courier Dover Publications, 2003.

[17] I. R. Epstein and J. A. Pojman, *An Introduction to Nonlinear Chemical Dynamics: Oscillations, Waves, Patterns, and Chaos: Oscillations, Waves, Patterns, and Chaos*. Oxford University Press, USA, 1998.

[18] S. H. Strogatz, *Sync: The emerging science of spontaneous order*. Hyperion, 2003.

[19] A. Pikovsky, M. Rosenblum, and J. Kurths, *Synchronization: a universal concept in nonlinear sciences*, vol. 12. Cambridge university press, 2003.

[20] J. Buck and E. Buck, “Mechanism of rhythmic synchronous flashing of fireflies fireflies of southeast asia may use anticipatory time-measuring in synchronizing their flashing,” *Science*, vol. 159, no. 3821, pp. 1319–1327, 1968.

[21] I. Z. Kiss, Y. Zhai, and J. L. Hudson, “Emerging coherence in a population of chemical oscillators,” *Science*, vol. 296, no. 5573, pp. 1676–1678, 2002.

[22] B. Blasius, A. Huppert, and L. Stone, “Complex dynamics and phase synchronization in spatially extended ecological systems,” *Nature*, vol. 399, no. 6734, pp. 354–359, 1999.

[23] C. M. Ticos, E. Rosa Jr, W. B. Pardo, J. A. Walkenstein, and M. Monti, “Experimental real-time phase synchronization of a paced chaotic plasma discharge,” *Physical review letters*, vol. 85, no. 14, pp. 2929–2932, 2000.

[24] R. Roy and K. S. Thornburg Jr, “Experimental synchronization of chaotic lasers,” *Physical Review Letters*, vol. 72, no. 13, pp. 2009–2012, 1994.

[25] V. Petrov, Q. Ouyang, and H. L. Swinney, “Resonant pattern formation in a chemical system,” *Nature*, vol. 388, no. 6643, pp. 655–657, 1997.

[26] K. Wiesenfeld, P. Colet, and S. H. Strogatz, “Synchronization transitions in a disordered josephson series array,” *Physical review letters*, vol. 76, no. 3, pp. 404–407, 1996.

[27] M. C. Cross and P. C. Hohenberg, “Pattern formation outside of equilibrium,” *Reviews of Modern Physics*, vol. 65, no. 3, p. 851, 1993.

[28] F. Brochard, E. Gravier, and G. Bonhomme, “Transitions to spatiotemporal chaos and turbulence of flute instabilities in a low-β magnetized plasma,” *Phys. Rev. E*, vol. 73, p. 036403, 2006.

[29] E. Ott, *Chaos in dynamical systems*. Cambridge university press, 2002.

[30] S. Strogatz, *Nonlinear dynamics and chaos: with applications to physics, biology, chemistry and engineering*. Perseus Books Group, 2001.

[31] K. Kaneko and K. Kaneko, *Theory and applications of coupled map lattices*. John Wiley & Sons Chichester, 1993.

[32] M. I. Rabinovich, P. Varona, A. I. Selverston, and H. D. I. Abarbanel, "Dynamical principles in neuroscience," *Rev. Mod. Phys.*, vol. 78, pp. 1213–1265, Nov 2006.

[33] S. Wolfram, "Statistical mechanics of cellular automata," *Reviews of modern physics*, vol. 55, no. 3, p. 601, 1983.

[34] P. Bak, C. Tang, and K. Wiesenfeld, "Self-organized criticality: An explanation of the 1/f noise," *Physical review letters*, vol. 59, no. 4, pp. 381–384, 1987.

[35] B. Ibarz, J. M. Casado, and M. A. F. Sanjuán, "Map-based models in neuronal dynamics," *Physics Reports*, vol. 501, no. 1, pp. 1–74, 2011.

[36] E. M. Izhikevich, "Neural excitability, spiking and bursting," *International Journal of Bifurcation and Chaos*, vol. 10, no. 06, pp. 1171–1266, 2000.

[37] T. M. Antonsen, R. Faghih, M. Girvan, E. Ott, and J. Platig, "External periodic driving of large systems of globally coupled phase oscillators," *Chaos: An Interdisciplinary Journal of Nonlinear Science*, vol. 18, no. 3, pp. 037112–037112, 2008.

[38] L. Gammaitoni, P. Hänggi, P. Jung, and F. Marchesoni, "Stochastic resonance," *Reviews of Modern Physics*, vol. 70, no. 1, p. 223, 1998.

[39] K. Kaneko, "Chaotic but regular posi-nega switch among coded attractors by cluster-size variation," *Physical Review Letters*, vol. 63, no. 3, pp. 219–223, 1989.

[40] G. Perez, C. Pando-Lambruschini, S. Sinha, and H. A. Cerdeira, "Nonstatistical behavior of coupled optical systems," *Physical Review A*, vol. 45, no. 8, p. 5469, 1992.

[41] K. Kaneko, "Spatiotemporal chaos in one-and two-dimensional coupled map lattices," *Physica D: Nonlinear Phenomena*, vol. 37, no. 1, pp. 60–82, 1989.

[42] K. Kaneko, "Clustering, coding, switching, hierarchical ordering, and control in a network of chaotic elements," *Physica D: Nonlinear Phenomena*, vol. 41, no. 2, pp. 137–172, 1990.

[43] K. Kaneko, "Globally coupled circle maps," *Physica D: Nonlinear Phenomena*, vol. 54, no. 1, pp. 5–19, 1991.

[44] S. C. Manrubia and A. S. Mikhailov, "Mutual synchronization and clustering in randomly coupled chaotic dynamical networks," *Physical review E*, vol. 60, no. 2, p. 1579, 1999.

[45] D. Zanette and A. Mikhailov, "Condensation in globally coupled populations of chaotic dynamical systems," *Physical Review E*, vol. 57, pp. 276–281, 1998.

[46] A. Kuznetsov and J. Kurths, "Stable heteroclinic cycles for ensembles of chaotic oscillators," *PHYSICAL REVIEW-SERIES E-*, vol. 66, no. 2; PART 2, pp. 026201–026201, 2002.

[47] A. Koseska, E. Volkov, A. Zaikin, and J. Kurths, "Inherent multistability in arrays of autoinducer coupled genetic oscillators," *Physical Review E*, vol. 75, no. 3, p. 031916, 2007.

[48] A. Koseska, E. Ullner, E. Volkov, J. Kurths, and J. Garcia-Ojalvo, "Cooperative differentiation through clustering in multicellular populations," *Journal of theoretical biology*, vol. 263, no. 2, pp. 189–202, 2010.

[49] D. Golomb and J. Rinzel, “Clustering in globally coupled inhibitory neurons,” *Physica D: Nonlinear Phenomena*, vol. 72, no. 3, pp. 259–282, 1994.

[50] K. Miyakawa and K. Yamada, “Synchronization and clustering in globally coupled salt-water oscillators,” *Physica D: Nonlinear Phenomena*, vol. 151, no. 2, pp. 217–227, 2001.

[51] W. Wang, I. Z. Kiss, and J. Hudson, “Experiments on arrays of globally coupled chaotic electrochemical oscillators: Synchronization and clustering,” *Chaos: An Interdisciplinary Journal of Nonlinear Science*, vol. 10, no. 1, pp. 248–256, 2000.

[52] W. Wang, I. Z. Kiss, and J. L. Hudson, “Clustering of arrays of chaotic chemical oscillators by feedback and forcing,” *Physical review letters*, vol. 86, no. 21, pp. 4954–4957, 2001.

[53] E. L. Berlow, “Strong effects of weak interactions in ecological communities,” *Nature*, vol. 398, no. 6725, pp. 330–334, 1999.

[54] S. Sinha and S. Sinha, “Evidence of universality for the may-wigner stability theorem for random networks with local dynamics,” *Physical Review E-Statistical, Nonlinear and Soft Matter Physics*, vol. 71, no. 2, pp. 020902_1–020902_4, 2005.

[55] S. Sinha and S. Sinha, “Robust emergent activity in dynamical networks,” *Physical Review E*, vol. 74, no. 6, p. 066117, 2006.

[56] S.-H. Yook, H. Jeong, A.-L. Barabási, and Y. Tu, “Weighted evolving networks,” *Physical Review Letters*, vol. 86, no. 25, pp. 5835–5838, 2001.

[57] C. Li and G. Chen, “A comprehensive weighted evolving network model,” *Physica A: Statistical Mechanics and its Applications*, vol. 343, pp. 288–294, 2004.

[58] Y. Jiang, “Globally coupled maps with time delay interactions,” *Physics Letters A*, vol. 267, no. 5, pp. 342–349, 2000.

[59] J. L. Rogers and L. T. Wille, "Phase transitions in nonlinear oscillator chains," *Physical Review E*, vol. 54, no. 3, pp. R2193–R2196, 1996.

[60] S. E. d. S. Pinto and R. L. Viana, "Synchronization plateaus in a lattice of coupled sine-circle maps," *Physical Review E*, vol. 61, no. 5, p. 5154, 2000.

[61] C. Woellner, S. Lopes, R. Viana, and I. Caldas, "Clustering and diffusion in a symplectic map lattice with non-local coupling," *Chaos, Solitons & Fractals*, vol. 41, no. 5, pp. 2201–2215, 2009.

[62] G. Tang, K. Xu, and L. Jiang, "Synchronization in a chaotic neural network with time delay depending on the spatial distance between neurons," *Physical Review E*, vol. 84, no. 4, p. 046207, 2011.

[63] C. Masoller, A. C. Martì, and D. H. Zanette, "Synchronization in an array of globally coupled maps with delayed interactions," *Physica A: Statistical Mechanics and its Applications*, vol. 325, no. 1, pp. 186–191, 2003.

[64] A. C. Martì and C. Masoller, "Delay-induced synchronization phenomena in an array of globally coupled logistic maps," *Physical Review E*, vol. 67, no. 5, p. 056219, 2003.

[65] A. C. Martì and C. Masoller, "Synchronization of globally coupled non-identical maps with inhomogeneous delayed interactions," *Physica A: Statistical Mechanics and its Applications*, vol. 342, no. 1, pp. 344–350, 2004.

[66] H. Daido and K. Nakanishi, "Aging transition and universal scaling in oscillator networks," *Physical review letters*, vol. 93, no. 10, p. 104101, 2004.

[67] H. Daido and K. Nakanishi, "Aging and clustering in globally coupled oscillators," *Physical Review E*, vol. 75, no. 5, p. 056206, 2007.

[68] D. Pazó and E. Montbrió, "Universal behavior in populations composed of excitable and self-oscillatory elements," *Physical Review E*, vol. 73, no. 5, p. 055202, 2006.

[69] G. Tanaka, Y. Okada, and K. Aihara, "Phase transitions in mixed populations composed of two types of self-oscillatory elements with different periods," *Physical Review E*, vol. 82, no. 3, p. 035202, 2010.

[70] E. Barreto, B. Hunt, E. Ott, and P. So, "Synchronization in networks of networks: The onset of coherent collective behavior in systems of interacting populations of heterogeneous oscillators," *Physical Review E*, vol. 77, no. 3, p. 036107, 2008.

[71] E. Montbrió, J. Kurths, and B. Blasius, "Synchronization of two interacting populations of oscillators," *Physical Review E*, vol. 70, no. 5, p. 056125, 2004.

[72] J. H. Sheeba, V. Chandrasekar, A. Stefanovska, and P. V. McClintock, "Asymmetry-induced effects in coupled phase-oscillator ensembles: Routes to synchronization," *Physical Review E*, vol. 79, no. 4, p. 046210, 2009.

[73] I. V. Belykh, V. N. Belykh, and M. Hasler, "Blinking model and synchronization in small-world networks with a time-varying coupling," *Physica D: Nonlinear Phenomena*, vol. 195, no. 1, pp. 188–206, 2004.

[74] R. Amritkar and C.-K. Hu, "Synchronized state of coupled dynamics on time-varying networks," *Chaos*, vol. 16, no. 1, pp. 015117_1–015117_5, 2006.

[75] A. Mondal, S. Sinha, and J. Kurths, "Rapidly switched random links enhance spatiotemporal regularity," *Physical Review E-Statistical, Nonlinear and Soft Matter Physics*, vol. 78, no. 6, p. 066209, 2008.

[76] J. F. Lindner, B. S. Prusha, and K. E. Clay, "Optimal disorders for taming spatiotemporal chaos," *Physics Letters A*, vol. 231, no. 3, pp. 164–172, 1997.

[77] W. L. Shew, H. A. Coy, and J. F. Lindner, “Taming chaos with disorder in a pendulum array,” *American Journal of Physics*, vol. 67, p. 703, 1999.

[78] C. J. Tessone, C. R. Mirasso, R. Toral, and J. D. Gunton, “Diversity-induced resonance,” *Physical review letters*, vol. 97, no. 19, p. 194101, 2006.

[79] F. Sagués, J. M. Sancho, and J. García-Ojalvo, “Spatiotemporal order out of noise,” *Rev. Mod. Phys.*, vol. 79, pp. 829–882, Jul 2007.

[80] A. L. Hodgkin and A. F. Huxley, “A quantitative description of membrane current and its application to conduction and excitation in nerve,” *The Journal of physiology*, vol. 117, no. 4, p. 500, 1952.

[81] E. M. Izhikevich, *Dynamical systems in neuroscience: the geometry of excitability and bursting*. The MIT press, 2007.

[82] R. FitzHugh, “Impulses and physiological states in theoretical models of nerve membrane,” *Biophysical journal*, vol. 1, no. 6, pp. 445–466, 1961.

[83] J. Nagumo, S. Arimoto, and S. Yoshizawa, “An active pulse transmission line simulating nerve axon,” *Proceedings of the IRE*, vol. 50, no. 10, pp. 2061–2070, 1962.

[84] C. Morris and H. Lecar, “Voltage oscillations in the barnacle giant muscle fiber,” *Biophysical journal*, vol. 35, no. 1, pp. 193–213, 1981.

[85] J. Hindmarsh and R. Rose, “A model of neuronal bursting using three coupled first order differential equations,” *Proceedings of the Royal society of London. Series B. Biological sciences*, vol. 221, no. 1222, pp. 87–102, 1984.

[86] M. Courbage and V. Nekorkin, “Map based models in neurodynamics,” *International Journal of Bifurcation and Chaos*, vol. 20, no. 06, pp. 1631–1651, 2010.

[87] D. R. Chialvo, “Generic excitable dynamics on a two-dimensional map,” *Chaos, Solitons & Fractals*, vol. 5, no. 3, pp. 461–479, 1995.

[88] N. F. Rulkov, "Modeling of spiking-bursting neural behavior using two-dimensional map," *Phys. Rev. E*, vol. 65, p. 041922, Apr 2002.

[89] A. T. Fechner, "Schweigg j," *Chen. Phys*, vol. 53, p. 141, 1828.

[90] W. Ostwald, "Periodisch veränderliche reaktionsgeschwindigkeiten," *Physikalische Zeitschrift*, vol. 1, no. 8, pp. 87–88, 1899.

[91] W. C. Bray, "A periodic reaction in homogeneous solution and its relation to catalysis.," *Journal of the American Chemical Society*, vol. 43, no. 6, pp. 1262–1267, 1921.

[92] W. C. Bray and H. A. Liebhafsky, "Reactions involving hydrogen peroxide, iodine and iodate ion. i. introduction," *Journal of the American Chemical Society*, vol. 53, no. 1, pp. 38–44, 1931.

[93] B. P. Belousov, "A periodic reaction and its mechanism," *Compilation of Abstracts on Radiation Medicine*, vol. 147, no. 145, p. 1, 1959.

[94] A. T. Winfree, "The prehistory of the belousov-zhabotinsky oscillator," *Journal of Chemical Education*, vol. 61, no. 8, p. 661, 1984.

[95] R. J. Field, M. Burger, *et al.*, *Oscillations and traveling waves in chemical systems*. Wiley New York etc., 1985.

[96] P. W. Atkins and J. De Paula, *Atkins' physical chemistry*, vol. 8. Oxford University Press Oxford, 2006.

[97] I. Prigogine, *Thermodynamics of irreversible processes*. Thomas, 1955.

[98] I. Prigogine and G. Nicolis, *Self Organization in Non-Equilibrium Systems*. J. Wiley and Sons, New York, 1977.

[99] A. J. Lotka, "Contribution to the theory of periodic reactions," *The Journal of Physical Chemistry*, vol. 14, no. 3, pp. 271–274, 1910.

[100] A. J. Lotka, “Undamped oscillations derived from the law of mass action.,” *Journal of the american chemical society*, vol. 42, no. 8, pp. 1595–1599, 1920.

[101] V. Volterra, “Fluctuations in the abundance of a species considered mathematically,” *Nature*, vol. 118, pp. 558–560, 1926.

[102] R. J. Field and R. M. Noyes, “Oscillations in chemical systems. iv. limit cycle behavior in a model of a real chemical reaction,” *The Journal of Chemical Physics*, vol. 60, p. 1877, 1974.

[103] I. Prigogine and R. Lefever, “Symmetry breaking instabilities in dissipative systems. ii,” *The Journal of Chemical Physics*, vol. 48, p. 1695, 1968.

[104] J. J. Tyson, “Some further studies of nonlinear oscillations in chemical systems,” *The Journal of Chemical Physics*, vol. 58, p. 3919, 1973.

[105] R. M. May, “Will a large complex system be stable?,” *Nature*, vol. 238, pp. 413–414, 1972.

[106] B. Haider, A. Duque, A. R. Hasenstaub, and D. A. McCormick, “Neocortical network activity in vivo is generated through a dynamic balance of excitation and inhibition,” *The Journal of neuroscience*, vol. 26, no. 17, pp. 4535–4545, 2006.

[107] V. Braitenberg and A. Schüz, *Cortex: statistics and geometry of neuronal connectivity*, vol. 249. Springer Berlin, 1998.

[108] C. van Vreeswijk and H. Sompolinsky, “Chaos in neuronal networks with balanced excitatory and inhibitory activity,” *Science*, vol. 274, no. 5293, pp. 1724–1726, 1996.

[109] C. van Vreeswijk and H. Sompolinsky, “Chaotic balanced state in a model of cortical circuits,” *Neural computation*, vol. 10, no. 6, pp. 1321–1371, 1998.

[110] K. Kaneko, “Globally coupled chaos violates the law of large numbers but not the central-limit theorem,” *Physical review letters*, vol. 65, no. 12, pp. 1391–1394, 1990.

[111] G. Perez, S. Sinha, and H. A. Cerdeira, “Order in the turbulent phase of globally coupled maps,” *Physica D: Nonlinear Phenomena*, vol. 63, no. 3, pp. 341–349, 1993.

[112] W. Chang and D. Z. Jin, “Spike propagation in driven chain networks with dominant global inhibition,” *Physical Review E*, vol. 79, no. 5, p. 051917, 2009.

[113] Z. Füredi and J. Komlós, “The eigenvalues of random symmetric matrices,” *Combinatorica*, vol. 1, no. 3, pp. 233–241, 1981.

[114] T. Hogg, B. A. Huberman, and J. M. McGlade, “The stability of ecosystems,” *Proceedings of the Royal Society of London. B. Biological Sciences*, vol. 237, no. 1286, pp. 43–51, 1989.

[115] P. J. Davis, *Circulant matrices*. John Wiley & Sons, New York, 1979.

[116] P. Gade and R. Amritkar, “Spatially periodic orbits in coupled-map lattices,” *Physical Review E*, vol. 47, no. 1, p. 143, 1993.

[117] J. H. Sheeba, V. Chandrasekar, and M. Lakshmanan, “Event-related desynchronization in diffusively coupled oscillator models,” *Physical review letters*, vol. 103, no. 7, p. 074101, 2009.

[118] J. H. Sheeba, V. Chandrasekar, and M. Lakshmanan, “General coupled-nonlinear-oscillator model for event-related (de) synchronization,” *Physical Review E*, vol. 84, no. 3, p. 036210, 2011.

[119] C. Dockstader, W. Gaetz, D. Cheyne, F. Wang, F. X. Castellanos, and R. Tannock, “Meg event-related desynchronization and synchronization deficits during basic

somatosensory processing in individuals with adhd," *Behav Brain Funct*, vol. 4, no. 8, pp. 1–13, 2008.

[120] B. Musizza, A. Stefanovska, P. V. McClintock, M. Paluš, J. Petrovčič, S. Ribarič, and F. F. Bajrović, "Interactions between cardiac, respiratory and eeg-δ oscillations in rats during anaesthesia," *The Journal of physiology*, vol. 580, no. 1, pp. 315–326, 2007.

[121] J. H. Sheeba, A. Stefanovska, and P. V. McClintock, "Neuronal synchrony during anesthesia: a thalamocortical model," *Biophysical journal*, vol. 95, no. 6, pp. 2722–2727, 2008.

[122] A. Palmigiano, J. Pastor, R. G. de Sola, and G. J. Ortega, "Stability of synchronization clusters and seizurability in temporal lobe epilepsy," *PloS one*, vol. 7, no. 7, p. e41799, 2012.

[123] M. Jiang and P. Ma, "Coherence resonance induced by rewiring in complex networks," *Chaos: An Interdisciplinary Journal of Nonlinear Science*, vol. 19, no. 1, pp. 013115–013115, 2009.

[124] V. Volman and M. Perc, "Fast random rewiring and strong connectivity impair subthreshold signal detection in excitable networks," *New Journal of Physics*, vol. 12, no. 4, p. 043013, 2010.

[125] H. Chen, J. Zhang, and J. Liu, "Enhancement of neuronal coherence by diversity in coupled rulkov-map models," *Physica A: Statistical Mechanics and its Applications*, vol. 387, no. 5, pp. 1071–1076, 2008.

[126] R. C. Hilborn, "A simple model for stochastic coherence and stochastic resonance," *American Journal of Physics*, vol. 72, p. 528, 2004.

[127] Q. Y. Wang, Q. S. Lu, and G. R. Chen, “Subthreshold stimulus-aided temporal order and synchronization in a square lattice noisy neuronal network,” *EPL (Europhysics Letters)*, vol. 77, no. 1, p. 10004, 2007.

[128] X. Pei, L. Wilkens, and F. Moss, “Noise-mediated spike timing precision from aperiodic stimuli in an array of hodgekin-huxley-type neurons,” *Physical review letters*, vol. 77, no. 22, p. 4679, 1996.

[129] C. Zhou, J. Kurths, and B. Hu, “Array-enhanced coherence resonance: nontrivial effects of heterogeneity and spatial independence of noise,” *Physical review letters*, vol. 87, no. 9, p. 098101, 2001.

[130] Y. Shinohara, T. Kanamaru, H. Suzuki, T. Horita, and K. Aihara, “Array-enhanced coherence resonance and forced dynamics in coupled fitzhugh-nagumo neurons with noise,” *Physical Review E*, vol. 65, no. 5, p. 051906, 2002.

[131] J. Tyson and S. Kauffman, “Control of mitosis by a continuous biochemical oscillation: Synchronization; spatially inhomogeneous oscillations,” *Journal of Mathematical Biology*, vol. 1, no. 4, pp. 289–310, 1975.

[132] K. Bar-Eli, “On the stability of coupled chemical oscillators,” *Physica D: Nonlinear Phenomena*, vol. 14, no. 2, pp. 242–252, 1985.

[133] E. I. Volkov and V. A. Romanov, “Bifurcations in the system of two identical diffusively coupled brusselators,” *Physica Scripta*, vol. 51, no. 1, p. 19, 1995.

[134] D. G. Aronson, G. B. Ermentrout, and N. Kopell, “Amplitude response of coupled oscillators,” *Physica D: Nonlinear Phenomena*, vol. 41, no. 3, pp. 403–449, 1990.

[135] A. Koseska, E. Volkov, and J. Kurths, “Detuning-dependent dominance of oscillation death in globally coupled synthetic genetic oscillators,” *EPL (Europhysics Letters)*, vol. 85, no. 2, p. 28002, 2009.

[136] M. Dolnik and M. Marek, “Extinction of oscillations in forced and coupled reaction cells,” *The Journal of Physical Chemistry*, vol. 92, no. 9, pp. 2452–2455, 1988.

[137] M. F. Crowley and I. R. Epstein, “Experimental and theoretical studies of a coupled chemical oscillator: phase death, multistability and in-phase and out-of-phase entrainment,” *The Journal of Physical Chemistry*, vol. 93, no. 6, pp. 2496–2502, 1989.

[138] K. Tsaneva-Atanasova, C. L. Zimliki, R. Bertram, and A. Sherman, “Diffusion of calcium and metabolites in pancreatic islets: killing oscillations with a pitchfork,” *Biophysical journal*, vol. 90, no. 10, pp. 3434–3446, 2006.

[139] R. E. Mirollo and S. H. Strogatz, “Amplitude death in an array of limit-cycle oscillators,” *Journal of Statistical Physics*, vol. 60, no. 1-2, pp. 245–262, 1990.

[140] G. B. Ermentrout, “Oscillator death in populations of âĂIJall to allâĂİ coupled nonlinear oscillators,” *Physica D: Nonlinear Phenomena*, vol. 41, no. 2, pp. 219–231, 1990.

[141] D. Ramana Reddy, A. Sen, and G. L. Johnston, “Time delay induced death in coupled limit cycle oscillators,” *Physical Review Letters*, vol. 80, no. 23, pp. 5109–5112, 1998.

[142] S. H. Strogatz, “Nonlinear dynamics: Death by delay,” *Nature*, vol. 394, no. 6691, pp. 316–317, 1998.

[143] A. Prasad, J. Kurths, S. K. Dana, and R. Ramaswamy, “Phase-flip bifurcation induced by time delay,” *Physical Review E*, vol. 74, no. 3, p. 035204, 2006.

[144] A. Prasad, S. K. Dana, R. Karnatak, J. Kurths, B. Blasius, and R. Ramaswamy, “Universal occurrence of the phase-flip bifurcation in time-delay coupled systems,” *Chaos: An Interdisciplinary Journal of Nonlinear Science*, vol. 18, no. 2, pp. 023111–023111, 2008.

[145] M. Toiya, V. K. Vanag, and I. R. Epstein, “Diffusively coupled chemical oscillators in a microfluidic assembly,” *Angewandte Chemie*, vol. 120, no. 40, pp. 7867–7869, 2008.

[146] M. Toiya, H. O. González-Ochoa, V. K. Vanag, S. Fraden, and I. R. Epstein, “Synchronization of chemical micro-oscillators,” *The Journal of Physical Chemistry Letters*, vol. 1, no. 8, pp. 1241–1246, 2010.

[147] F. Rossi, V. K. Vanag, E. Tiezzi, and I. R. Epstein, “Quaternary cross-diffusion in water-in-oil microemulsions loaded with a component of the belousov- zhabotinsky reaction,” *The Journal of Physical Chemistry B*, vol. 114, no. 24, pp. 8140–8146, 2010.

[148] I. R. Epstein and K. Showalter, “Nonlinear chemical dynamics: oscillations, patterns, and chaos,” *The Journal of Physical Chemistry*, vol. 100, no. 31, pp. 13132–13147, 1996.

[149] K. Tomita, “Chaotic response of nonlinear oscillators,” *Physics Reports*, vol. 86, no. 3, pp. 113–167, 1982.

[150] M. Dolnik, I. Schreiber, and M. Marek, “Experimental observations of periodic and chaotic regimes in a forced chemical oscillator,” *Physics Letters A*, vol. 100, no. 6, pp. 316–319, 1984.

[151] M. R. Guevara and L. Glass, “Phase locking, period doubling bifurcations and chaos in a mathematical model of a periodically driven oscillator: A theory for the entrainment of biological oscillators and the generation of cardiac dysrhythmias,” *Journal of mathematical biology*, vol. 14, no. 1, pp. 1–23, 1982.

[152] A. T. Winfree, *The geometry of biological time*, vol. 12. Springer, 2001.

[153] L. Glass, M. R. Guevara, J. Belair, and A. Shrier, “Global bifurcations of a periodically forced biological oscillator,” *Physical Review A*, vol. 29, no. 3, p. 1348, 1984.

[154] M. N. Stolyarov, V. A. Romanov, and E. I. Volkov, “Out-of-phase mixed-mode oscillations of two strongly coupled identical relaxation oscillators,” *Physical Review E*, vol. 54, no. 1, p. 163, 1996.